# A Comprehensive Volcanic Hazard Assessment for Mount Meager Volcanic Complex, B.C.

**by**

**Rachel Warwick**

B.Sc., Simon Fraser University, 2017

Thesis Submitted in Partial Fulfillment of the
Requirements for the Degree of
Master of Science

in the
Department of Earth Sciences
Faculty of Science


SIMON FRASER UNIVERSITY
Fall 2020

## Declaration of Committee

| | |
|---|---|
| **Name:** | **Rachel Warwick** |
| **Degree:** | **Master of Science** |
| **Title:** | **A Comprehensive Volcanic Hazard Assessment for Mount Meager Volcanic Complex, B.C.** |
| **Committee:** | **Chair: Brendan Dyck**<br>Assistant Professor, Earth Sciences |
| | **Glyn Williams-Jones**<br>Supervisor<br>Professor, Earth Sciences |
| | **Jeffrey Witter**<br>Committee Member<br>Adjunct Professor, Earth Sciences |
| | **Melanie Kelman**<br>Committee Member<br>Physical Scientist<br>Geological Survey of Canada |
| | **Nathalie Vigouroux**<br>Examiner<br>Instructor, Earth and Environmental Sciences<br>Douglas College |

## Abstract

Mount Meager Volcanic Complex located in south-western British Columbia exhibits possible volcanic activity in the form of hydrothermal features such as several hot springs around the base and a fumarole field in the northeast corner of the complex. Operational infrastructure, including a run-of-river hydroelectric project, is present in the vicinity of the volcano and a significant population exists only 60 km downstream. Up until now, no volcanic hazard assessment or accompanying map existed for Mount Meager. Hazard assessments are important tools used to understand, manage and reduce the risks associated with volcanic environments. This thesis investigates the potential primary volcanic hazards associated with a future explosive eruption at Mount Meager. These hazards are identified as lahars, pyroclastic density currents and volcanic ash. With the use of numerical modelling programs, the distribution, timescales, intensity of inundation and other parameters are investigated. Finally, a suite of scenario-based preliminary hazard maps have been produced to visually display these hazards as a communication tool. This information relays hazard information to stakeholders with a vested interest in the potential risks involved with any future explosive volcanic event from Mount Meager.



**Keywords**: Mount Meager; Volcanic Hazard Modelling; Lahar; Pyroclastic Flow; Tephra; Canadian Volcano

## Acknowledgements

There are many people that I would like to extend my gratitude for their input and guidance through these past few years of completing my Master's. First, thank you to my senior supervisor, Dr. Glyn Williams-Jones for the opportunity to work on this exciting project and for going above-and-beyond to offer research guidance and educational opportunities and facilitating field research. I am also extremely grateful for the input and words of encouragement from my other committee members Dr. Jeff Witter and Dr. Melanie Kelman throughout my Master's degree.

I would also like to acknowledge Jennifer Harrison (University of Bristol) who completed the numerical modelling of tephra distribution with TephraProb. This was an invaluable component and addition to the volcanic hazard analysis for this hazard assessment.

Thank you to everyone (past and present) in the physical volcanology lab group for all the time they have taken out of their day to assist me in small and sometimes big challenges and for being there when I needed to bounce around ideas or share a laugh. You have all helped me immeasurably over the past few years. Specifically thank you to Gioachino Roberti for providing me with so much material, information, and expertise about Mount Meager and for initial guidance of using VolcFlow. And also to Yannick Le Moigne for his guidance in using and troubleshooting issues with VolcFlow. Thank you to Antonina Calahorrano who was a part of initial investigations of statistical analysis of wind patterns across Mount Meager. I would also like to thank many others in the SFU Earth Science department who have either helped me throughout my years in the department or who have been there for great discussions and laughs, and made my experience in the department wonderful.

Next, I would like to thank the many individuals for their assistance in various aspects of navigating the numerical models chosen for each hazard. Thank you to Valentin Gueugneau for answering my questions about lahar and pyroclastic flow modelling in VolcFlow, Francisco Vasconez for also offering guidance in lahar modelling with VolcFlow and lahar modelling in LAHARZ. Thank you to everyone at the Cascades Volcano Observatory who offered guidance and suggestions upon listening to my discussion about my research in November 2018. Specifically, thank you to Sarah

Ogburn for her guidance and suggestions for pyroclastic flow modelling of Mount Meager for providing me with additional reading material about volcanic hazard assessments available for U.S. volcanoes.

Finally, thank you so much to my friends and family who have offered support through words of encouragement, guidance and patiently listening to my ideas or challenges. Especially, thank you to my parents, whom without their support and unquestioning belief in all my hopes and dreams, I would not be where I am today.

# Table of Contents

# List of Tables

# List of Figures

## List of Acronyms

| | |
|---|---|
| DEM | Digital Elevation Model |
| MMVC | Mount Meager Volcanic Complex |
| PDCs | Pyroclastic Density Currents |

# Chapter 1.

# Introduction

The Mount Meager Volcanic Complex (Mount Meager) is a glacier-clad volcanic massif in south-western British Columbia. Several stratovolcano peaks comprise the structure of the volcanic system, resulting in a complex topographic terrain. Mount Meager has a 2 million year history of intermittent explosive volcanism (Read, 1990). It is currently in a state of quiescence; the last eruption occurred 2360 calendar years B.P. from the Bridge River vent on the eastern flank of Plinth Peak (Hickson et al., 1999). It currently has an active hydrothermal system manifested by a fumarole field and multiple hot springs. The fumaroles (Figure 1.1) were first seen at the surface of Job Glacier in 2016, in the north-east section of the complex (Venugopal et al., 2017; Roberti et al., 2018).

Currently, there is no volcanic hazard assessment outlining the potential multifaceted hazards related to the next phase of volcanic activity. A hazard and risk assessment was completed by Friele et al. (2008) and Friele (2012) to address the landslide risk at Mount Meager. The comprehensive volcanic hazard assessment developed in this thesis will mark one of the first of its kind in the Canadian context.

Volcanic hazard assessments and accompanying maps are vital tools used to understand, manage and reduce the risk posed by volcanic environments in many countries around the world. While western Canada lies in a zone of active tectonics, with five volcanic belts (Hickson, 1994; Edwards & Russell, 1999), this region of Canada remains vulnerable to volcanic activity. The risk is exacerbated due to limited knowledge of the recent geologic history, a poor understanding of eruptive dates, and a lack of targeted monitoring efforts to gather background volcanic signals from any potentially active systems in British Columbia or Yukon. A report by Stasiuk et al. (2003) identified the vulnerability of Canadian society to possible eruptions - and noted that in the past 10,000 years, 49 volcanic eruptions have occurred. Widespread concern has not been given to potential volcanic activity due to many factors including: the fact that volcanoes are mostly remote across western Canada, the Canadian population is dispersed and because of the short colonial history in Canada has no written record of first-hand

experience of an eruption. For this reason, the creation of volcanic hazard maps, targeted monitoring, and management plans have not been a priority for those involved in geohazard management across western Canada. Far more prevalent and ongoing hazards such as forest fires, floods and earthquakes have garnered the attention from government, scientists and the public up until now.

The objective of this project was to produce a comprehensive volcanic hazard assessment for Mount Meager, informed by a scenario-based approach of numerically modelling the expected hazards. Three governing scenarios represent plausible eruptive episodes that could be expected from the volcanic complex in the future. The development of these scenarios was informed by the known geologic history of the volcano and eruption parameters from analogous volcanic systems.

The challenges faced by this study include limited geologic data available for Mount Meager beyond the studies focused on the last eruption 2360 cal yr. B.P., as well as no existing framework for addressing future volcanic hazards and their impacts. Not only does the lack of data prove a problem for informing the likely eruptive parameters from this volcano, it precludes an understanding of the particular volcanic hazards that could stem from an eruption and their sphere of impact. This project endeavors to create a hazard assessment, despite the limited data. This project will therefore stand as a framework for the further development of volcanic hazard assessments for other Canadian volcanoes.

Specific stakeholders that will benefit from the production of this hazard map for Mount Meager include: Squamish-Lillooet Regional District managers, the Lil'wat Nation community, Emergency Management BC, and Natural Resources Canada (NRCan). This assessment can be used to prioritize mitigation strategies and inform a monitoring program, with a greater understanding of the hazard characteristics that can be expected from a future eruption.

## 1.1. Background

Mount Meager, part of the Garibaldi Volcanic Belt (GVB), is 150 km northwest of Vancouver, and 65 km northwest of Pemberton. It is bordered by Meager Creek and the upper Lillooet River which flow along the base of the volcanic complex (Figure 1.1).

From the volcano, the upper Lillooet River flows down valley towards Pemberton, the closest population center. These rivers follow known tectonic lineaments trending NE-SW and NW-SE respectively (Grasby et al., 2020). The upper reaches of the complex are partially covered by several alpine glaciers. The northernmost and highest peak of the complex is Plinth Peak at 2677 m.a.s.l. (463824 E, 5610505 N 10U), valley bases have an elevation of ~ 500 m.a.s.l. and therefore the local relief is about 2200 m.a.s.l. The complex has been subjected to dynamic Quaternary processes, such as dissection by glacier advance and retreat, from the large continental-scale Cordilleran ice sheet (Clague & Ward, 2011), and modern alpine glaciers (Roberti et al., 2018) as well as extensive hydrothermal alteration (Venugopal, 2019).

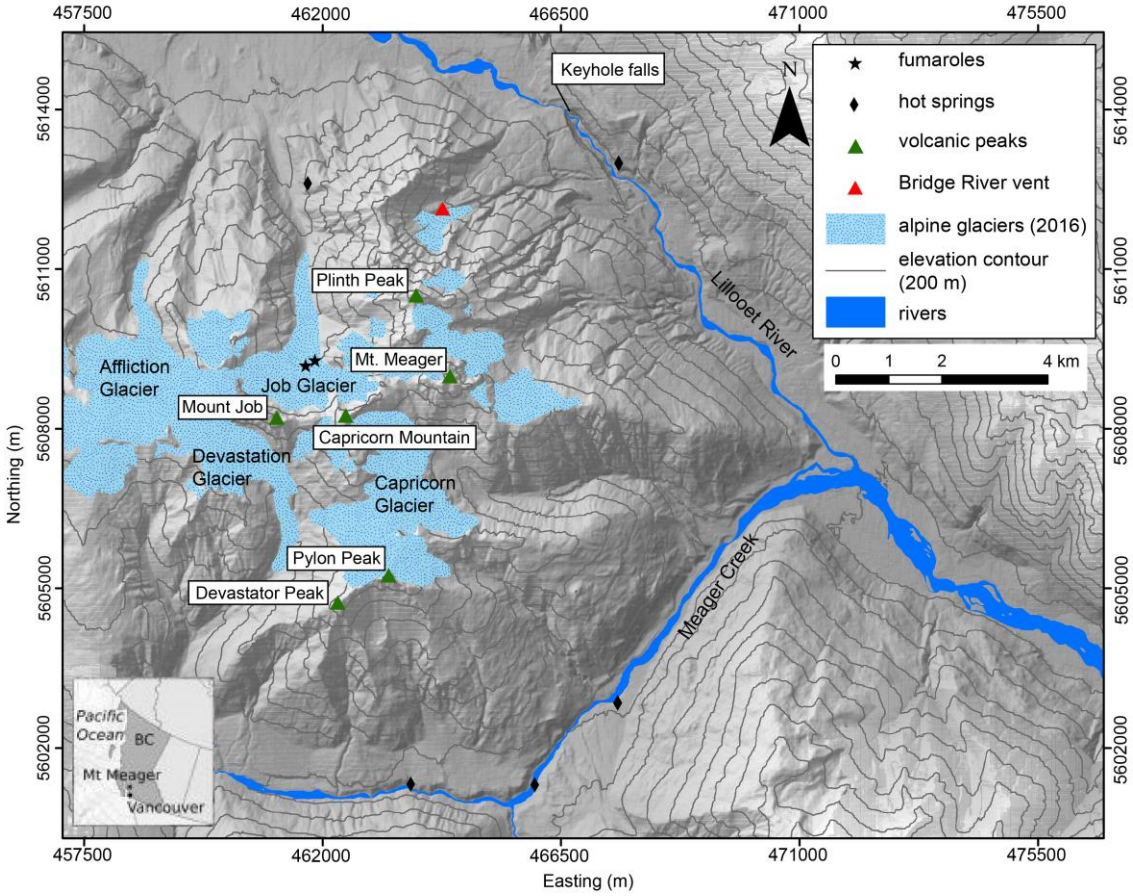


**Figure 1.1** **Overview of the Mount Meager Volcanic Complex (MMVC). Includes the extent of modern alpine glaciers as of 2016, mapped by Roberti et al. (2018). The locations of hot springs (black diamonds) and fumaroles (black stars) represent surface expression of hydrothermal activity. Inset map identifies the location of MMVC in the context of British Columbia. All coordinates are in UTM Zone 10, WGS 1984.**

The GVB, is part of the northern segment of the Cascadia Subduction Zone (Green et al., 1988; Read, 1990) (Figure 1.2). The subduction zone is segmented into two volcanic arcs: the High Cascades Arc to the south and the GVB in the north (Mullen & Weis, 2013; Mullen et al., 2018; Venugopal, 2019). Volcanism of the GVB is related to subduction of the northern end of the Juan de Fuca Plate beneath the North American Plate (Green et al., 1988). Volcanism in the GVB is characterized by much lower eruption rates due to a younger and hotter subducting plate relative to magmatism in the High Cascades (Green & Harry, 1999; Mullen et al., 2018). In addition, many volcanoes in the GVB exhibit relatively low relief due to the combination of high rates of uplift (Farley et al., 2001) and a long history of glacier cover (resulting in glaciovolcanism, reduced rock strength, and glacial scouring);  this includes, but is not limited to, interaction with the Cordilleran ice sheet in the Pleistocene (Wilson & Russell, 2018).

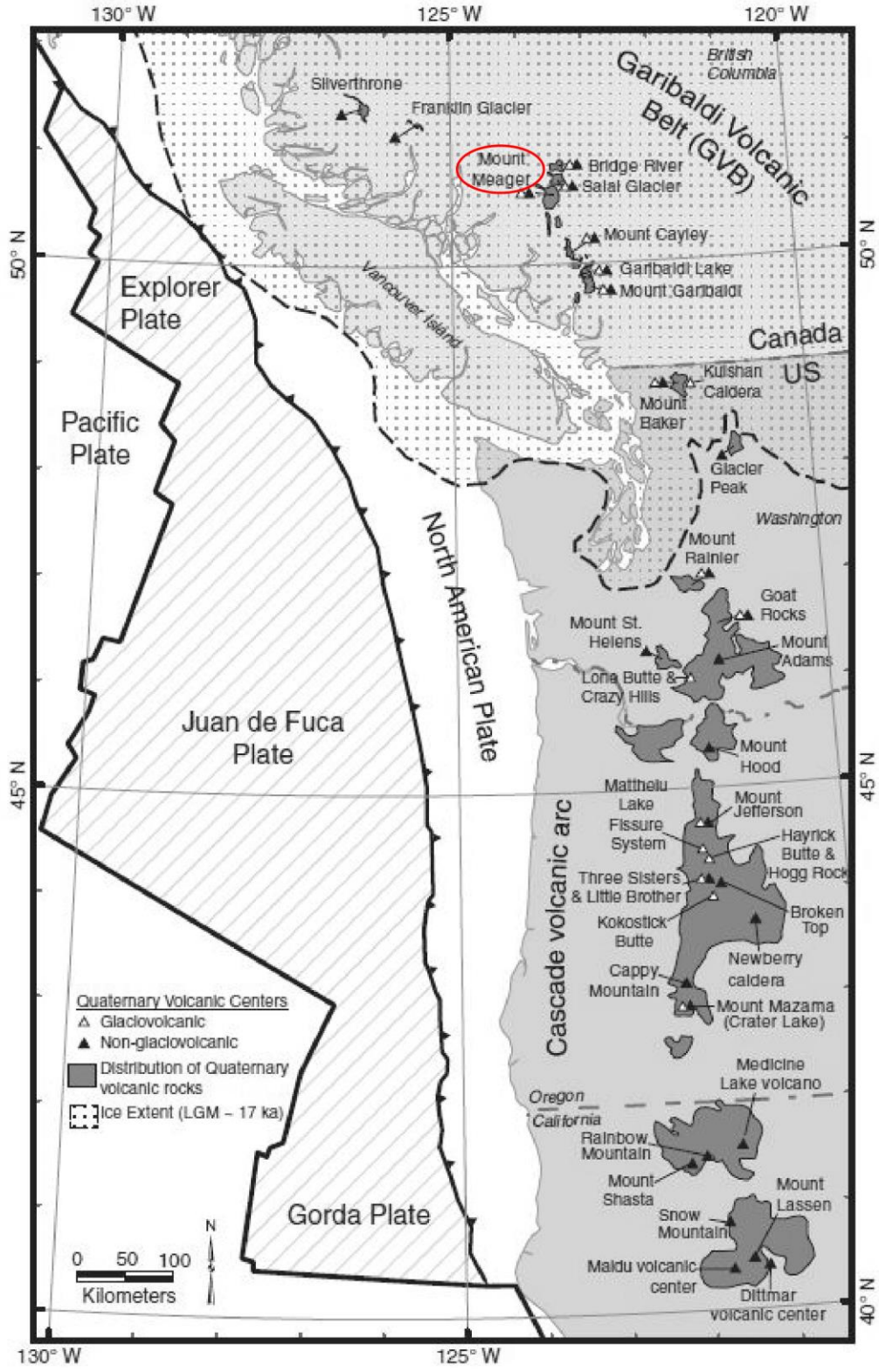


**Figure 1.2** **Map showing location of Mount Meager (circled in red) in relation to the tectonic setting of the Cascade volcanic arc in the Pacific North-West. Modified from Wilson & Russell (2018), used with permission of the GSA.**

Despite being a large volcanic system, Mount Meager is far more recognized for its history of frequent, large-scale mass-wasting events. In 2010, the largest landslide in Canadian history (~$53 \times 10^6$ $m^3$) occurred on the flanks of Capricorn Mountain, flowing into a portion of the upper Lillooet River, with a maximum path length of 12.7 km (Guthrie et al., 2012; Roberti et al., 2017). The high frequency of landslides occurring around the Mount Meager massif has led past geologists to label this area as the most landslide prone site in Canada (Read, 1990).

## 1.2. Geologic History

The 2 million year eruptive history of Mount Meager has constructed several peaks, resulting in the complex that stands today (Read, 1990; Farley et al., 2001). Mapping by Read (1990) and Hickson et al. (1999) shows that volcanism at this complex can be split into three periods: early- and late-stage rhyodacite, and a middle stage of andesitic activity. The eruptive suite includes pyroclastic deposits, overlapping andesite and rhyodacite lavas, and rhyodacite to dacite domes, as well as peripheral basaltic lavas (Read, 1990; Hickson et al., 1999). The volcanic deposits are believed to be about 600 m thick and overlie Mesozoic plutonic and metamorphic basement rocks (Read, 1990; Roberti, 2018).

Extensive work by a number of researchers (e.g., Simpson et al., 2006; Friele et al., 2008; Friele, 2012) has documented the long record of landslides and established a hazard and risk assessment based on the large-scale and frequent landslides prevalent throughout the complex. Work has continued to document recent mass-wasting events and identify unstable slopes throughout the massif (Guthrie et al., 2012; Hetherington, 2014; Roberti et al., 2017). Only one of the documented debris-flow events has been directly associated with the last eruption (Simpson et al., 2006). A question remains regarding what relationship might exist between an abrupt large landslide failure and the depressurization of the underlying magmatic plumbing system, possibly triggering an eruption as explored by Roberti (2018).

## 1.3. Eruption sequence and hazards of the 2360 calendar years B.P. eruption

The last eruption from Mount Meager occurred 2360 cal yr B.P. (Clague et al., 1995; Hickson et al., 1999), and was the most recent eruption within the GVB and last major explosive eruption within Canada. That eruption, with a Volcano Explosivity Index (VEI) of 4, is believed to have been episodic; the subsequent emplacement of volcanic products possibly lasted weeks to months, starting as a sub-plinian style eruption and waning to vulcanian style activity (Hickson et al., 1999; Andrews et al., 2014; Campbell et al., 2016).

The vent responsible for the latest eruption is located at 1500 m.a.s.l. elevation, on the northeastern flank of Plinth Peak and is no longer exposed at the surface. This vent sits atop older volcanic material comprising the Plinth Assemblage, which differs petrographically from the products of the Pebble Creek Formation (PCF), the deposit from the 2360 cal yr B.P. eruption (Hickson et al., 1999).

The PCF - also referred to as the Bridge River Assemblage in older publications - consists of the eruptive products stemming from the 2360 cal yr B.P. eruption. They locally fill the nearby Lillooet Valley. Proximal mapped deposits comprise fallout pumice, channelized pyroclastic density currents, volcanic and non-volcanic debris flows, a dacite lava flow and a catastrophic outburst flood (which can also be described as a secondary lahar). Visible ashfall associated with the eruption has been identified as far away as ~ 548 km E-NE from Mount Meager (Jensen et al., 2019).

The timescale and sequence of events of the 2360 cal yr B.P. eruption have been studied by many researchers (e.g., Stasiuk et al., 1996; Hickson et al., 1999; Stewart, 2002; Michol et al., 2008 Andrews et al., 2014). While the explosive phase of the eruption may have only lasted a few hours to a few days, the emplacement of subsequent deposits may have lasted for years after the initial highly explosive phase. These subsequent deposits include non-welded ignimbrite (indicative of eruption column collapse, or diminished energy in the eruption column) occurring during or immediately preceding the cessation of violent explosive activity. Welded block and ash flows (BAF), with an estimated volume of 0.15 $km^3$, stem from the collapse of lava domes being extruded onto the oversteepened side of Plinth Peak. The extrusion of lava domes and

flows could have lasted days to years after the onset of eruption. These deposits are overlain by a non-welded block and ash flow that accumulated in the Lillooet River valley over 1-2 months (Andrews et al., 2014). The welded BAF formed a 110 m high tall dam directly below the vent which impounded the river and created a temporary lake. The subsequent catastrophic collapse of the dam lead to rapid draining of the temporary lake, leaving behind hyperconcentrated volcaniclastic flood deposits, identified at the base of Mount Meager, and correlated to deposits 45-60 km downstream (Friele et al., 2005; Friele et al., 2008). This flood, a secondary volcanic hazard, has been estimated to have occurred over the course of 4 hours, depositing a volume of $5 \times 10^7$ $m^3$ (Andrews et al., 2014). The final phase of active eruption is represented by a single dacitic lava deposit on the flanks of Plinth Peak with a thickness of 15 m to 20 m (Stasiuk et al., 1996; Hickson et al., 1999). Field observations show that it does not extend to the base of Mount Meager in the Lillooet Valley.

Finally, the ash cloud distribution and ash deposition are directly related in time to the expulsion of pyroclastic material from the eruption. The fallout pumice deposit trends 63° east-northeast and calculations by Hickson et al. (1999) suggest the height of the eruption column was 15-20 km. A timescale has not been estimated for the propagation of the ash cloud stemming from this particular eruption. In the case of the 1980 eruption of Mt. St. Helens (which can be considered as an analogous volcanic system), the eruption column rose 25 km in 30 minutes (Wolfe, 1995) and the ash cloud crossed the continental U.S. in three days. A similar timeframe of ash dispersal from the 2360 cal yr B.P. eruption of Mount Meager would be plausible.

## 1.4. Future Volcanic Hazards

Three volcanic hazards, associated with explosive eruptions, have been chosen for the development of the hazard assessment: lahar flows, pyroclastic density currents (PDCs) and volcanic ash (ashfall). Fatalities from volcanic eruptions are historically correlated to higher population density in proximity to a volcano and the occurrence of lahar flows and PDCs, which are proximal hazards (Auker et al., 2013). Volcanic ash is one of the most widespread products of explosive eruptions, being transported in the atmosphere. These primary hazards individually encompass both proximal and proximal-to-distal regions of impact. Lahar flows and PDCs are proximal hazards (impact zone range from the massif, up to 65 km away), while volcanic ash deposition and distribution

includes distal impact (deposition could impact regions over 500 km away, given a large explosive eruption and strong prevailing winds). These particular hazards stand to cause the most destruction to human activity and their livelihood upon impact, not only being a threat to human life, but also to vital infrastructure, social and economic human activity and to the surrounding environment. Choosing to highlight and investigate the impacts of these three volcanic hazards will best inform emergency managers and stakeholders for emergency response plans and policy considerations.

Deposits attributed to all three hazard phenomena are visible in the landscape around Mount Meager stemming from the last major eruption. While this is the record of only one eruption, it is evidence of a major event and the capability of an eruptive episode. The destructive effects and impacts caused by these hazards are well-known and have been felt from the recent eruptions of several similar analogous volcanoes. Among many recent, well-documented volcanic eruptions around the world, the tragedies of Nevado del Ruiz (1985) and Mt. St Helens (1980) stand out. These are subduction zone related, glacier-clad stratovolcanoes, with well-documented eruptive events, and deposits. Their geologic histories highlight a myriad of eruptive scenarios for eruption magnitude, parameters and hazardous outcomes. The 1985 eruption of Nevado del Ruiz was catastrophic, killing tens of thousands of people. This eruption produced ashfall and pyroclastic density currents, but it was the large lahars that wiped out towns, causing the most destruction. The lahar that destroyed Armero travelled more than 70 kilometres before burying the town (Voight, 1990). The explosive eruption of Mt. St. Helens in 1980 was also multi-hazardous, causing a lateral blast, several PDCs and lahar flows; ashfall from this eruption was recorded in several states in the aftermath (Wolfe & Pierson, 1995).

These hazards have been chosen as being primary in nature, meaning that they are syneruptive hazards, are the most-likely to occur during an explosive phase of activity at Mount Meager and have the widest impact on people and infrastructure. One or all of these hazards may occur during the next phase of eruptive activity at Mount Meager. Secondary hazards and/or noneruptive hazards are not accounted for in this thesis. Secondary hazards include post-eruptive induced lahars, floods, and forest fires. Noneruptive hazards are non-volcanic mass movements, which are known to be common around the massif (Evans, 1987; Jordan, 1994; Bovis & Jakob, 2000; Friele & Clague, 2004; Friele et al., 2008; Simpson et al., 2006; Guthrie et al., 2012;

Hetherington, 2014; Roberti, 2018). In the following section each volcanic hazard is described and their impacts summarized.

### 1.4.1. Pyroclastic Density Currents

Pyroclastic density currents (PDCs) are hot (~200-700°C), rapid flows (reaching speeds of 10 – 100 m/s) of volcanic gas and particles (e.g., Druitt, 1998; Scott et al., 2008). PDCs are often conceptualized as dense-dilute coupled flows that include both flow and surge components. The morphological components of this flow include the dense, basal avalanche and the overriding dilute, turbulent cloud of ash and gas (surge component) (Denlinger, 1987; Valentine, 1987; Burgisser & Bergantz, 2002; Ogburn & Calder, 2017). Pyroclastic flows are often confined by topography. A pyroclastic surge can travel uphill or across water and sometimes extends upwards and outwards from a pyroclastic flow (Carey et al., 1996). There are a few distinct processes that can cause the initiation of a PDC during volcanic unrest. PDCs can be generated from the high vertical collapse of an eruptive column, a directed volcanic blast, or from the collapse fronts of lava domes and flows (Wolfe, 1995). While segments of PDCs can travel independently of the topography, leaving mantled deposits, their flow path is often dictated by topography, confined by valleys and flowing from high to low elevations. Principally, the gravity driven flow will travel down the flank of a volcano once the mixture is denser than the surrounding atmosphere and can resist upward convective and buoyant factors.

PDCs are the most deadly volcanic hazard, given their rapid speed, heat and mass. They are known to completely level vegetation in their path, and the toxic gas and ash cloud is catastrophic, causing asphyxiation for any living being in the path of propagation. This was the case for most causes of fatality and a large area of damaged forest after the eruption of Mt. St. Helens (Bernstein et al., 1986). It is understood that survival is only possible for victims on the periphery of a dilute phase. According to a study by Auker et al. (2013), PDCs account for one third of all volcanic activity related fatalities. However, this statistic takes into account all known volcanic events and fatalities that include volcanoes in close proximity to population centres. While this phenomena is complex, unpredictable and deadly, the impact footprint is often limited to a few kilometres to tens of kilometres from the vent. The footprints are largely

determined by the energy of the eruption, and volume of collapsed material entrained into the flow (Brown et al., 2015).

Based on mapping by Hickson et al. (1999), the welded block and ash flow at Mount Meager can be traced 5.5 km downstream from the inferred vent location. While it is likely that the stratigraphic record does not capture the true runout length of PDCs from the last eruption, this short travel distance is still useful for informing the possible footprint of future PDCs at Mount Meager.

The generation of PDCs may also contribute to the instigation of lahar flows. Hot material from these events has been documented to deposit onto the surface of glaciers, which leads to melting and incorporation of the pyroclastic material, generating a lahar (Fagents & Baloga, 2006).

### 1.4.2. Lahar Flows

Also known as volcanic debris flows or mudflows, lahars are fast flowing mixtures of water and sediment originating from a volcanic source (Smith & Fritz, 1989). They are gravity-driven, channelized flows that can travel 10s of m/s and long distances, or induce flooding conditions affecting areas at even greater distances (Brown et al., 2015). Lahars typically reach their peak velocity on the flanks of the volcano, where the valley morphology is steep and narrow and lose speed with increased distance. Peak flow velocities of the lahars on the flanks of Nevado del Ruiz, stemming from the 1985 eruption, reached 17 m/s (Pierson et al., 1990).

Lahars are variable in terms of mechanisms of occurrence, flow rheology and hydraulic properties both across all events and within the same event. Flow rheology and hydraulic properties are related to the mixture of the flow (in reference to the ratio of debris to water comprising the flow). The debris composition can vary depending on the amount, type, and size distribution of incorporated sediment. Lahar rheology changes through the duration of advance based on the addition or loss of sediment and water, a process known as bulking and debulking (Vallance, 2000).

Depending on their mechanism of occurrence, they can be considered primary (syneruptive) or secondary volcanic hazards. Syneruptive mechanisms of occurrence include: mixing of water with unconsolidated or poorly consolidated volcanic debris,

eruptions within crater lakes, interaction of hot pyroclastic material with water, snow and ice, and ice melt induced by geothermal heating beneath an ice cap (Waythomas, 2014). The geothermally induced melting of ice may also be a secondary hazard depending on the timing of the lahar. Other post-eruptive mechanisms of occurrence include remobilization of volcanic sediments following intense rainfall, outbreak of lakes impounded by unconsolidated volcanic sediment, or an evolution of large debris avalanches sourced from volcanic material (Fagents & Baloga, 2006). During eruptive activity, volcanoes with snow and ice caps are particularly susceptible to the generation of large lahars due to the formation of PDCs, which are a common outcome of explosive activity. PDCs thermally and mechanically erode and melt ice cover, generating significant volumes of water. It is this dynamic interaction that produces more melt water and thus larger volume lahars than other volcanic processes that melt ice (Waythomas, 2014). The long-term possibilities of lahar initiation can seriously impede recovery efforts and relocation of displaced communities following the volcanic eruption (Pierson et al., 2014).

Primary lahars are included in this hazard assessment for Mount Meager because this complex is capped by alpine glaciers with near constant fumarolic activity making it susceptible to geothermally-generated lahars or ice and PDC interaction triggered lahars during an eruption. As mentioned earlier, a lahar deposit is prevalent in the Pebble Creek formation stratigraphy. This originated from the catastrophic failure and subsequent rapid draining of a temporary lake at the site of Keyhole Falls within the Lillooet Valley.

Lahars, ultimately, are landscaping events, altering the topographical characteristics of the environment upon which they are deposited. During propagation, they are highly destructive, causing structural damage to anything in their paths, including buildings, roads and bridges. Lahar deposits fill river valleys, which inhibits the natural carrying capacity for normal river discharge, making the rivers highly susceptible to flooding or changing river morphology after the deposition of the lahar (Wolfe, 1995). While lahars are responsible for many fatalities associated with volcanic eruptions (>35,000) (Auker et al., 2013), these fatalities can be avoided with early-warning systems and effective land-use planning (Pierson et al., 2014).

### 1.4.3. Volcanic ash

Explosive eruptions violently eject a mixture of hot gas and tephra from the vent of origin, generating an eruption column. Tephra is any highly fragmented volcaniclastic particles ejected during an eruption (Fisher, 1964). This mixture is propelled upwards by the energy of the eruption itself, gas expansion and the difference in material density, where this mixture is typically less dense than air. The eruption column extends upwards into the atmosphere until it is no longer buoyant. Particles fall out of the column once the energy to remain in suspension diminishes (Carey & Sparks, 1986). Simply put, larger particles drop out of suspension closer to the vent leaving ash-sized particles (< 2 mm diameter) to travel as an ash cloud, with the tephra fragment size and blanket thickness decreasing further away from the vent, up to several hundred kilometers downwind of the vent (Pyle, 1989). The term volcanic ash, strictly refers to particles ejected by a volcano that are ≤ 2 mm in diameter (Fisher & Schmincke, 1984).

Of all volcanic hazards, volcanic ash has the potential to affect the greatest number of people because it can be distributed over large areas. Impacts include: damage to critical infrastructure (Wilson et al., 2012), costly clean-up measures, agricultural damage (Thompson et al., 2017), aviation disruption (Guffanti et al., 2009), and air quality concerns (Horwell & Baxter, 2006).

Volcanic ash clouds have the ability to temporarily change weather conditions. As an example, the ash cloud attributed to the 1980 eruption of Mt. St. Helens caused a short period of darkness in Spokane, Washington, 400 km away from the volcano. This ash cloud spread across the U.S. in 3 days and circled the Earth in 15 days (Global Volcanism Program, 1980). In this regard, what may appear to be a remote volcano, is no longer a remote, secluded problem, as they have the ability to affect global air traffic. As an example, the 2010 eruption of Iceland's Eyjafjallajökull volcano prompted intermittent air traffic shutdown across many parts of Europe for several weeks. In total the International Air Transport Association estimated the total loss for the airline industry was US $1.7 billion due to the shutdowns in response to that eruption (Budd et al., 2011).

Specifically concerning Mount Meager, the dominant prevailing wind patterns are the westerlies, with some deviation from this norm. This has implications for the most-

likely direction of volcanic ash propagation and deposition. Within one year, daily wind conditions are variable, therefore impacting the direction of possible ash cloud propagation. Duration, radius and dispersion of the ash cloud can also be affected by the height of the eruption column. Volcanic ash particles that remain in the lower atmosphere (troposphere) will fall within a few hours, affected by gravitational settling and weather conditions. Particles that reach the upper atmosphere (~11 km, stratosphere) may remain there for several years (Prata & Rose, 2015).

## 1.5. Introduction to hazard maps

Volcanic hazard maps are a visual tool that can be used to communicate spatial volcanic hazard information to designated audiences, such as emergency managers, land planners and government officials in addition to the interested and potentially impacted general public. Selective temporal information may also be included if that serves the desired message for communication. Hazard maps represent a common reference point that may be referred to by all stakeholders and interested parties when formulating subsequent risk assessments and hazard and mitigation plans (Lindsay & Robertson, 2018). The content and visuals of hazard maps vary immensely due to many factors, these include: type of information being communicated, method of acquiring data for display, quality and quantity of data, desired audience, political sensitivities, and societal considerations (Thompson et al., 2017). An extensive review of volcanic hazard maps categorized these documents into five main types: geology-based, integrated qualitative type, modelling-based, probabilistic type and administrative based (Brown et al., 2015). The study found that geology-based hazard maps were the most commonly generated. These maps integrate the information of past events to inform the hazard map of a specific volcanic system, based on the fundamental geologic concept of uniformitarianism (the past is the key to the future). This is a sound approach where the geologic history of a site is well understood and believed to be well constrained. Modelling-based hazard maps display hazard information derived from the numerical modelling of specific hazards. These have become more prevalent with the advent of improved computer technology and processing power and improvements in the understanding of the geophysical parameters driving each hazard type. Modelling-based hazard studies can be further categorized as deterministic (a straightforward narrative approach, where the set of specific inputs dictates the output), probabilistic (includes

elements of randomness) or a hybrid between the two (Ang et al., 2020; Rouwet et al., 2017). Probabilistic hazard maps are garnering more interest in the volcanological community for their ability to quantify that statistical probability of occurrence of a hazard and capture the non-linear behaviours of volcanic events. However, probabilistic assessments require the knowledge of past events from the system (at best) or parameter input from analogue volcanoes. Furthermore, this approach remains computationally expensive in comparison to other available methodologies.

With consideration of the Canadian context (remote volcanoes with limited geologic data), the best approach for generating a hazard map centres on the modelling-based type, using deterministic methods. The volcanic system of Mount Meager is not well constrained, with information only available from one prior eruption. The available geology has informed the type of eruption to consider and the hazards to focus on for modelling efforts.

## 1.6. Thesis outline

This thesis is primarily an investigation of the major hazard phenomena that could occur during the next volcanic eruption at Mount Meager. The following chapters detail the rationale, procedure and development of the volcanic hazard assessment organized by three governing scenarios that describe a range of eruptive magnitudes and outcomes from this system. This project has been guided by a few key research questions:

- What are the main hazards of concern for future eruptive activity at Mount Meager?
- How does one develop an effective hazard assessment and map for a relatively remote volcanic system with limited geologic or background volcanic data?
- What are the expected impacts from a future explosive eruption at Mount Meager?

These questions are investigated and addressed in five chapters and supporting appendices.

- Chapter 1 (this chapter) presents the general introduction, background and motivation for this thesis and begins to answer the first research question.

- Chapter 2 describes the governing scenarios of this thesis. The procedure, parameters and numerical model programs are presented in order to tackle the second question.

- Chapter 3 presents the results of each hazard simulation.

- Chapter 4 discusses the outcomes of the simulations, comments on the use of each numerical model for other volcanic systems in Canada and presents the scenario-based volcanic hazard maps for Mount Meager.

- Chapter 5 provides general conclusions and comments on future work that should be considered for Mount Meager and other volcanic systems in Canada.

# Chapter 2.

# Methods

The hazard assessment and accompanying map for this project is modelling-based, which is described as a “scenario-based application of simulation tools” (Calder et al., 2015). This was chosen as the best approach for developing a volcanic hazard assessment for Mount Meager based on the quantity and type of data available. Sufficient historical eruption data for Mount Meager is not available, as only one past eruption, the 2360 cal yr B.P. eruption, is well-constrained (Stasiuk et al. 1996; Hickson et al. 1999). A wide-ranging geologic dataset containing well-constrained data from several past eruptions would be required to develop a geologically-based hazard assessment, a common type of hazard assessment produced by the hazard analysis community (Calder et al., 2015). For the numerical simulations of each volcanic hazard, common input data required include: Digital Elevation Models (DEM), geological information known for Mount Meager and analogue volcanic eruption data.

## 2.1. The governing scenarios

The use of scenarios to compile and organize potential outcomes serves to capture and showcase the range of eruptive possibilities and resulting hazards that could be reasonably expected to occur from an explosive eruptive phase of Mount Meager. This is especially beneficial in developing a narrative for effective communication of the multi-hazard phenomena stemming from a volcanic eruption (Ang et al., 2020). The scenarios used for this project are guided by the VEI scale, showcasing an increase in eruptive magnitude. The basis of characterization of the VEI scale encompasses eruptive magnitude (force) and volume of erupted material (Newhall & Self, 1982). This is appropriate for the basis of scenarios for the volcanic ash hazards but not directly related, in practice, to the size of PDCs or lahars, which have additional parameters that may influence their size and region of impact (e.g., Kataoka et al., 2018). The organization of scenarios is based on the comparable size of input parameter values and are therefore consistently presented together as individual scenarios, with scenario 1 being the smallest magnitude eruption (or smallest input of initial conditional values) and scenario 3 being the largest magnitude of initial input conditions.

The Volcanic Explosivity Index (VEI) has been widely adopted as the scale to characterise and compare explosive volcanic events. This scale, which ranges from 0 to 8, incorporates the volume of erupted material and the height of the eruptive column (Newhall & Self, 1982). The last eruption from Mount Meager was characterised as VEI 4 (Andrews et al. 2014), which describes an eruptive volume ~$10^8$-$10^9$ $m^3$ and column height between 10-25 km (Newhall & Self, 1982).

Other stratovolcanoes of similar composition to Mount Meager have exhibited a range of explosivities both across their known geologic history and within a specific eruptive episode. This includes Mt. St. Helens eruptive ranges of VEI 2-5 (Wolfe & Pierson, 1995), the multi-phase eruption (from effusive style to vulcanian style with VEI up to 3) of Soufriere Hills Volcano, Montserrat (Wadge et al., 2014) and a range of VEI characterizations, from a recent VEI 1-2 eruption and past eruptions ≥ VEI 3, for eruptions from Cotopaxi Volcano, Ecuador (Bernard et al., 2016).

Given that stratovolcanoes can exhibit a range of explosive magnitudes across their history or even within a single eruptive phase, the governing scenarios (Table 2.1) are guided by the parameters often exhibited in a VEI 1-5 eruption, capturing a variety of plausible eruptive magnitudes for a future eruption at Mount Meager. Each volcanic hazard is modelled with input parameters corresponding to appropriate values consistent with the designated VEI value. For the scope of this project, each hazard is modelled across three VEI conditions, as a worst case (VEI 5), mid-range (VEI 3) and low energy eruption (VEI 1-2).

**Table 2.1 Eruption scenarios and the corresponding parameter values used in numerical models**

| Scenario | Explosivity | Tephra Characteristics | Lahar Flow Characteristics | Example |
|---|---|---|---|---|
| 1 | VEI 1-2 | Plume height: 5 km asl<br>Erupted volume: 0.0001 $km^3$<br>Eruption duration: 1 hour | Volume: 1-3 × $10^6$ $m^3$<br>Runout length: 15 – 18 km | Cotopaxi volcano eruption 2015 (Bernard et al., 2016; Global Volcanism Program, 2016) |
| 2 | VEI 3 | Plume height: 27 km asl<br>Erupted volume: 0.0390 $km^3$<br>Eruption duration: 45 minutes | Volume: 5 × $10^7$ $m^3$<br>Runout length: 60 – 100 km | Nevado del Ruiz 1985 eruption<br>(Herd, 1986) |
| 3 | VEI 5 | Plume height: 24 km asl<br>Erupted volume: 1.4 $km^3$<br>Eruption duration: 9 hours | Volume: 5 × $10^8$ $m^3$<br>Runout length: 80 – 100 km | Mt. St. Helens 1980 eruption<br>(Wolfe , 1995) |

These scenarios do not describe the succession of events that could happen during the onset of an eruption. The scope of this project has involved numerically modelling each hazard individually onto the landscape at the time of the DEM generation (i.e., 2015-2016). This project does not aim to encompass all possible scenarios and no comments are made that allude to which case (VEI) is the most likely. That level of analysis would require a rigorous monitoring network and further studies.

## 2.2. Topographic Controls: DEM

Common among all numerical modelling of lahars and PDCs was the input requirement of a DEM. It was necessary to use the most up-to-date topographic data available. This is particularly necessary at Mount Meager due to the ever changing topographic environment. For example, a landslide in 2010 significantly changed the morphology of the river bed at the confluence of Meager Creek and upper Lillooet River (Guthrie et al., 2012; Roberti et al., 2018), which could affect the propagation of subsequent geophysical flows.

Lidar (Light Detection and ranging) available for the massif of Mount Meager was acquired in summer 2015 (southern half of volcano) and 2016 (northern half of volcano). The resolution of the generated DEM was 1 metre (Roberti et al., 2018). This data

covered the Mount Meager massif as well as a small portion of the upper Lillooet Valley. In total, the flat surface area coverage was 432 $km^2$. While 1 m resolution is advantageous for many purposes - such as analyzing the landscape for landslide scars, evidence of past landslide activity and land instability - numerical models used in this study were unable to process simulations efficiently with high DEM resolution. For efficiency and due to time constraints of running the computer models, the resolution of this DEM was downsampled to a resolution appropriate for the individual numerical model. This will be subsequently indicated as input parameters for each hazard in subsections below. Other DEMs included 20 metre resolution data acquired from Shuttle Radar Topography Mission (SRTM) in order to extend the surface area and capture greater distances outside of the central massif; the total area of that DEM was 4020 $km^2$. This data set will be indicated as an input parameter for each individual model (or individual simulation where applicable).

The numerical models involved in the generation of tephra hazard footprints were independent of DEMs. The presentation of these hazards is provided on a topographical map in order to show the geographical context of the area and extent that these hazards encompass. Tephra transport and tephra fall-out depends on atmospheric conditions rather than topography on a regional scale (Biass et al., 2016; Mastin et al., 2013).

## 2.3. Numerical Models

An aim of this project was to test different numerical models currently available for the simulation of each individual volcanic hazard. This has resulted in use of two numerical model programs for each hazard, each with a different computational approach to the simulation.

The numerical model programs allow for the simulation of hazards with predefined input parameters. Given the lack of geological evidence, using computer software can give an understanding of the potential inundation footprint, timeframe and topographical modifications that may result from the generation of specific hazardous phenomenon following an eruption at Mount Meager. Table 2.2 provides a summary of the numerical models used for each type of hazard. The specific numerical model programs are further discussed in subsequent sections of this chapter.

**Table 2.2 Numerical models chosen for simulating each type of volcanic hazard**

| Hazard type | Numerical model |
|---|---|
| Lahar | LAHARZ |
| | VolcFlow |
| Pyroclastic Density Currents | LAHARZ, proximal hazard tool |
| Volcanic ash | Ash3d (for ashfall & cloud dispersion) |
| | TephraProb (for ashfall) |

### 2.3.1. Pyroclastic Density Current modelling programs and parameters

The numerical modelling method used to simulate pyroclastic debris currents is the ΔH/L energy cone. Ogburn & Calder (2017) completed a study of several popular PDC model methods and their applications for hazard assessments. Other programs investigated include TITAN2D and a recalibrated version of LAHARZ specific to PDC modelling and VolcFlow. The energy cone model is included in the LAHARZ package as the proximal hazard tool; it offers a quick approximation of runout distance. The energy cone method is an empirical model based on statistical analysis that forecasts runout length.

#### *ΔH/L energy cone*

The energy cone method applied to PDC runout forecasting, proposed by Sheridan (1979), incorporates the relationship of the ΔH/L ratio vs. flow volume. The ratio states that ΔH is the fall height of the flow, and L is the runout length. This method depicts the outer extent of PDCs as an energy line (or fully encompassing cone) and incorporates both the dilute and concentrated segments of a pyroclastic flow. The energy cone method is included in LAHARZ software (further explained in section 2.3.2) as a proximal hazard tool, generating the cone over a digital elevation model (Schilling 1998). This parameter refers to the notion that along a slope, a geophysical flow will move due to potential energy which converts to kinetic energy minus friction. The energy cone refers to the area of the slope where frictional loss is balanced by conversion of potential to kinetic energy (Sheridan, 1979). This ratio is equivalent to the basal friction angle (Scheidegger, 1973). This method does not inherently model the surge or dense

basal avalanche component of a PDC as it does not simulate channelization or directionality, it merely covers the interfluves that may potentially be impacted by these flows (Ogburn & Calder, 2017). This model also does not inherently model the timeframe of inundation.

For this project, the values of ΔH/L ratio were determined from designated volumes of input based on ΔH/L vs. volume regressions from FlowDat as compiled and formulated by Ogburn (2016, 2012). Due to the lack of extractable information of multiple PDC events for Mount Meager (from separate eruptions), the regressions were derived from the global FlowDat database using data from over 120 block-and-ash flow type deposits (equation 2.2). The following equations are used to determine the ΔH/L ratio entered into the LAHARZ proximal hazard tool to systematically draw the energy cone:

$$\log(\Delta H/L) = -0.14(V) - 0.97 \quad (2.1)$$

Or

$$\Delta H/L = 0.11(V^{-0.14}) \quad (2.2)$$

The regression coefficient for this dataset is $R^2 = 0.61$.

The FlowDat database includes data from more PDC deposits but the regression equations chosen for this work incorporate only block and ash flow (BAF) data, simulating a dome collapse. This methodology was followed because the only evidence from the last eruption of a PDC deposit was a block and ash flow (Michol et al., 2008; Stewart et al., 2003). The dynamics of a column collapse PDC deposit are not known for Mount Meager. In following this reasoning, guesses do not need to be made for the height at which the collapse would occur, with the ΔH parameter being integral to this method of mapping potential extents of PDC deposits. The initiation points for PDC modelling was generated from the apex of all known volcanic peaks (see green triangles in Figure 2.1).

For this modelling procedure, topography was represented by the same SRTM DEM used for LAHARZ lahar modelling. This DEM dataset was used to model the energy cone for the three governing scenarios, the resolution of this DEM was 20 m.

**Table 2.3 Input parameters for PDC modelling with ΔH/L method**

| Parameter | Scenario 1 | Scenario 2 | Scenario 3 |
|---|---|---|---|
| Volume | $1\times10^5$ m$^3$ | $1\times10^6$ m$^3$ | $1\times10^7$ m$^3$ |
| ΔH/L | 0.4 | 0.3 | 0.2 |

A key limitation of the ΔH/L cone method is that it does not simulate channelization and directionality of flow progress, therefore unrealistically covering all interfluves stemming from the indicated start point (Ogburn & Calder, 2017). For this reason, the area of potential inundation cannot be commented on.

## 2.3.2. Lahar modelling programs and parameters

Two computer modelling packages have been used to simulate possible impact areas of lahars stemming from an eruption from Mount Meager. The motivation behind choosing the two programs, LAHARZ and VolcFlow, aligns with the goals of the overall project of finding user-friendly, open-access programs. LAHARZ is a semi-empirically based model, while VolcFlow is a geophysical-based approach. Other software programs used in the hazard modelling community to model lahar flows include the two-phase shallow layer model TITAN2D (Patra et al., 2005; Williams et al., 2008), hydrodynamics model Delft3D (Carrivick et al., 2009) and FLO-2D (Charbonnier et al., 2018).

Modelling included capturing lahar propagation stemming from key drainage basins of the massif where volcanic deposits are present (Figure 2.1). These specific drainage basins were chosen based on field evidence of volcanic deposits being present, as mapped by Read (1990) and Stasiuk et al. (1996) and informed by basins containing unstable slopes delineated by Roberti et al. (2018). The drainage basins captured in the hazard assessment - including Devastator Creek, Capricorn Creek, Mt. Meager and Job Creek basin - strategically capture drainage from the south, east and north flanks of the complex. Currently, volcanic activity is manifested as a fumarole field within the Job Creek basin. Simulations should cover the pathways of any future flows even if they stem from basins not included by the four chosen ones, the exception being small scale events with inundation limits restricted within the basin in which they are initiated. This logic is followed through for modelling undergone in both LAHARZ and VolcFlow with the motivation for that being twofold – i.e. the four points of initiation

capture the major drainage basins and points of interest surrounding the volcanic massif, and keeping the initiation points the same across both models will allow for appropriate comparison of results. The same drainage basins are used as initiation points for both programs; however, the coordinates for initiation points differ due to input requirements that will be explained further in the next two sections.

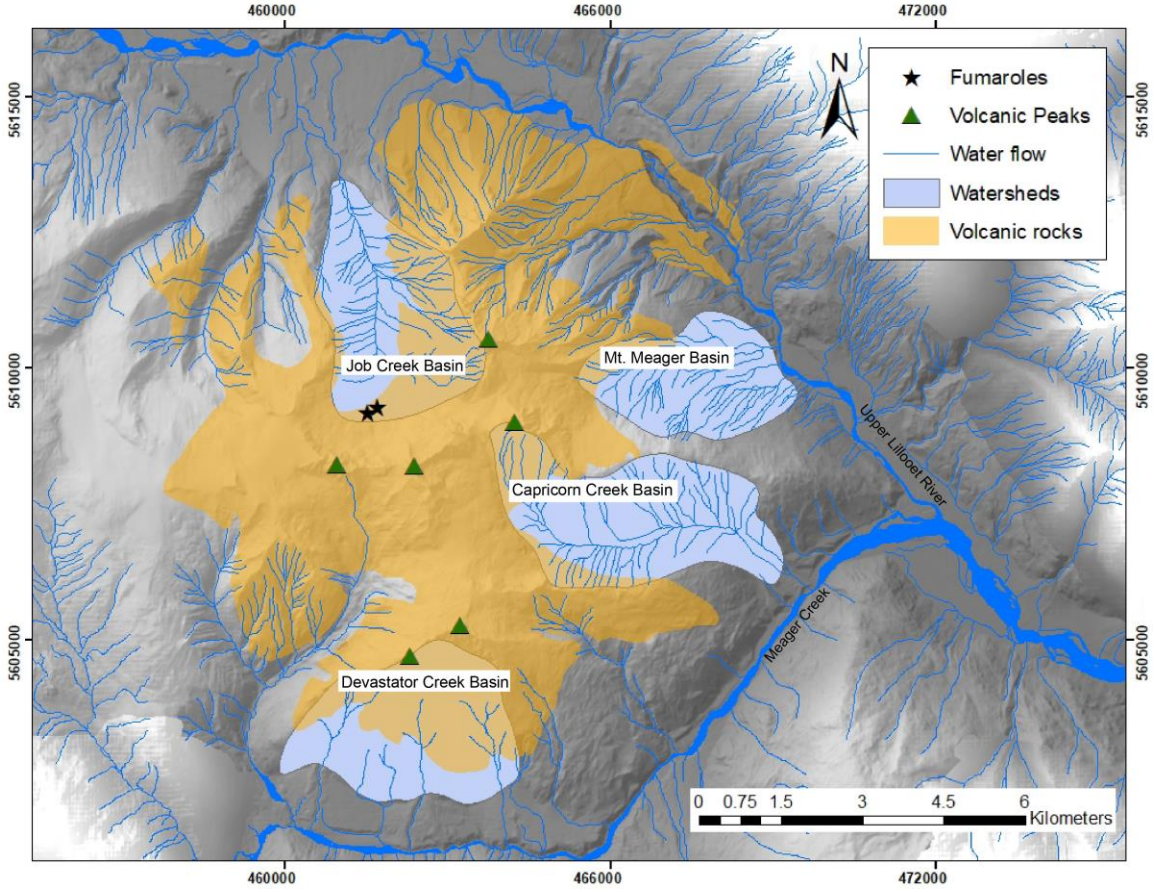


**Figure 2.1 Drainage basins captured by lahar modelling with LAHARZ and VolcFlow, all coordinates UTM Zone 10N, NAD 83.**

### *LAHARZ*

Produced by the United States Geological Survey, LAHARZ offers an automated approach to mapping potential areas of gravitational flow inundation. It was principally designed for lahars (Iverson et al., 1998; Schilling, 1998) but also recalibrated for debris flows and rock avalanches (Griswold & Iverson, 2008), and most recently for PDCs (Widiwijayanti et al., 2009). This is a GIS-based software package that uses predictive equations to calculate inundation limits based on user-specified volumes “filling” a DEM representation of local topography. The program output constructs a nested set of

inundation-hazard zones, with each zone representing the user-specified volume of input (Iverson et al., 1998). LAHARZ is a semi-empirical program based on correlations between lahar deposit volume (V), valley cross sectional area ($A_{cross}$) and planimetric area ($B_{plan}$) (Iverson et al., 1998; Schilling, 1998). The two equations relating these parameters were derived from statistical analysis of multiple lahar paths and assume that the evolving mass moves downstream with constant bulk density, mass and volume; where C = 0.05 and c = 200 are constant calibrated coefficients (Iverson et al., 1998).

$$Across = CV^{\frac{2}{3}}, (2.3)$$

$$Bplan = cV^{\frac{2}{3}}, (2.4)$$

The workflow of LAHARZ requires a multi-step process (Iverson et al., 1998; Schilling, 1998). First, a hydrologic grid based on the DEM is prepared, tracing hydrologic flow lines that join pixels ranging from maximum to minimum. This grid (stream grid) indicates slope directions and the possible stream valleys. Next, a proximal hazard zone is created, which represents the separation between the lahar erosive area and accumulation area. The intersection of this boundary with a hydrologic line will represent the start point of the lahar simulation. The proximal hazard zone is obtained from the ratio of the vertical drop from volcano apex (H) to zone of lahar deposition (L). The next step is to select the initial (and if preferred, final) pixels of the lahar, thus specifying the drainage basins being simulated. Finally, lahar volumes are specified in LAHARZ (up to four volumes) and lahar inundation can be simulated. Full details of the computation procedure are presented by Iverson et al., (1998) and Schilling (1998) explaining the calculations of $A_{cross}$ and $B_{plan}$ within the algorithms supporting LAHARZ. The calculations stop and the simulated lahar-inundation zones are drawn when the recorded planimetric area is ≥ $B_{plan}$, or when the program encounters a user-specified end point or the end of the DEM.

Following initial steps, two different DEMs datasets were selected to provide a DEM representation of topography. The LiDAR dataset was used for all three governing scenarios and was downsampled to 5 metre resolution because LAHARZ cannot run with a DEM less than 5 m resolution (Muñoz-Salinas et al., 2009). A second DEM was derived from interferometry from the Shuttle Radar Topography Mission (SRTM). This DEM provided a coarser resolution of 20m. This was used on the three governing

scenarios and to test a fourth scenario with the purpose of selecting a volume capable of reaching the town of Pemberton, 65 km downstream of the massif. This coarser resolution DEM was chosen partly due to access to topography coverage reaching a distal endpoint and to test the performance of LAHARZ on a reduced resolution.

A value of 0.4 was used for the $\Delta H/L$ ratio. This value produced a boundary line across all drainages that roughly corresponds with the mouth of each drainage, which in this case is assumed as the point at which lahar deposition starts. Initiation points were informed by the results of the algorithm selecting start points of stream flow intersected by the proximal hazard boundary. Exact coordinates corresponding to the four drainage basins are listed below (Table 2.4).

**Table 2.4 Coordinates of initiation points for lahar simulations in four drainage basins on Mount Meager for LAHARZ. Coordinates in UTM Zone 10**

| Drainage Basin | Coordinates (m) | Elevation (m) |
|---|---|---|
| Devastation creek | 464,165.279 5,601,196.996 | 686 |
| Job Creek | 460,779.893 5,614,204.007 | 809 |
| Mt. Meager | 469,179.724 5,609,902.275 | 440 |
| Capricorn Creek | 469,052.454 5,606,262.348 | 584 |

The three governing scenarios were followed for deciding the volumes to simulate across all basin simulations. A fourth scenario was added in order to model a flow reaching Pemberton. Furthermore, previous LAHARZ modelling for simulating debris flows from Mount Meager had been conducted by Simpson et al. (2006), which also acted as a guide for deciding upon volume estimates for model inputs. Previous modelling had volumes of $1\times10^6$ $m^3$, $1\times10^7$ $m^3$, $1\times10^8$ $m^3$ and $1\times10^9$ $m^3$. Moreover, a lahar deposit from the 2360 cal yr B.P. eruption has been estimated as a volume of $5\times10^7$ $m^3$ by Andrews et al. (2014), although this has been interpreted as a possible outburst flood, therefore making it a secondary lahar deposit. The volume increments are consistent with the logarithmic scaling of LAHARZ (Iverson et al., 1998), other than the large scale scenario. Table 2.5 lists the volumes chosen for each scenario and includes a real world example of an analogue volcanic event with similar volumes.

**Table 2.5 Volume constraints for lahar simulation modelling with LAHARZ**

| Scenario | Volume ($m^3$) | Example |
|---|---|---|
| 1 (VEI ≤ 2) | $1\times10^6$ | Cotopaxi 2015, ~ 50,000 $m^3$ (Global Volcanism Program, 2016) |
| 2 (VEI 3) | $1\times10^7$ | Nevado del Ruiz 1985, 1.6 x $10^7$ $m^3$ (Pierson et al., 1990) |
| 3 (VEI 4-5) | $1x10^8$ | Mt. St. Helens 1980, two lahar flows, each ~$10^7$ $m^3$ (Iverson, 1997) |
| Large volume | $5\times10^9$ | Osceola, Mount Rainier, 5000 B.P., 4.0 x $10^9$ $m^3$ (Vallance & Scott, 1997) |

The output nested inundation footprints often exhibit unrealistic lateral inundation areas in the form of ragged edges (Muñoz-Salinas et al., 2009). Theoretically, these ragged edges should be reduced with higher resolution DEMs which accurately depict channel cross sections, an important parameter calculated within the LAHARZ algorithm. However, Munoz-Salinas et al. (2009), showed that this was not the case due to the nature of the calculations filling each cross section and maximizing the planimetric area until a new stream grid cell is processed. The final mapped outputs of this study display the boundaries of lahar inundation as smooth lines for display purposes. In the case of hazard mapping at Mount Meager, a few metres of inaccuracy as a result of smoothing the boundaries should not impede future interpretations and hazard management due to the remoteness of the area. However, a further limitation of the model methodology dictates that the calculated planimetric area of inundation will be the same for all runout pathways describing one scenario.

Another limitation of this model is the assumption that the mass moves as bulk density, mass and volume. This does not account for lahar behaviour of bulking and debulking (Vallance, 2000; Fagents & Baloga, 2006), which would have implications for the total runout of the flow.

### *VolcFlow*

VolcFlow is a geophysical model, run in Matlab, developed by the Laboratoire Magmas et Volcans, and designed to simulate gravitational flows capturing the mass flow behaviour in time and space (Kelfoun & Vallejo Vargas, 2016). It has been applied to debris flows, dilute and concentrated components of pyroclastic flows, landslide derived tsunamis, lava flows (Kelfoun & Vallejo Vargas, 2016), and lahars (Gueugneau, 2014). Flows are modelled using depth-averaged equations of mass and momentum

conservation on a topography linked coordinate system where x and y parallel the local topography. VolcFlow differs from other mass-flow numerical models by providing the opportunity to solve for several types of rheological equations (e.g., frictional, viscous, or plastic) (Kelfoun & Vallejo Vargas, 2015; Ogburn & Calder, 2017). This feature is manifested by the choice of the retarding stress parameter, which is user-defined by manipulating the value of cohesion. Other input parameters also manipulate the physical flow characteristics including: internal and basal friction angle, viscosity and a dimensionless parameter that defines turbulent or collisional stress. The flow is simulated with the position, thickness and velocity calculated at each time step for each pixel of the grid. VolcFlow records a movie of the simulated flow, offering observational insight of the dynamics of the flow. Other outputs offered or easily extractable from the software include deposit thickness, final volume and maximum velocity. Several versions of the code now exist, including a single-layer and two-layer model. Due to access and for simplification purposes, the single-layer model has been used for the lahar modelling of this project. The code and more information can be found on the VolcFlow webpage (http://lmv.univ-bpclermont.fr/volcflow/).

The DEM used for lahar simulations in VolcFlow was the LiDAR. The resolution of the DEM can be adjusted and downsampled within the program; coarser resolution shortens the runtime of the model calculations. For this reason, coarse resolutions (60 m – 100 m) were chosen to set up the simulations and test efficiency. The resolution used for the generation of each final result simulation is included in Chapter 3 (Table 3.3).

While the four general initiation localities are kept the same for lahar modelling in LAHARZ and VolcFlow, the location on slope differs. Locations chosen for VolcFlow involve points mostly starting midway down the slope. In the case of Job Creek basin, this location is roughly placed at the terminus of the glacier as of 2016 observations. For the other three locations, the start points are located at the boundary of the volcanic massif and its underlying basement rock (which is exposed as described in Chapter 1). The equations behind VolcFlow solve for momentum and mass balance, therefore placing the locations at these points captures both the failure of dominantly volcanic material and the momentum achieved on each of the slopes. Furthermore, the shape of both the initiation point and the location that acts as the discharge point can be manipulated in the software. However, for the sake of timing, a particular shape was not created, and thus discharge is modelled as a point source. This is therefore a

simplification of lahar flow rheology and does not account for the bulking and debulking behaviour of lahar flows. The particular locations are noted in Table 2.6 below. For consistency purposes, the coordinates are presented as UTM coordinates although these points are entered in the program as x and y coordinates based on the dimensions of the topographic template used in VolcFlow by the user.

**Table 2.6 Coordinates of initiation points for lahar simulations in four drainage basins on Mount Meager for VolcFlow. Coordinates in UTM Zone 10**

| Drainage basin | Coordinates (m) | Elevation (m) |
|---|---|---|
| Devastation Creek | 462,479.297 5,603,740.798 | 1560 |
| Capricorn Creek | 465,372.786 5,606,721.071 | 1230 |
| Mt. Meager | 466,089.279 5,609,843.160 | 1450 |
| Job Creek | 461,437.895 5,611,956.127 | 1075 |

The physical input parameters for Mount Meager lahar flow modelling with VolcFlow were informed by two examples of previous work done to model lahars using the code, those being Gueugneau (2014) efforts modelling the Armero disaster from Nevado del Ruiz eruption 1985 and the reconstruction of lahars from the 1698 eruption of Carihuairazo (Vasconez et al., 2017).

The lahar is simulated as draining from the point source as a single pulse, by signaling the program to add mass at the designated discharge rate until total initial volume has been reached. The simulation is stopped when maximum velocity is consistently low (below 3 m/s) or had read out low values as the program was running. The maximum velocity parameter reported as the program is running represents the maximum velocity at the time stamp within the flow, and not necessarily the toe of the flow. The input parameters remain the same for each drainage basin and differ only by initial volume for each scenario. Table 2.7 presents the input parameters chosen for VolcFlow lahar simulations. Only governing scenarios 2 and 3 were simulated in VolcFlow. Scenario 1 yielded insignificant runout results.

**Table 2.7 Input parameters for lahar simulation modelling with VolcFlow for two scenarios**

| Parameters | Scenario 2 | Scenario 3 |
|---|---|---|
| Coefficient of Turbulence | 0.01 dimensionless | |
| Viscosity | 0.01 Pa.s | |
| Density | 1600 kg/m$^3$ | |
| Cohesion | 500 Pa | |
| Internal and basal friction angles | 0° | |
| Maximum time | 3 hours | 4 hours |
| Initial volume | 1×10$^7$ m$^3$ | 1×10$^8$ m$^3$ |
| Discharge rate | 47000 m$^3$/s | |

With this iteration of modelling, the physical parameters of the flow remained constant, which is a simplification of the lahar flow dynamics as it does not account for bulking and debulking behaviour. In particular, the interaction with additional fluid components is not included, such as the natural river discharge are present in the area. This is an additional step that can be incorporated into the model and would likely facilitate a longer run-out path and higher flow velocity.

## 2.3.3. Volcanic ash modelling and parameters

Two volcanic ash dispersal and transport models (VADTM) were used to address the tephra hazard, USGS Ash3d program and the TephraProb package. There are numerous VATDM in use by volcanic ash scientists and Volcanic Ash Advisory Centres (VAACs) around the world - examples being FALL3D, HYSPLIT (Bonadonna et al., 2012). Ash3d and TephraProb were chosen for being freely available, and for their ease of access and use. Ash3d produces files depicting both the propagation of the ash cloud hazard (outlying spatial and temporal propagation) and the depositional footprint of the ash. TephraProb models the deposition footprint and incorporates built in analysis of that footprint. The output results from TephraProb are also probabilistic in nature due to the capabilities of the software. The web interface version of Ash3d used for this project is not inherently probabilistic.

### *Ash3d*

Ash3d is a finite-volume, eulerian model produced and administered by the United States Geological Survey (Schwaiger et al., 2012), that forecasts airborne volcanic ash concentration and tephra deposition. It was developed in response to the need for time-sensitive tephra modelling after the 2010 eruption of Eyjafjallajökull volcano in Iceland. It has demonstrated success in recreating tephra transport and deposition of the 2009 eruption of Mt. Redoubt (Mastin et al., 2013a) and is being used for risk assessments for Hekla Volcano (Falkenstrøm et al., 2014) and Taupo Volcano (Barker et al., 2019).

Tephra transport is simulated in a three-dimensional domain of cells by calculating the flux of tephra particles of all sizes through cell walls. The simulation begins with tephra being injected at a constant rate into the column of cells above the volcano's coordinates. Numerical modelling is achieved with calculations being made for time dependent, downwind advection by wind transport, turbulent diffusion, fall velocity and tephra source parameters. The overarching formula for this is:

$$\frac{\partial q}{\partial t} + \nabla\big((u + v_s)q\big) - \nabla(K\nabla q) = S, \text{ (2.5)}$$

Where q is the concentration of a particle grain size, u is the velocity field, $v_s$ is the settling velocity of the ash particles, S is the rate of mass influx per volume per unit time into the plume and K is the diffusivity (Schwaiger et al., 2012).

The advection term is solved using the Donor Cell Upwind method. The diffusion term is calculated at the end of each time step; it is a function of local meteorological conditions but default settings have set K=0 (Mastin et al., 2013b). Deposition is achieved once tephra falls through the cell boundary that represents the ground surface.

Ash3d is hosted by the USGS and accessed through a web interface. The wind files are obtained from the National Oceanic and Atmospheric Administration (NOAA) Global Forecast System numerical weather prediction model, downloaded four times daily at 000,0600,1200 and 1800 UTC (Mastin et al., 2013b). Although Ash3d is capable of allowing several user specified parameters (such as diffusivity, multiple eruptive pulses and multiple grain sizes), the web interface accessed for this project only included critical parameters for modelling. Those included the volcano name, plume

height, eruption start time, duration, erupted volume and hours of simulation. Model resolution is adjusted to obtain outputs within 10 minutes or less (Schwaiger et al., 2012).

Continuing with the three governing scenarios, input parameters were chosen based on appropriate eruptive parameters for each size of eruption, with consideration of the three VEI values. Adjustable parameters are stated below (Table 2.8).

**Table 2.8 Input parameters for modelling ash hazards with Ash3d**

| Parameter | Scenario 1 | Scenario 2 | Scenario 3 |
|---|---|---|---|
| Volcano Site | Latitude: 50.633, Longitude: -123.500, Elevation: 2680.106 m | | |
| Plume height | 4.77 km a.s.l. | 27 km a.s.l. | 23.68 km a.s.l. |
| Simulation Duration | 24.00 hours | 24.00 hours | 24.00 hours |
| Eruption Duration | 1.00 hour | 45 minutes | 9.00 hours |
| Erupted Volume | 0.0001 $km^3$ | 0.0390 $km^3$ | 0.2420 $km^3$ |

A number of parameters are set to default values explained and defined in the user manual for Ash3d (Mastin et al., 2013b), stated herein. For airborne ash simulations, a single fine grain size (0.01 mm) with negligible settling velocity is considered. Also, in airborne simulations, only 5 percent of the total erupted volume is considered for cloud propagation. Ash deposition simulations calculate the deposition of seven grain size bins (4, 2, 1, 0.5, 0.25, 0.125 and 0.625 mm). The calculation of deposition is only possible within a few hundred kilometres beyond the volcano. The methodology of completing this component of hazard modelling was carried out by logging into the web interface nearly daily for a year, capturing near real-time wind conditions for that duration.

This is a quasi-probabilistic approach due to the nature of parameters chosen and analyzed in this method. The only parameters that were varied across the time-span of running the scenarios were the atmospheric wind conditions. All eruption parameters remained the same for the entire duration of running this project.

For each scenario, deposition data was organized by resulting deposit thickness values. Data was compiled in ArcGIS to produce a probabilistic analysis, assessing tephra accumulation (deposition) exceeding 0.9 mm and 9.9 mm. These values were

chosen in order to process Ash3d data similarly to TephraProb outputs, which, for this project assess the probability of tephra accumulation ≥ 1 mm, 10 mm and 100 mm.

Limitations of this model include that deposition is simulated by sedimentation, not accounting for outlying considerations (such as rain induced deposition and dynamic localized weather conditions). Another limitation of this iteration of the model is that the eruption event is simulated as a single pulse event where ash is injected into the column at a constant rate and that grain size distribution also remains constant, throughout all elevations of the model.

### *TephraProb*

The basic computation behind TephraProb, based on the Tephra2 model (Bonadonna et al., 2005), uses the advection-diffusion equation to determine the tephra mass accumulation given varying eruption scenarios differing by eruptive and wind conditions. The purpose of this package is to produce a probabilistic hazard assessment for tephra fallout (Biass et al., 2016b). TephraProb incorporates a total grain-size distribution (TGSD) file to account for particle aggregation processes. During computation, the model samples input parameters for each run (making it a probabilistic assessment). For this project, the sampling of plume height is logarithmic and both plume height and TGSD integration steps are set to 50. Within the scope of this project, only a single eruption scenario was investigated (the program has the capability to test multiple eruption scenarios). Choosing the single eruption scenario fixes input values to constrain upper limit parameters over variable wind conditions. The eruption range scenario randomly samples a range of input values and stochastically samples the wind conditions at each run (Bonadonna et al., 2005). Wind data used for the TephraProb analysis was obtained from NOAA Reanalysis 1 dataset, which involves wind conditions on one 2.5° resolution grid at 17 height levels. This dataset provides 4 wind profiles per day for the years chosen, which for this project involved wind profiles from 2006 to 2011. A user manual (Biass et al., 2016a) is available, provided by the developers of TephraProb which defines each parameter included in the program.

TephraProb presents the results using three types of outputs: probability maps, hazard curves and probabilistic isomass maps. These three visual outputs display the probability of exceeding a given tephra accumulation accounting for geographic location, tephra accumulation threshold and its associated exceedance probability. The

thresholds of concern that have been applied to data produced for the Mount Meager simulations are: 1 kg/m$^2$ to account for air quality restrictions (personal respiratory distress, and air traffic), 10 kg/m$^2$ to account for electric failure, minor roof damage, and crop damage and 100 kg/m$^2$ which can lead to roof/building damage (Biass et al., 2017).

In addition to the guiding principles of the three governing scenarios, an additional scenario is presented for work done to recreate the 2360 cal yr BP eruption in Appendix D. In all cases other than scenario 1, different wind direction restrictions were tested; this was done in order to analyze impacts for pre-specified regions of interest (based on populous regions of British Columbia and areas of economic importance) and the effects of tephra dispersal given specified wind restrictions, the specifications and results are included in Appendix D.

All parameters are taken from reported average values in the literature. This includes the aggregation coefficient, maximum aggregation diameter, diffusion coefficient and total grainsize distribution (Biass et al., 2016b), and fall time threshold (Bonadonna et al., 2005; Biass et al., 2016b). Lithic and pumice density are based on density ranges reported by (Scollo et al., 2008).

**Table 2.9 TephraProb input parameters for the three governing scenarios**

| Parameter | Scenario 1 | Scenario 2 | Scenario 3 |
|---|---|---|---|
| VEI | < 3 | 3-4 | > 5 |
| Grid resolution (m) | 1000 | 2500 | 2500 |
| Plume height (km a.s.l.) | 10-15 | 15-20 | 20-40 |
| Erupted Mass (kg) | 1 x $10^8$ – 1x $10^{11}$ | 1 x $10^9$ – 1 x $10^{12}$ | 5 x $10^{11}$ - 5 x $10^{13}$ |
| TGSD range (Φ) | -6 – 8 | -5 – 9 | -4 – 10 |
| Median diameter (Φ) | -3 – 0 | -1 – 2 | 0 – 4 |
| Sorting (Φ) | 1 – 2 | 2.5 | 3 – 4 |
| Aggregation coefficient | 0.3-0.7 | 0.3-0.7 | 0.3-0.7 |
| Lithic density (km/m3) | 2600 | 2400 | 2200 |
| Pumice density (kg/m3) | 1000 | 700 | 500 |
| Diffusion coefficient (m/s2) | 10 | 500 | 2500 |
| Fall-time threshold (s) | 50 | 500 | 6000 |
| Eruption duration (hours) | 2-4 | 4-10 | 12-120 |

Numerical modelling within TephraProb allows for accurate depictions of tephra deposition up to a couple of hundred kilometres beyond the vent location (Biass et al., 2016a), which constrains the total spatial domain that can be accounted for. This program is limited in validity of the outcome to only model tephra fallout to a few hundred kilometres around the vent due to the wind profile being homogenous horizontally and temporally (but vertically stratified).

# Chapter 3.

# Numerical Model Results

Model outputs vary depending on the specific hazards and specific capabilities of the software used. In this chapter the results of each numerically modelled volcanic hazard are presented. This includes a collection of maps and tables detailing inundation areas, propagation time-scales and deposit specifications as provided by the individual programs.

## 3.1. Pyroclastic Density Current Hazard Zones

### 3.1.1. ΔH/L energy cone

Modelling using the LAHARZ proximal hazard tool was used to delineate the extent of pyroclastic runout length expected for the three governing scenarios. Figure 3.1 presents the output from this modelling, combining the results from all start points into a single runout profile across the three scenarios.

Successive boundary lines represent the maximum runout length of the simulated pyroclastic flow scenario with the areal extent shown as shaded relief (Figure 3.1). No comment is made regarding the total area covered by the simulation because this method does not model channelization or directionality and therefore portrays unrealistic coverage of the flow, both in terms of the basal avalanche component and surge.

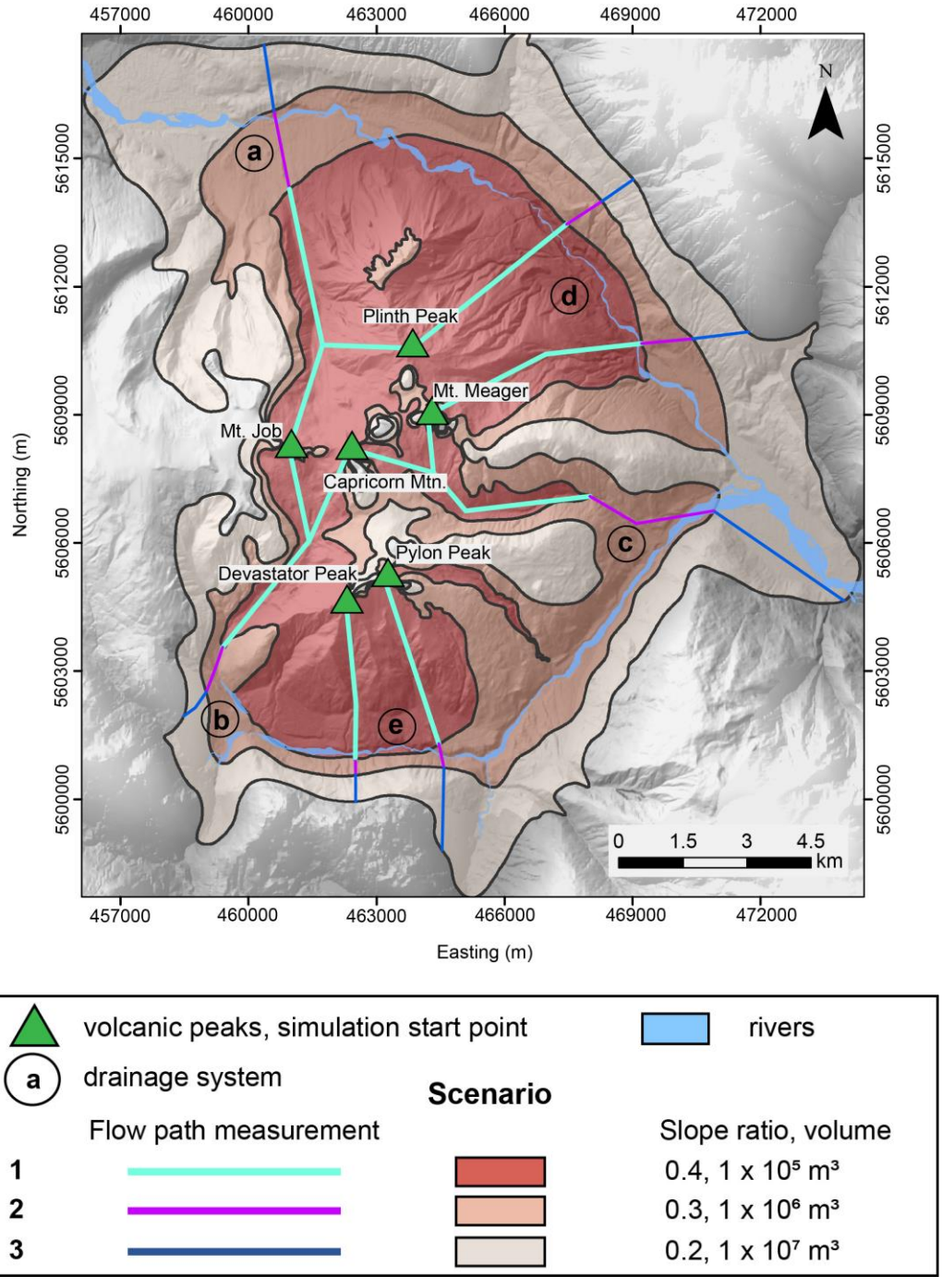


**Figure 3.1** **Combined results of PDC scenarios modelled with the ΔH/L method. The shaded relief displays the possible area that could be impacted from PDC events given the input parameters selected for a dome collapse PDC event. The coloured lines (turquoise for scenario 1, pink for scenario 2 and blue for scenario 3) represent the line where the runout length extent measurement was made, based on planar measurements. All coordinates are in UTM Zone 10 NAD 83.**

Table 3.1 shows an amalgamation of the individual runout lengths measured from the apex of volcanic peaks - that served as the initiation points - to the corresponding boundary line (Figure 3.1). Individual simulations for each volcanic peak treated as a separate entity are presented in Appendix B, along with runout measurements for each scenario. A letter code identifies drainage systems that the simulations indicate could be impacted by PDCs (Figure 3.1).

**Table 3.1 Runout lengths (km) from the combined simulation of PDC initiation at all known volcanic peaks of the massif**

| Drainage system | Scenario 1 | Scenario 2 | Scenario 3 |
|---|---|---|---|
| *Mt. Job* | | | |
| a | 6.2 | 8.1 | 9.6 |
| b | 5.4 | 6.5 | 7.3 |
| *Plinth Peak* | | | |
| a | 5.6 | 7.5 | 9.0 |
| d | 4.7 | 5.6 | 6.5 |
| *Mt. Meager* | | | |
| d | 5.3 | 6.5 | 7.7 |
| c | 5.3 | 8.4 | 12.2 |
| *Capricorn Mountain* | | | |
| c | 6.0 | 9.1 | 12.8 |
| b | 5.5 | 6.6 | 7.4 |
| *Pylon Peak* | | | |
| e | 4.0 | 4.5 | 6.5 |
| *Devastator Peak* | | | |
| e | 3.5 | 4.0 | 4.6 |

The simulated runout lengths vary from 3.5 km – 6.2 km with scenario 1 parameters, 4.0 km – 9.1 km with scenario 2 parameters and 4.6 km – 12.8 km with scenario 3 parameters. Scenario 1 parameters show Meager Creek being inundated from a PDC stemming from Devastator Peak, and Lillooet River inundated from Plinth Peak and Mt. Meager PDC's. Both Meager Creek and Lillooet River are subsequently simulated to be inundated from a PDC stemming from any volcanic apex given scenario 2 and 3 parameters. Based on the volcanic peaks used as starting points, the PDC

hazard does not encompass the entire massif - the western edge is absent of inundation from this hazard.

## 3.2. Lahar Inundation

### 3.2.1. LAHARZ

The potential lahar inundation zones are presented in Figure 3.2 as generated by LAHARZ. This includes the three governing scenarios based on volumes of lahar flow in addition to the fourth scenario, intended to identify the flow volume required to reach the village of Pemberton, the nearest population centre to Mount Meager. Each lahar scenario presented on the map represents the merged volume using a tool provided by the LAHARZ software. The simulated flows are intended to represent primary flow hazards and are considered as single pulse events (Schilling, 1998).

Table 3.2 lists the individual results of each scenario from the four separate points of origin. Runout length includes the length from point of origin to the end of the modelled flow (horizontal planar distance). Inundation area includes total planimetric area covered by the separate flow scenario. The area was calculated from unedited shapefiles generated in LAHARZ, which include unrealistic jagged edges. Refer to Appendix A for individual simulated flows that have not been smoothed. For presentation purposes, the “jagged edges” have been smoothed in subsequent maps.

**Table 3.2 Summary of quantitative output values as a result of modelling the lahar hazard with LAHARZ for three governing scenarios of eruptions. Results from modelling a fourth, additional scenario are included, which simulates the inundation of Pemberton, the closest population center downstream of Mount Meager**

| | Scenario 1 | Scenario 2 | Scenario 3 | Scenario 4 |
|---|---|---|---|---|
| | | | | |
| Source (Lat, Lon, Elev, m) | Devastator Peak drainage basin (464,165.279 5,601,196.996, 686) | | | |
| Run out length (km) | 11.5 | 20.1 | 39.9 | 77.9 |
| Inundation area ($km^2$) | 2 | 9 | 43 | 126 |
| | | | | |
| Source (Lat, Lon, Elev m) | Job Creek drainage basin (460,779.893 5,614,204.007, 809) | | | |
| Run out length (km) | 9.6 | 21.5 | 40.6 | 76.8 |
| Inundation area ($km^2$) | 2 | 9 | 43 | 126 |
| | | | | |
| Source (Lat, Lon, Elev m) | Mt. Meager drainage basin (469,179.724 5,609,902.275, 440) | | | |
| Run out length (km) | 7.6 | 14.5 | 34.4 | 72.9 |
| Inundation area ($km^2$) | 2 | 9 | 43 | 126 |
| | | | | |
| Source (Lat, Lon, Elev m) | Capricorn Creek drainage basin (469,052.454 5,606,262.348, 584) | | | |
| Runout length (km) | 6.6 | 13.4 | 33.4 | 72.2 |
| Inundation area ($km^2$) | 2 | 9 | 43 | 126 |

The outputs for runout length vary while inundation area does not. This is because operationally, the planimetric area is pre-determined based on the scaling arguments of the program LAHARZ. The volume parameter remains the same across all scenarios and therefore, the planimetric area will be the same calculated value for all equivalent scenarios. The program sums the cumulative planimetric area (equation 2.4) until the total inundation area ($B_{plan}$) is reached, finishes filling the DEM and draws the lahar inundation hazard zone (Iverson et al., 1998; Schilling, 1998).

Outputs from LAHARZ provide insight into the inundation footprint. LAHARZ does not inherently model flow velocity, time frame of inundation or deposit thickness, which are key factors that hazard management personnel (e.g., BC Emergency Management) have expressed interest in.

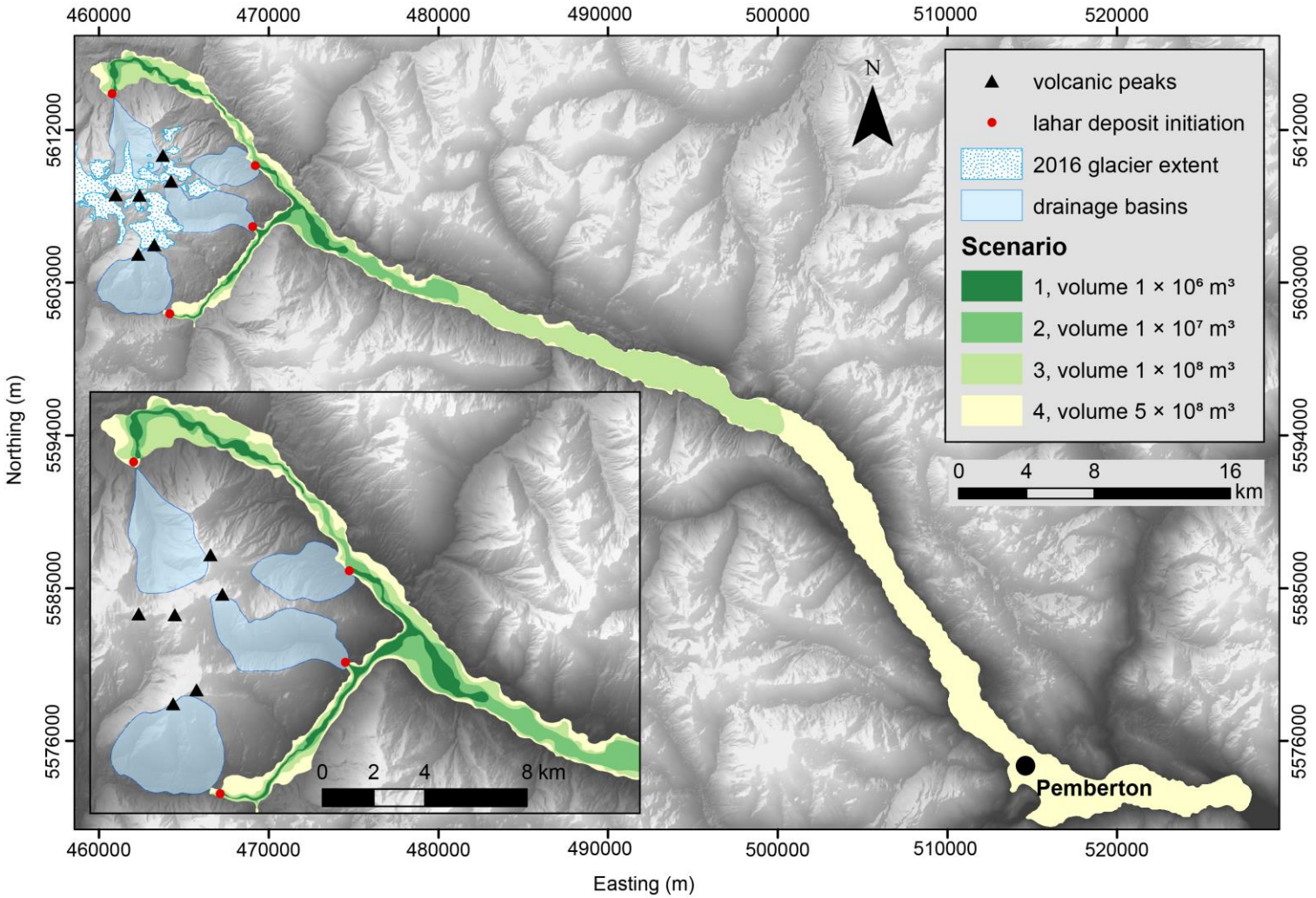


**Figure 3.2** **Scenario-based lahar flow hazard map modelled by LAHARZ. The spatial runout is presented for four scenarios, differentiated by flow volume input. Scenario's 1-3 represent the governing explosive eruption scenarios for a future eruption from Mount Meager. Scenario 4 models the flow volume required to inundate Pemberton, the closest downstream population centre from the volcano. The red dots indicate the start points entered in LAHARZ as the points where erosion ends and lahar deposition begins. All coordinates are in UTM Zone 10N, NAD 83.**

The length of single-event lahar flows are predicted as: 6.6 km – 11.5 km (scenario 1), 13.4 km – 21.5 km (scenario 2), and 33.4 km – 40.6 km (scenario 3). All simulated flows paths are directed towards terrain of lower topography, all eventually reaching Lillooet River, either directly (Job Creek and Mt. Meager flows) or indirectly (Devastator Peak and Capricorn Creek flows inundate Meager Creek first before entering Lillooet River).The fourth scenario simulates a lahar flow with a volume of $5 \times 10^8$ $m^3$ capable of inundating the town of Pemberton and beyond (a total runout length of 72.2 km to 77.9 km). This lahar flow follows the Lillooet River valley past Pemberton Meadows, Pemberton and reaching the mouth of Lillooet Lake, covering a total inundation area of 126 $km^2$.

### 3.2.2. VolcFlow

Modelling performed with VolcFlow has been synthesized with results subsequently presented on the DEM covering the Mount Meager Volcanic Complex in figures 3.2 to 3.4 for scenario 2 and 3.5 to 3.7 for scenario 3. A description of the results for each simulation, mainly focusing on the distribution of thickness values, is included. The average value of thickness is reported along with the standard deviation from the dataset of each simulation. This standard deviation, representing uncertainty of the average thickness value obtained for each flow simulation was calculated with a statistical analysis tool in QGIS (3.12.3). Table 3.3 includes information about the DEM resolution that each simulation was run with during the modelling stage, but for visual consistency, the figures are presented with the resulting flow overlain on the 5 m resolution DEM.

The aim of these simulations was to model the different conditions based on flow volume, the difference being $1 \times 10^7$ $m^3$ for scenario 2 and $1 \times 10^8$ $m^3$ for scenario 3. This was achieved in all cases but the values of volume output computed by the simulation are included in Table 3.3.

Total length and inundation area were measured after the simulation, mapping the point coordinates representing the final footprint of the simulated flow in ArcGIS. The resolution of these measurements are, therefore, consistent with the DEM resolution with which they were modelled. Total length was obtained using the planar length measurement tool in ArcGIS, measuring the length from the point of first simulated

deposition to furthest extent of flow deposition along the central axis of the flow. Inundation area represents the planimetric area covered by flow inundation. While total simulated time is included in the summary table, additional time stamps are indicated on the figures below for each individual simulation that report the timeframe of flow propagation at different stages of the lahar flow. The timeframe is an important parameter for hazard management that varies across the total flow propagation and depends on terrain slope and valley confinement. Additionally, elapsed computational run time (desktop computer) is included in the summary table.

**Table 3.3 Results from lahar simulation performed in VolcFlow**

| Basin | Devastation Creek | | Capricorn Creek | | Mt. Meager | | Job Creek | |
|---|---|---|---|---|---|---|---|---|
| Scenario | 2 | 3 | 2 | 3 | 2 | 3 | 2 | 3 |
| DEM resolution (m) | 20 | 60 | 20 | 20 | 40 | 20 | 20 | 100 |
| Max velocity (m/s) | 1.69 | 2.16 | 2.7 | 5.71 | 2.67 | 2.30 | 8.21 | 10.75 |
| Deposited volume ($10^7$ $m^3$) | 1.00 | 10.00 | 1.00 | 10.00 | 1.01 | 10.00 | 1.00 | 10.00 |
| Total length (km) | 18.2 | 34.9 | 11.57 | 27.8 | 11.72 | 29.15 | 17.9 | 35 |
| Inundation area ($km^2$) | 6.73 | 26.38 | 6.11 | 24.8 | 4.74 | 20.67 | 6.8 | 22.37 |
| Simulated time (hours) | 4 | 6 | 0.75 | 2 | 1.5 | 2.75 | 4 | 6 |
| Elapsed time computational | 6 hrs | 50 min | 1.6 hrs | 11 hrs | 29 min | 11 hrs | 14 hrs | 28 min |

The average value of thickness for a scenario 2 lahar flow stemming from Capricorn Creek drainage basin is 1.64 m ± 1.17 m (Figure 3.3). Areas of thickness reaching 3 m to 5 metres are concentrated in the backsplash section directed west of the confluence of Meager Creek and Capricorn Creek and the end section of the flow upon entry into Lillooet River. There are also small segments of thickness ranging from 4 m to 9 metres along Capricorn Creek (with one measurement of 15.9 metres in that section as well).

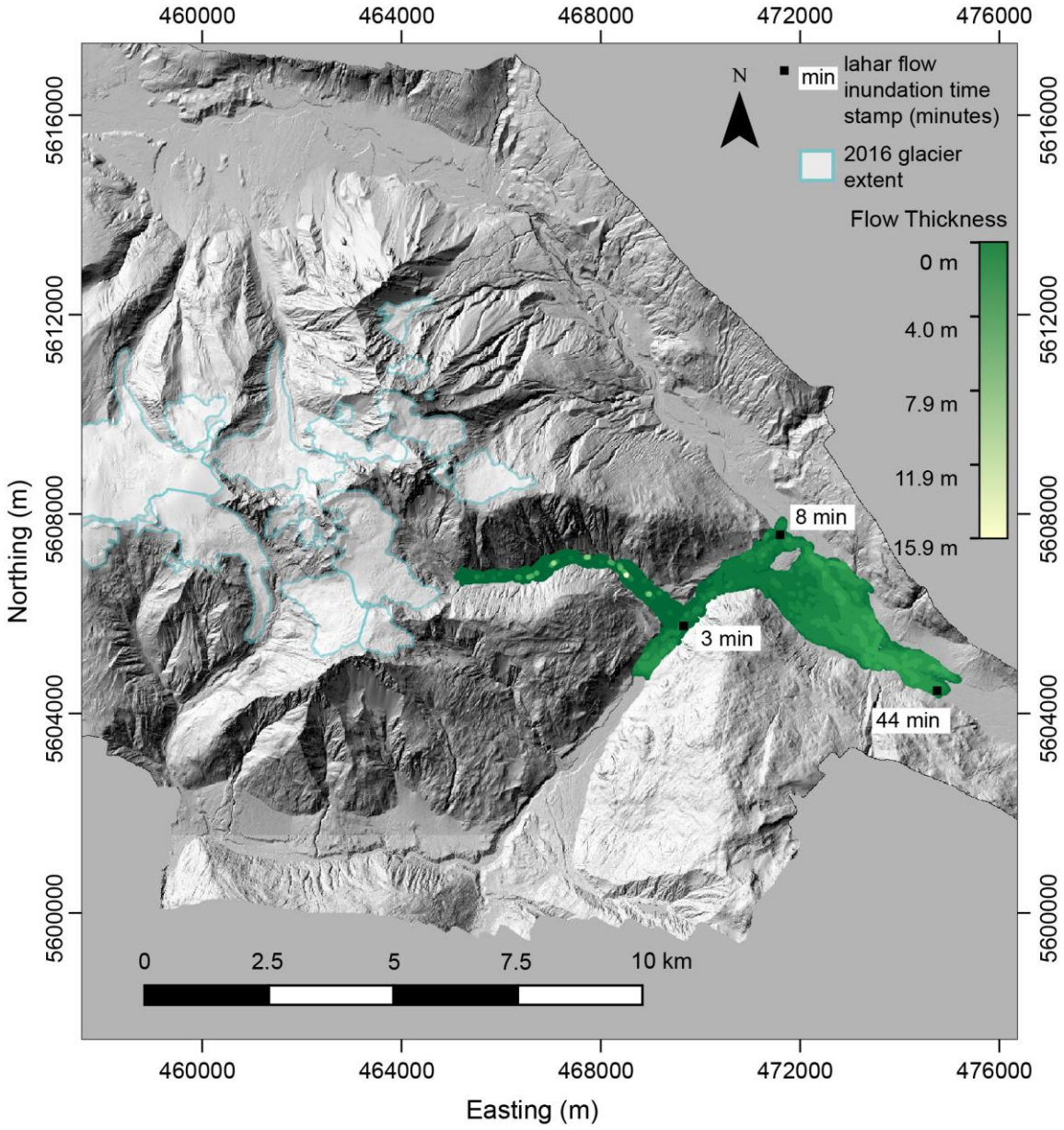


**Figure 3.3 Scenario 2 lahar inundation area and thickness stemming from Capricorn Creek drainage basin modelled in VolcFlow. Time stamps (in minutes) are approximate. All coordinates are in UTM Zone 10, NAD 83.**

The average value of thickness for a scenario 2 lahar flow initiated from Devastation Peak drainage basin is 1.47 m ± 1.17 m (Figure 3.4). Concentrated areas of thickness ranging from 3 m to 5 metres are simulated at the confluence of Meager Creek and Lillooet River extending to the toe of the simulated deposit as well as a small section in Meager Creek to the west of the confluence with Capricorn Creek. A few values of thickness ranging from 5 m to 7 m and a point of 13 m calculated thickness are

simulated within the area of the fan created at the entrance of the flow into Meager Creek, although the dominating value of thickness for this fan is below 1 m thickness.

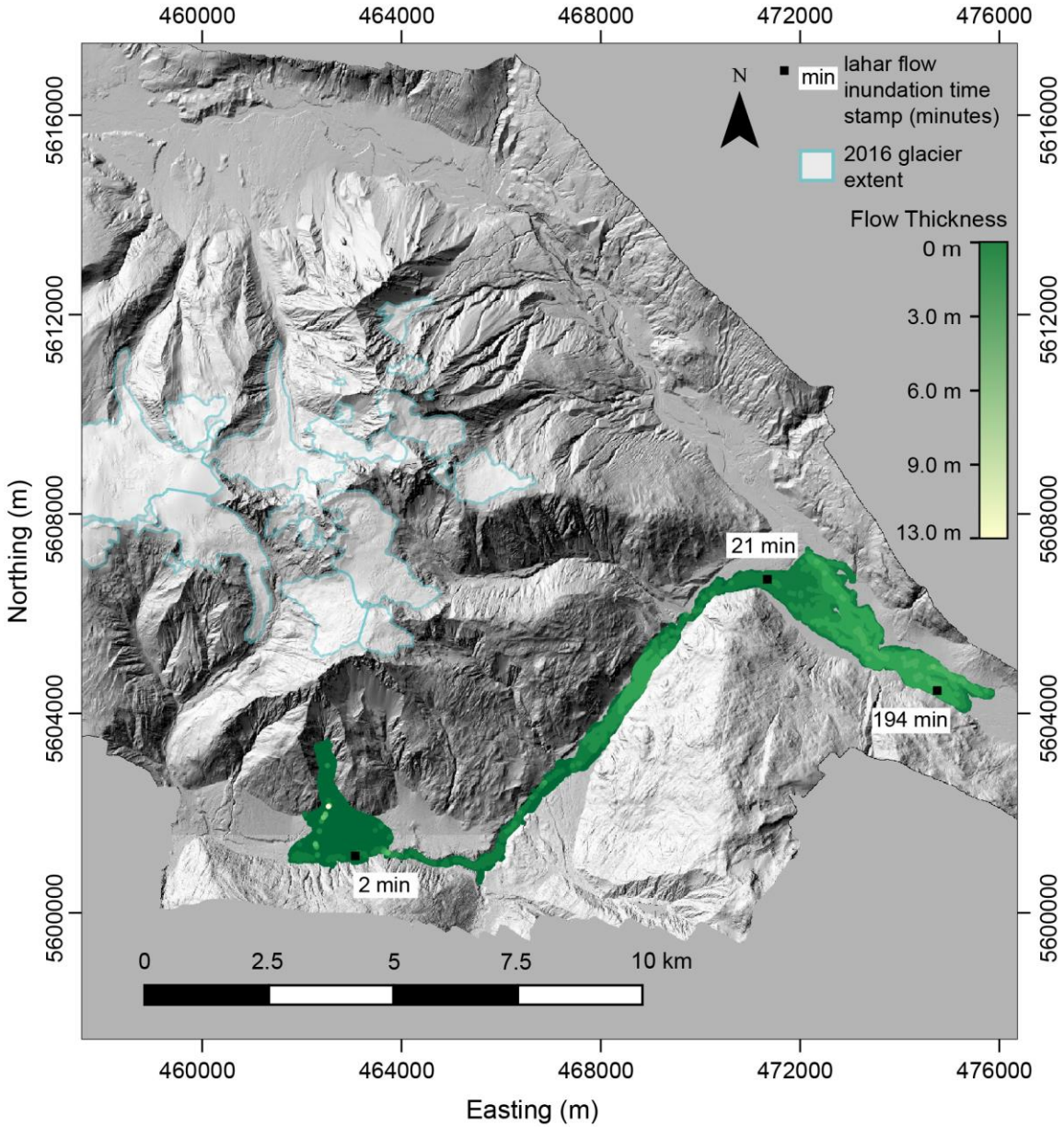


**Figure 3.4 Scenario 2 lahar inundation area and thickness stemming from Devastation Peak drainage basin modelled in VolcFlow. All time stamps (in minutes) are approximate. All coordinates are in UTM Zone 10, NAD 83.**

The average value of thickness for a scenario 2 lahar flow initiated from Mt. Meager drainage basin is 1.68 m ± 1.48 m (Figure 3.5). High values of thickness ranging from 3 m to 5 metres are again connected towards the end of the flow path (toe of the

flow) but do extend throughout the deposit in the Lillooet River. A few higher values of thickness occur within the channel of the drainage system (a range of 3 m to 9.1 m and a single value of 20 m occur).

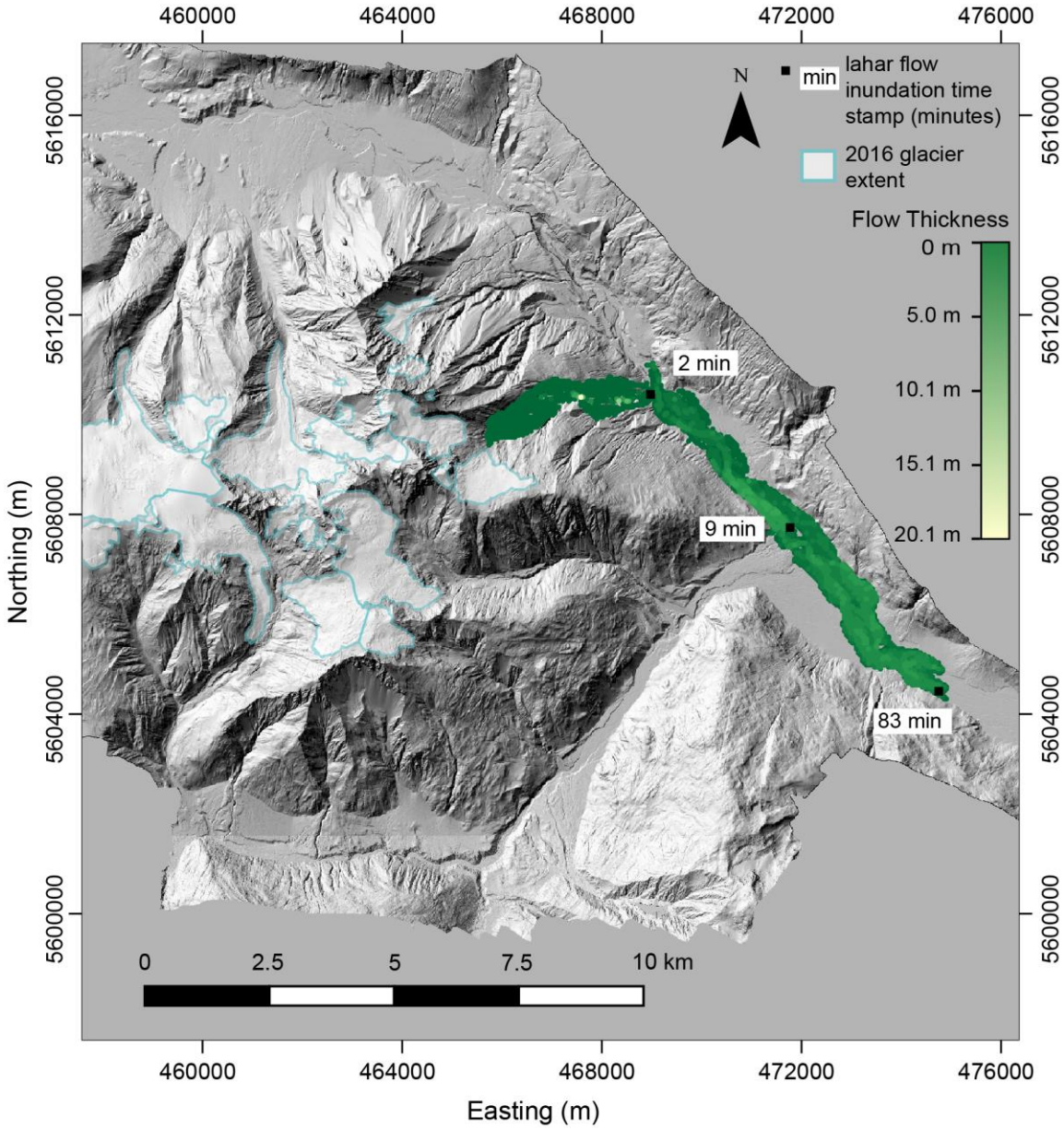


**Figure 3.5 Scenario 2 lahar inundation area and thickness stemming from Mt. Meager drainage basin modelled in VolcFlow. Time stamps (in minutes) are approximate. All coordinates are in UTM Zone 10, NAD 83.**

The average value of thickness for a scenario 2 lahar flow initiated from Job Creek drainage basin is 1.46 m ± 1.54 m (Figure 3.6). Areas of high values of thickness

concentration include the river channel ahead of Keyhole Falls, in a natural zone of valley confinement. In this section calculated values range from 6 m to 24 m and 41 m. Values of thickness downstream of Keyhole falls, towards the toe of the flow range are below 6 m, importantly being mostly below 2 m. This flow is also simulated to form a fan shape upon exiting the confines of Job Creek, as this area opens up into a natural wide valley portion of the Lillooet River. The thickness values calculated for this fan are all below 2 m.

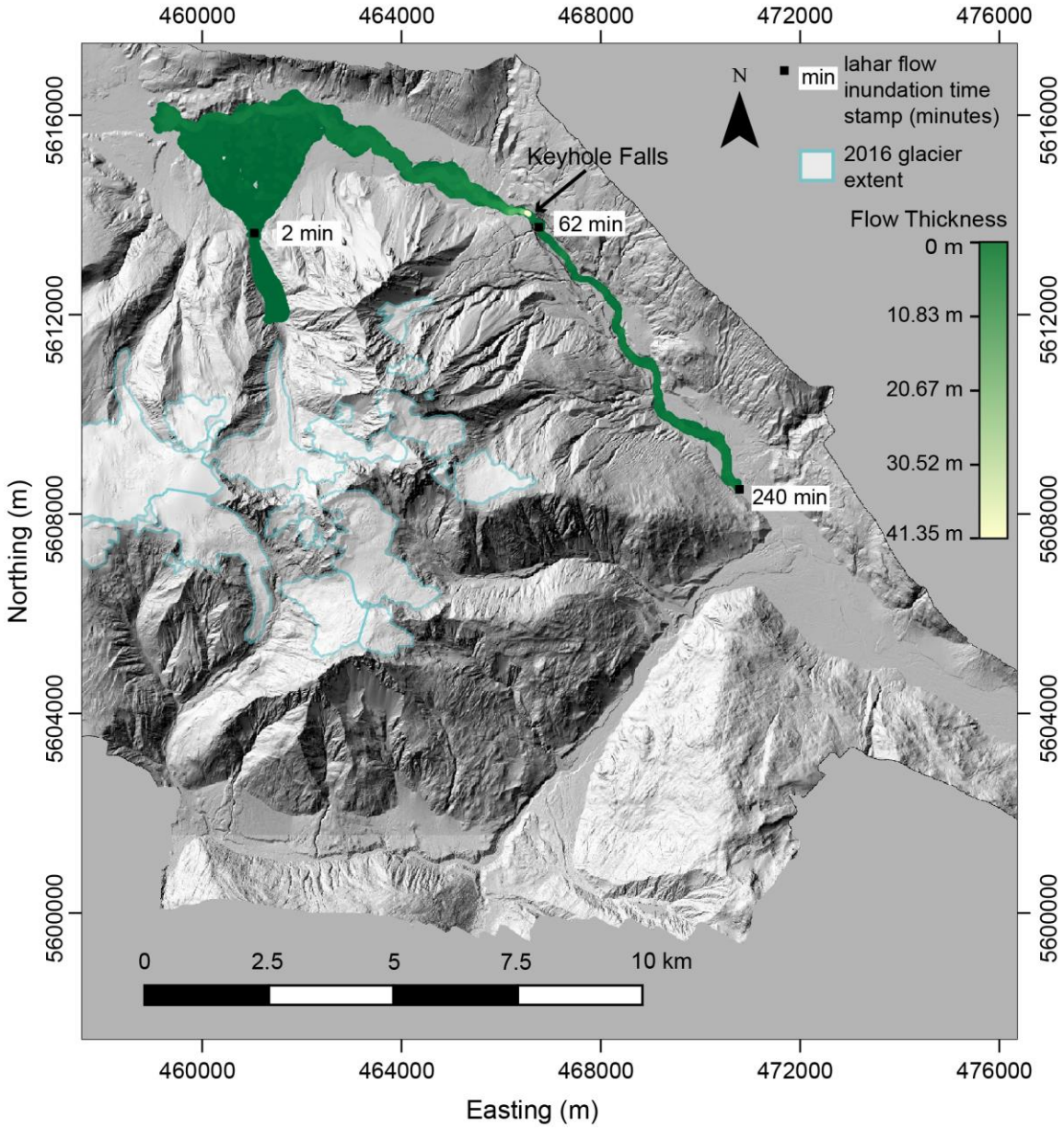


**Figure 3.6 Scenario 2 lahar inundation area and thickness stemming from Job Creek drainage basin modelled in VolcFlow. All time stamps (in minutes) are approximate. All coordinates are in UTM Zone 10, NAD 83.**

The average value of thickness for a scenario 3 lahar flow initiated from Capricorn Creek drainage basin 4.03 m ± 2.16 m (Figure 3.7). Concentrations of thickness values 5 m to 10.89 m are most pronounced starting at 3.7 km downstream of the confluence of Meager Creek and Lillooet River extending to the end of the flow, 20 km beyond the confluence. Segments of flow are also simulated to be deposited in

Meager Creek to the west of Capricorn Creek Valley, for a distance of 2 km (dominantly 2 m to 5 m thickness).

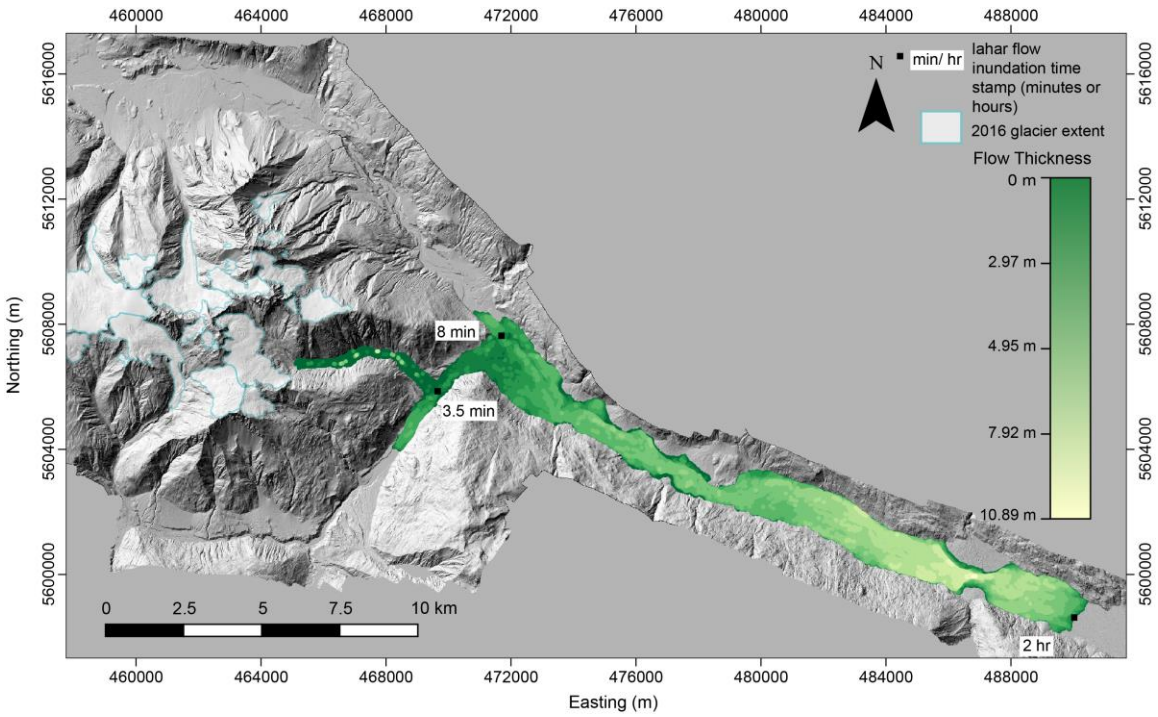


**Figure 3.7 Scenario 3 lahar inundation and thickness results modelled in VolcFlow for Capricorn Creek drainage basin. All time steps (in minutes or hours) are approximate. All coordinates are in UTM Zone 10 NAD 83.**

The average value of thickness for a scenario 3 lahar flow initiated from Devastation Peak drainage system is 3.69 m ± 2.18 m (Figure 3.8). Concentrated areas of thickness ranging from 5 m to 9 m are simulated 8.8 km past the confluence of Meager Creek and Lillooet River extending to the toe of the simulated deposit (20 km past the confluence). Small sections of high thickness values also occur at confining sections along Meager Creek ranging in values of 5 m to 12 m thickness. Again, the simulated fan deposited beyond the boundary of the massif is dominantly composed of thickness values below 1 m.

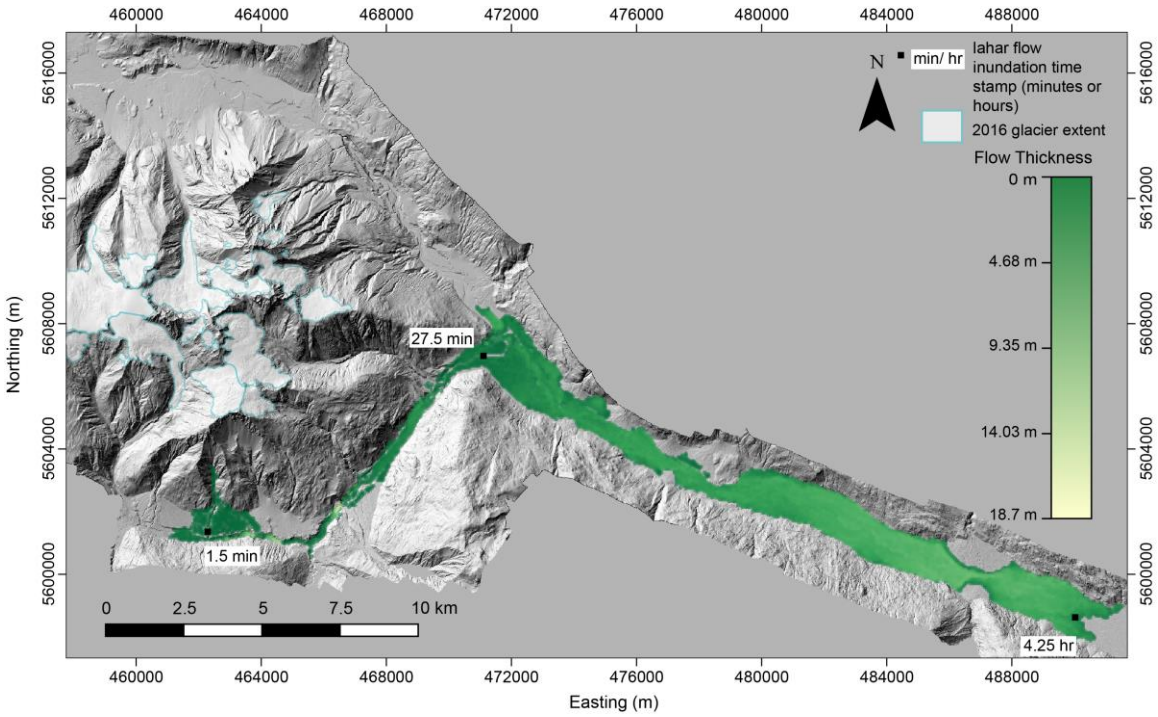


**Figure 3.8 Scenario 3 lahar inundation and thickness results modelled in VolcFlow for Devastation Peak drainage basin. All time steps (in minutes or hours) are approximate. All coordinates are in UTM Zone 10 NAD 83.**

The average value of thickness for a scenario 3 lahar flow from Mt. Meager drainage basin is 4.0 m ± 2.15 m (Figure 3.9). The average value of thickness for this flow is 4.0 m ± 2.15 m. High values of thickness ranging from 5 m to 9 m are concentrated towards the end of the flow path (toe of the flow) and the deposit shape follows the shape of the boundary of the river valley. A few higher values of thickness are simulated to be deposited within the channel of the drainage system (a range of 9 m to 12 m).

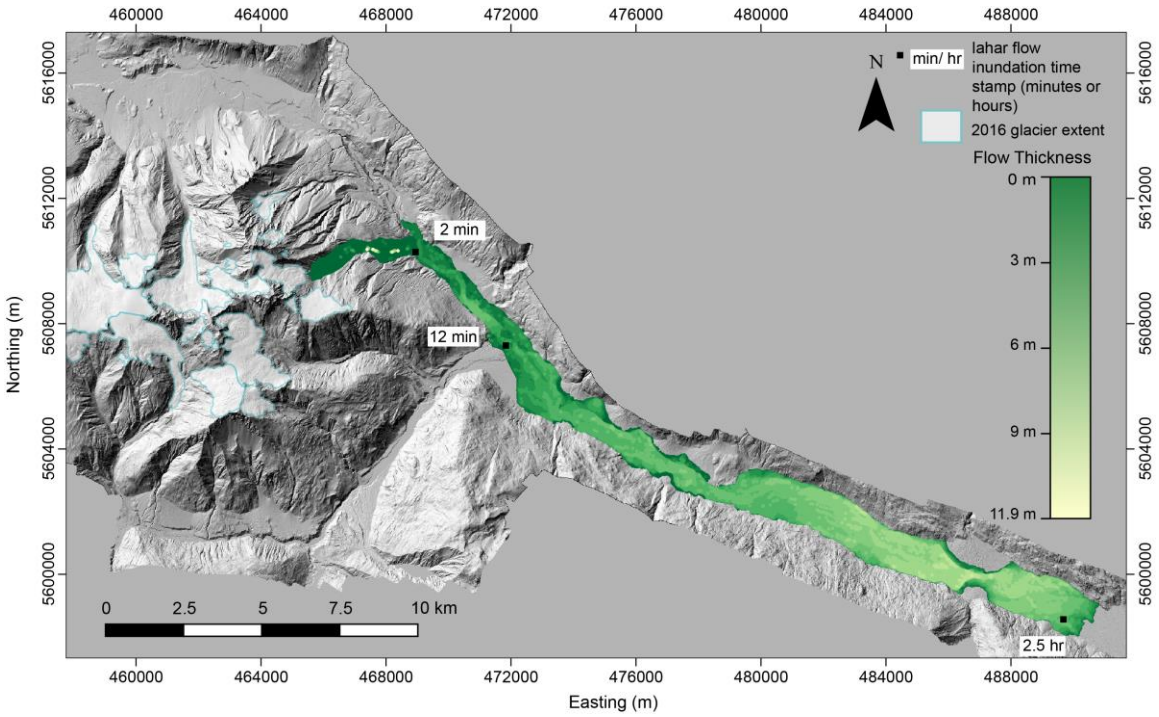


**Figure 3.9 Scenario 3 lahar inundation and thickness results modellled in VolcFlow for Mt. Meager drainage basin. All time stamps (minutes or hours) are approximate. All coordinates are in UTM Zone 10, NAD 83.**

The average value of thickness for a scenario 3 lahar flow from Job Creek basin is 3.49 m ± 2.6 m (Figure 3.10). Areas of high values of thickness concentration include the river channel ahead of Keyhole falls, in a natural zone of valley confinement. In this section calculated values range from 7 m to 18 m and 36 m in a section of high thickness values extending 2 km behind the falls (to the northwest). A section of high thickness values, in the range of 10 m to 27 m, also extends past the falls for 2 km. Beyond this point, extending to the toe of the flow, values of thickness dominantly range from 2 m to 5 m. This flow is also simulated to form a fan shape upon exiting the confines of Job Creek, mostly with a value of less than 1 m thickness. However, a small peripheral section of the fan (northwestern corner) has a simulated thickness value of about 5 m thickness.

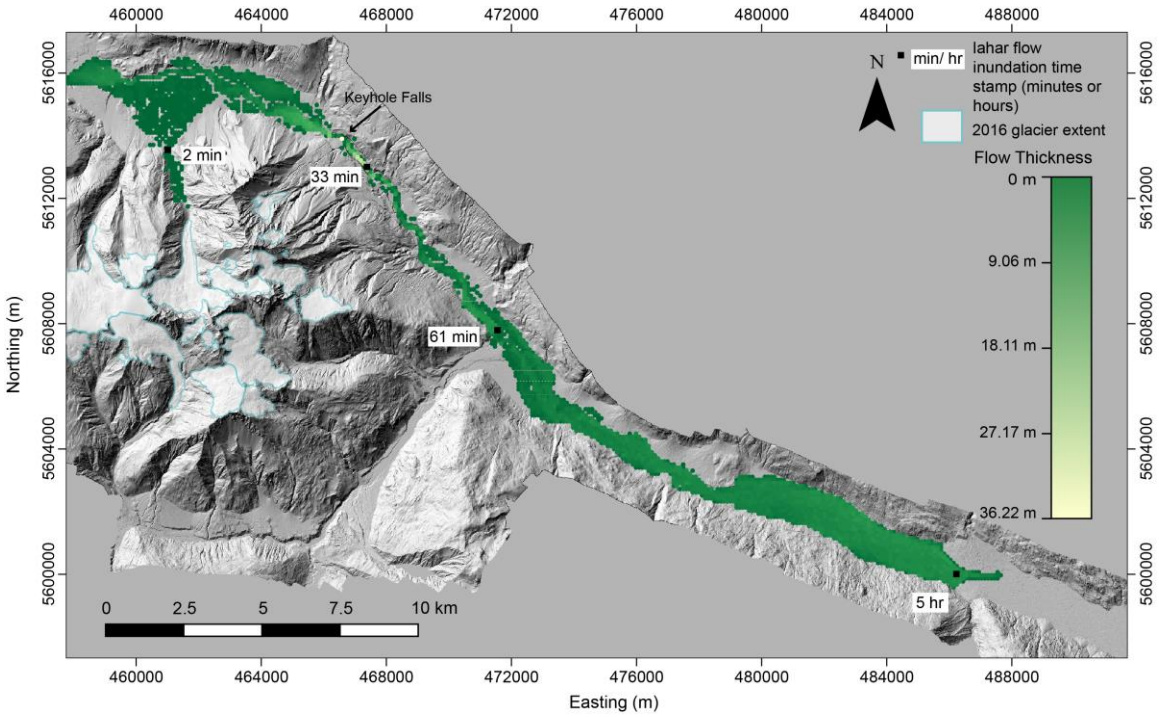


**Figure 3.10 Scenario 3 lahar inundation and thickness results modelled in VolcFlow for Job Creek drainage basin. All time steps (minutes or hours) are approximate. All coordinates are in UTM Zone 10 NAD 83.**

In all cases, flow direction is dominantly directed towards points of lower elevation. For flows stemming from the southern section of the massif, this results in flows entering Meager Creek and being directed east into Lillooet River. For flows stemming from the northern and eastern slopes of the massif this results in direct flow and deposition into the Lillooet River. Scenario 2 lahar flows are simulated to a distance of 11.57 km - 18.2 km and scenario 3 lahar flows are 27.8 km - 35 km.

Scenario 2 flows are all dominantly less than 2 m thick (1.46 m – 1.68 m) and scenario 3 flows less than 4 m (3.49 m – 4.03 m). The maximum value of lahar thickness occurs from Job creek for scenario 2 and 3. Maximum thickness values range from 13.0 m – 41.35 m (scenario 2) and 10.89 m – 36.22 m (scenario 3). Maximum thickness values occur at locations of valley confinement where the lahar flow is simulated to flow while being constricted. However, larger areas of thickness consistently occur near the toe of the lahar flow.

In all simulations (scenario 2 and 3), lahar flow inundation of the major valley bottom (Meager Creek or Lillooet River) occurs under 3.5 minutes (100 s – 210 s). Devastator Peak and Capricorn Creek lahar flows take 8 to 21 minutes (scenario 2) and

8 minutes to 27 minutes (scenario 3) to reach the Lillooet River. The scenario 2 Job Creek lahar flow is the only simulated flow that does not reach a distance past the confluence of Meager Creek and Lillooet River. At a total flow time of 4 hours, it is simulated to stop flow along the Lillooet River close to the southeastern corner of the base of the complex (ahead of the confluence). Otherwise, the scenario 3 lahar flow initiated from Job Creek reaches the point of confluence in 64 minutes and the scenario 2 and 3 lahar flow initiated from the Mt. Meager drainage basin reaches this point in under 10 minutes. The speed of lahar flows down the flanks of Mount Meager travel at 17-30 m/s (similar values between scenario 2 and 3) and slow down with distance from the source and travel over flatter topography.

### *Lahar Result Summary and Limitations*

It is clear that the present drainage pattern of the area on and surrounding the volcanic complex will dominate the trajectory of any lahar flow stemming from Mount Meager. The dominant water course at the base of Mount Meager is the Lillooet River, which all modelled flows enter and propagate downstream, either directly or indirectly if stemming from the southern sector of the complex. These flows are all constrained within the confines of the existing channel boundaries. This will be a reliable outcome for primary, single event lahars but may be altered if subsequent lahars occur within the same channel locations, where the deposition of previous pulses or events would have altered the terrain and therefore drainage pattern. However, it is reasonable to assume the dominant preferential direction of these flows (downstream) will remain the same as long as the channel path is not blocked - as occurred in 2360 cal yr B.P. eruption (Stewart, 2002). The modelling presented in this thesis shows that the flow deposits for scenario 2 and 3 will inundate the Lillooet River, which would cause catastrophic destruction to existing infrastructure and facilities within and close to the margins of the river. The models show that lahar deposits will be confined to the margins of existing stream channels, and flow path dictated by these channels.

Modelling focused on the assumption of the total volume of input stemming from the initiation point, as previously mentioned, does not accurately capture lahar behaviour of bulking and debulking. Streamflow from the in-situ drainage system of the area, could affect this process and increase mobility of the lahar flow.

The volume input for each scenario was based on observations of lahar flow volumes from other volcanoes around the world, and three different input volumes chosen for the sake of analyzing “what would happen” if that particular event of that volume were to occur from Mount Meager. The fourth lahar scenario included in this study suggests that a volume of 5 x $10^8$ $m^3$ would be required to reach Pemberton. An analysis of whether that volume of material is actually available or could occur from Mount Meager was not carried out. Although, Roberti et al. (2018) identified 12 potential landslide sites on the massif with a volume range $10^8$ – $10^9$ $m^3$. Calculations for Job Glacier, one of the glaciers on Mount Meager with current fumarolic activity, estimate the volume of the glacier to be ~7.5 × $10^7$ $m^3$ which could contribute meltwater to a lahar stemming from this drainage basin (see Appendix E). Melt contribution from a glacier ultimately will not include the entire calculated volume of the glacier, as it is unlikely the entire glacial mass would instantly melt and be incorporated into the lahar (or pyroclastic) flow. However, this value provides a real-world parameter for maximum ice melt contributing to the fluid component of any geophysical flow. Historically, large debris flows initiated from the flanks of Mount Meager have reached up to $10^9$ $m^3$ in volume (Friele et al., 2008). While these debris flows are not necessarily syneruptive and not characterized as a lahar in the literature, these multiple large volume debris flows give a volume range of material that could be incorporated into a lahar flow associated with a future eruption from Mount Meager.

## 3.3. Tephra Hazard

### 3.3.1. Ash3d

#### *Airborne Ash Dispersal*

The following figure displays a series of maps visualising the ash cloud cover results as frequency maps (Figure 3.11). These depict the individual airports in the Ash3d airport database that had a simulated occurrence of the propagated ash cloud during a run. Frequency has been classified by the size of the dot, referencing the number of simulations registering at each particular airport. The point features are the location of each day an airport reports ash cloud cover by the simulated runs as a visual representation of the simulated extent of the tephra.

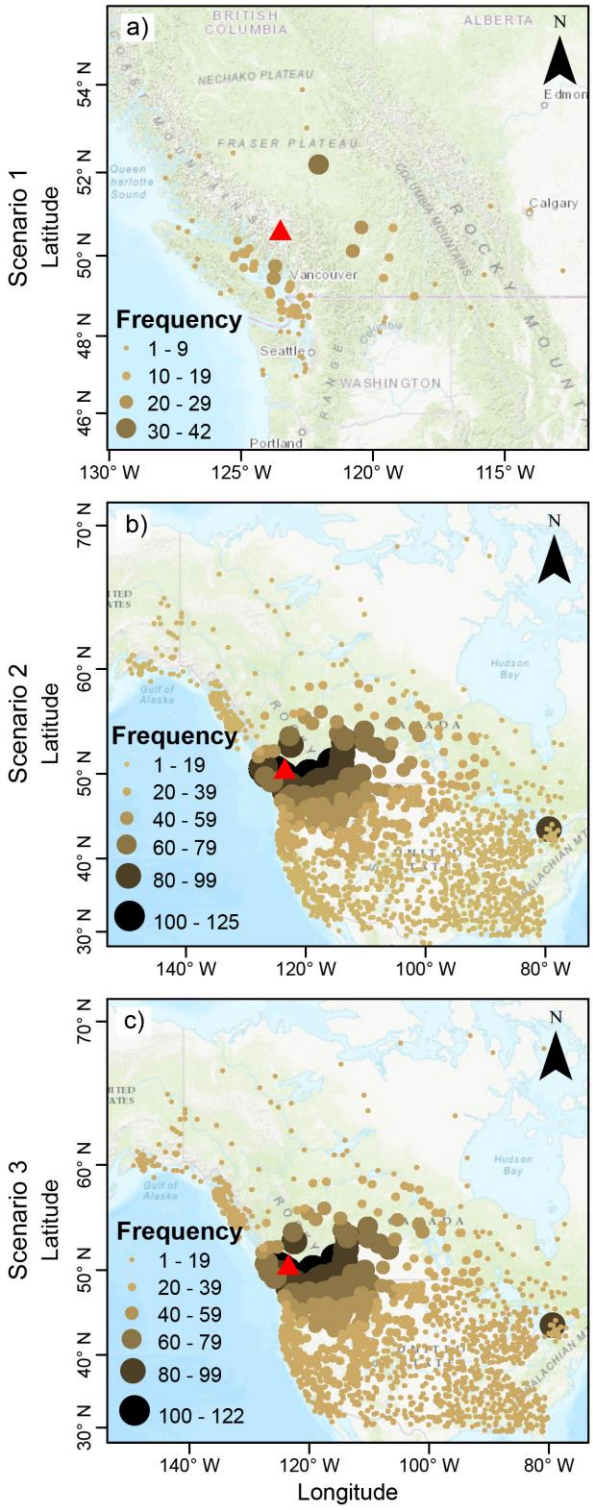


**Figure 3.11** **Instances of ash cloud cover over airports simulated for three eruption scenarios of Mount Meager. Represented as frequency distributions of each airport (number of simulated occurances of ash cloud cover per airport) for scenario 1 (a), scenario 2 (b), and scenario 3 (c). Mount Meager is indicated by the red triangle. Coordinate system is WGS 1984, World Mercator.**

Frequency maps show that the greatest concentrations of points are located in southwest British Columbia and northwest Washington. In frequency maps for scenario 2 and 3, individual points cannot be distinguished in this portion of total map area. A summary of the information for airborne ash dispersal for locations of interest in regards to each scenario, are shown in Table 3.4.

**Table 3.4 Ash arrival time and duration for selected locations surrounding Mount Meager as a representative summary of conditions of ash cloud propagation modelled in Ash3d**

| | | | | Ash arrival time (hh:mm) | | Ash cloud cover duration (hh:mm) | |
|---|---|---|---|---|---|---|---|
| *Scenario 1, total runs accounted for: 151* | | | | | | | |
| Airport | # of runs | Distance | Direction | range | average | range | average |
| Vancouver | 17 | 150 km | S | 2:43 -23:10 | 14:34 | 0:45-11:10 | 4:43 |
| Williams Lake | 33 | 189 km | NE | 4:05-23:46 | 14:19 | 0:13-14:02 | 3:05 |
| Powell River | 19 | 110 km | SW | 2:46-20:52 | 8:31 | 1:43-18:41 | 6:34 |
| Kamloops | 28 | 214 km | E | 4:24-21:53 | 11:59 | 0:37-14:57 | 3:59 |
| No ash reported | 42 | | | | | | |
| *Scenario 2, total runs accounted for: 194* | | | | | | | |
| Airport | # of runs | Distance | Direction | range | average | range | average |
| Vancouver | 105 | 150 km | S | 0:58-23:41 | 6:09 | 0:18-23:01 | 13:57 |
| Williams Lake | 136 | 189 km | NE | 0:52 - 22:48 | 7:24 | 1:11 - 22:57 | 14:33 |
| Powell River | 107 | 110 km | SW | 0:31-23:59 | 6:51 | 0:30-23:28 | 15:17 |
| Kamloops | 155 | 214 km | E | 0:39 – 22:16 | 5:00 | 1:08 -23:20 | 15:16 |
| Calgary | 92 | 655 km | NE | 2:52-23:19 | 11:26 | 0:40-21:07 | 9:44 |
| *Scenario 3, total runs accounted for: 136* | | | | | | | |
| Airport | # of runs | Distance | Direction | range | average | range | average |
| Vancouver | 113 | 150 km | S | 0:50 – 23:53 | 7:15 | 0:06 - 23:09 | 14:32 |
| Williams Lake | 133 | 189 km | NE | 0:58 -23:28 | 8:28 | 0:31-23:01 | 14:42 |
| Powell River | 104 | 110 km | SW | 0:29-23:41 | 7:24 | 0:18 -23:30 | 16:04 |
| Kamloops | 147 | 214 km | E | 0:38-23:48 | 5:55 | 0:12 - 23:21 | 15:57 |
| Calgary | 87 | 655 km | NE | 2:52-23:48 | 12:28 | 0:11 - 21:07 | 9:22 |

The scenario 1 eruption parameters model a significantly smaller eruption than the other two eruption scenarios and the extent of ash cloud propagation is either close to zero or very limited with respect to the time ash reaches major cities and how long it lingers. It takes a minimum of 2.75 hours to reach Vancouver (average cloud duration of 4.72 hours) as opposed to just under 1 hour for scenario 2 and 3 eruption parameters (average cloud duration over 13.95 hours). This discrepancy of time results is consistent for scenario 1 in comparison to scenario 2 and 3. Reasons for the discrepancies include inherent wind variations due to eruption height, seasonality affects, etc. The results for scenario 2 and 3 are incredibly similar. Comparing the ash arrival time results for the same cities shows a difference of 8 minutes or less. However, the average time that it takes the ash cloud to reach the same cities is less for scenario 2 than scenario 3 (a difference of under 1 hour). The average cloud duration over these cities is more for scenario 3 (less than 35 minutes), except for Calgary, where scenario 2 conditions simulate an average of 9.73 hours (as opposed to 9.37 hours for scenario 3).

Ash cloud simulations using the USGS Ash3d code show that the likelihood of ash cloud cover is concentrated in the area of the Pacific Northwest for, conditional upon the pre-defined eruption scenarios. For both scenario 2 and 3 eruption magnitudes, the ash cloud could travel all across North America, as recorded by the program's database of airports across North America.

### *Tephra Deposition*

The quasi-probabilistic analysis of one year of tephra deposition data produced by Ash3d shows that an eruption stemming from Mount Meager has the potential to impact the landscape at varying distances and in many directions surrounding the edifice. Distance is conditional on eruption scenario, with scenario 1(Figure 3.12 a,b) covering a significantly smaller distance than either scenario 2 (Figure 3.12 c,d) or scenario 3 (Figure 3.12 e,f). The probability of exceeding 0.9 mm tephra accumulation by 10% extends from 11 km to 21 km away from Mount Meager for scenario 1 (Figure 3.12 a). The corresponding contour line for scenario 2 extends from 348 km to 532 km away from Mount Meager (Figure 3.12 c) and 496 km to 755 km for scenario 3 (Figure 3.12 e).

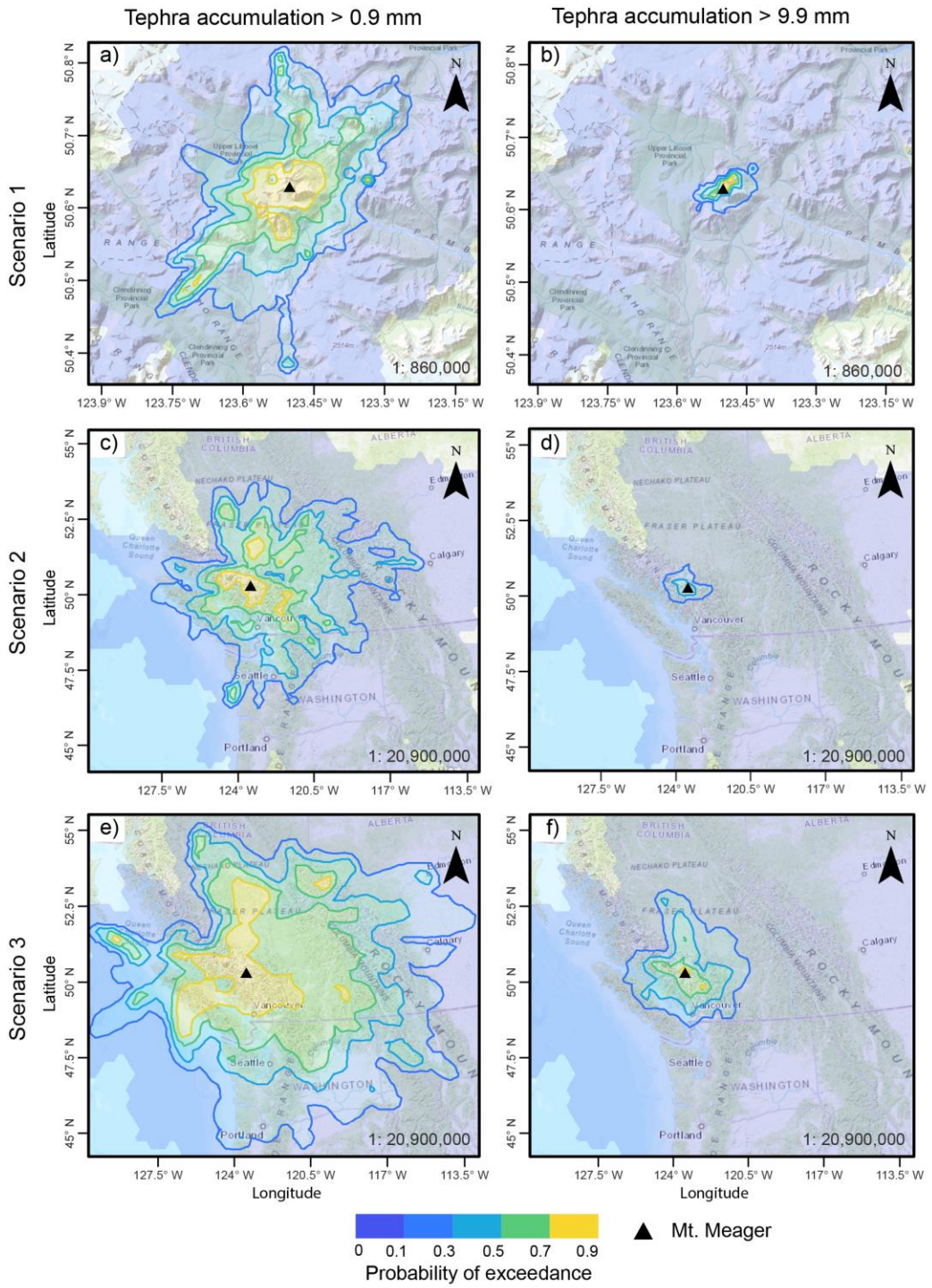


**Figure 3.12** **Spatial probability of exceeding tephra accumulation thresholds conditional on the eruption scenario modelled with USGS Ash3d. Scenario 1 a) for a tephra accumulation exceeding 0.9 mm, b) 9.9 mm; Scenario 2 c) 0.9 mm, d) 9.9 mm; Scenario 3 e) 0.9 mm, f) 9.9 mm. Contours indicate the probability starting at 0.1 and incrementally increased by an interval of 0.2, black triangle represents Mount Meager, the eruption source. Co-ordinate system is WGS 1984, World Mercator.**

Across all scenarios, the probability of exceeding the threshold criteria increases towards the coordinate of Mount Meager. The shapes of the boundary conditions show no trends of preferential direction of deposition. Regarding the shape, across all scenario's results with a threshold of 0.9 mm, the pattern of output is chaotic and, in some cases, contour pattern is disjointed showing small pockets of discontinuous regions of higher probability of exceeding the threshold. This is, in part, due to the method of using of using one year of wind profiles (as opposed to several years). It can be noted that in scenario 2 and 3, the furthest extension of the contour lines and shaded regions extends from volcano coordinate eastward, reaching a maximum distance of 532 km in scenario 2 and 755 km in scenario 3 towards the east for the contour representing a 10% probability of exceeding 0.9 mm. The shortest distance of this contour extends 347 km to the west in scenario 2 and 496 km north in scenario 3 (with an extended distance of 500 km westward in scenario 3).

In the case of scenario 1, the directions of maximum and minimum distance from the volcano coordinate differ from the other two scenarios in the case of a threshold of exceeding 0.9 mm tephra accumulation. The maximum distances of the contour line representing 10% probability are achieved 21 km towards the northeast and southwest. Minimum distances are recorded towards the east (11 km) and west (13 km).

At first appearance, the directionality of the scenarios deposit outputs are less chaotic with a threshold of 10 mm tephra accumulation. The maximum distance of contour lines also do not extend to the same distances as the results from the threshold of 0.9 mm tephra accumulation. The contour lines, and therefore distance of probabilistically exceeding 9.9 mm tephra accumulation, are closer to Mount Meager. In scenario 1, the 10% probability of exceeding 9.9 mm tephra accumulation extends to a maximum of 5 km eastward and minimum of 3.7 km westward. In scenario 2, this same contour boundary extends to a maximum of 93 km eastward and minimum of 46 km south. For scenario 3, the contour extends to the north at a maximum distance of 300 km, and a minimum distance of 199 km southward.

In all cases, the geographical area that receives the highest probability of exceeding the thresholds of tephra accumulation is southwestern British Columbia. The total distance and area covered increases from scenario 1 to 3 representing more energetic and explosive volcanic eruptions. The results show that the probability of

exceeding 0.9 mm tephra accumulation in scenario 2 and 3 also extend into Washington State and southwestern Alberta.

The results from both threshold values for scenario 1 show no population centres receiving tephra accumulation. The only area of importance that is simulated to be impacted by tephra deposition is Mount Meager. With the threshold of 9.9 mm tephra accumulation, no areas beyond the massif are simulated to receive tephra deposition. With a threshold of 0.9 mm tephra accumulation, Meager Creek and the upper Lillooet River are upwards of 50% probability of receiving this degree of tephra accumulation.

A list of cities and areas of importance (chosen based center of large population or important economic regions) is included in Table 3.5 corresponding to which areas have a probability of being impacted given the specified threshold. The cities listed is not a complete list of all cities covered by the statistical analysis and is only a summarized list of a few areas of interest or importance.

**Table 3.5 A summary of cities and geographic regions potentially impacted by ash accumulation within the boundaries of the probabilistic analysis of ash deposition data from Ash3d**

| | Probability of exceeding 0.9 mm tephra accumulation | | | | Probability of exceeding 9.9 mm tephra accumulation | | | |
|---|---|---|---|---|---|---|---|---|
| Scenario | 10% | 30% | 50% | 70% | 10% | 30% | 50% | 70% |
| 1 | Meager Creek and Upper Lillooet River | | | Volcanic Complex | Mount Meager Volcanic Complex | | | |
| 2 | Seattle, Kelowna, Vancouver Island, Banff, Quesnel | Williams Lake, Kamloops, Vancouver, Nanaimo, Bellingham | Campbell River, Northern Fraser Valley | Whistler, Pemberton | Pemberton | MMVC, Pemberton Meadows | N/A | |
| 3 | Calgary, Portland, | Prince George, Seattle | Vancouver, Vancouver Island Bellingham, Okanagan, Williams Lake | Pemberton, Whistler, North Shore Campbell River | Vancouver, Campbell River 100 Mile House, Kamloops | Squamish, North Shore | Pemberton, Whistler | MMVC |

There are several considerations for uncertainty regarding the results of tephra deposition obtained by Ash3d and presented here. The geostatistical wizard in ArcGIS software is unable to take into account stacked points (data with exact co-ordinate overlap), and a decision was made to carry on with the analysis by considering the maximum value of coincident points. Therefore, the analysis does not truly consider all points obtained in the numerical modelling and results in a potential difference on the order of 10s of km not accounted for in the probability boundaries. However, as a first order assessment within the degree of precision needed for this assessment, the distance of 10s of kilometres is acceptable. See Appendix C for a comparison in considering coincident points as the average value or maximum value. In addition, calling this a probabilistic analysis is false due to the limited time span that this analysis covers and the fact that only wind data is varied for a modelling simulation where eruption parameters could also be represented by a range. The outcome therefore is a combination of deterministic and probabilistic criteria.

### 3.3.2. TephraProb

TephraProb produces results for modelled tephra deposition which are presented as maps of the spatial distribution of probabilities that exceed specified tephra accumulations (Figure 3.13). Only results from the unrestricted wind profiles are tabulated and included (Table 3.6) in order to assess the probability of tephra accumulation based on the statistical distribution of wind conditions. The TephraProb package allows users to constrain the sampling of wind conditions to pre-defined directions around the volcano in order to assess the volcanic ash accumulation hazard at specific sites, conditional upon a specific wind scenario (see Appendix D).

From all results of non-restricted wind profiles for all tephra deposition thresholds, a clear pattern of directionality is present in tephra deposition, that being dominantly directed towards the northeast. This is indicative from the pattern of contour lines outlining the probability of exceeding the tephra deposition threshold (Figure 3.13). The central axis of this direction is similar in all scenarios except scenario 3. This direction is dominantly 45° NE in scenario 1 and 2. It is 65° NE for scenario 3. It is also consistent across all scenarios that the contours representing probability values of exceeding the threshold of tephra accumulation are geographically closer to Mount Meager, the origin point, for exceeding 100 kg/m$^2$ as opposed to 1 kg/m$^2$.

The sphere of sizable impact from a scenario 1 eruption is restricted to a proximal distance surrounding Mount Meager (Figure 3.13 a,b,c). The furthest extent of the 10% contour probabilistically exceeding 10 kg/m$^2$ of tephra accumulation is within a range of 30 – 55 km from Mount Meager. Only two locations are noted below in Table 3.6 (Gold Bridge is beyond the smallest contour value included on the maps), both with small or zero populations. These two sites are notable landmarks in the vicinity of Mount Meager that have simulated tephra deposition within the scope of this scenario. Lillooet River has less than 80% probability of exceeding the accumulation of 1 kg/m$^2$ of tephra, less than 70% with a threshold of 10 kg/m$^2$, and less than 50% probability with a threshold of 100 kg/m$^2$, with all values of accumulation presenting their own problems and difficulties for access and activity and the natural environment of the water course.

Modelling shows that Pemberton has the potential to be impacted by tephra accumulation exceeding the thresholds of 1 kg/m$^2$ or 10 kg/m$^2$ for scenario 2 and

exceeding any of the thresholds for scenario 3. Scenario 3 parameters simulate that Vancouver may also be impacted by tephra accumulation exceeding 1 kg/$m^2$ or 10 kg/$m^2$. Finally, Kamloops and Williams Lake are only included in the computational grid for scenario 3 and are therefore not captured within the scope of scenario 2 parameters.

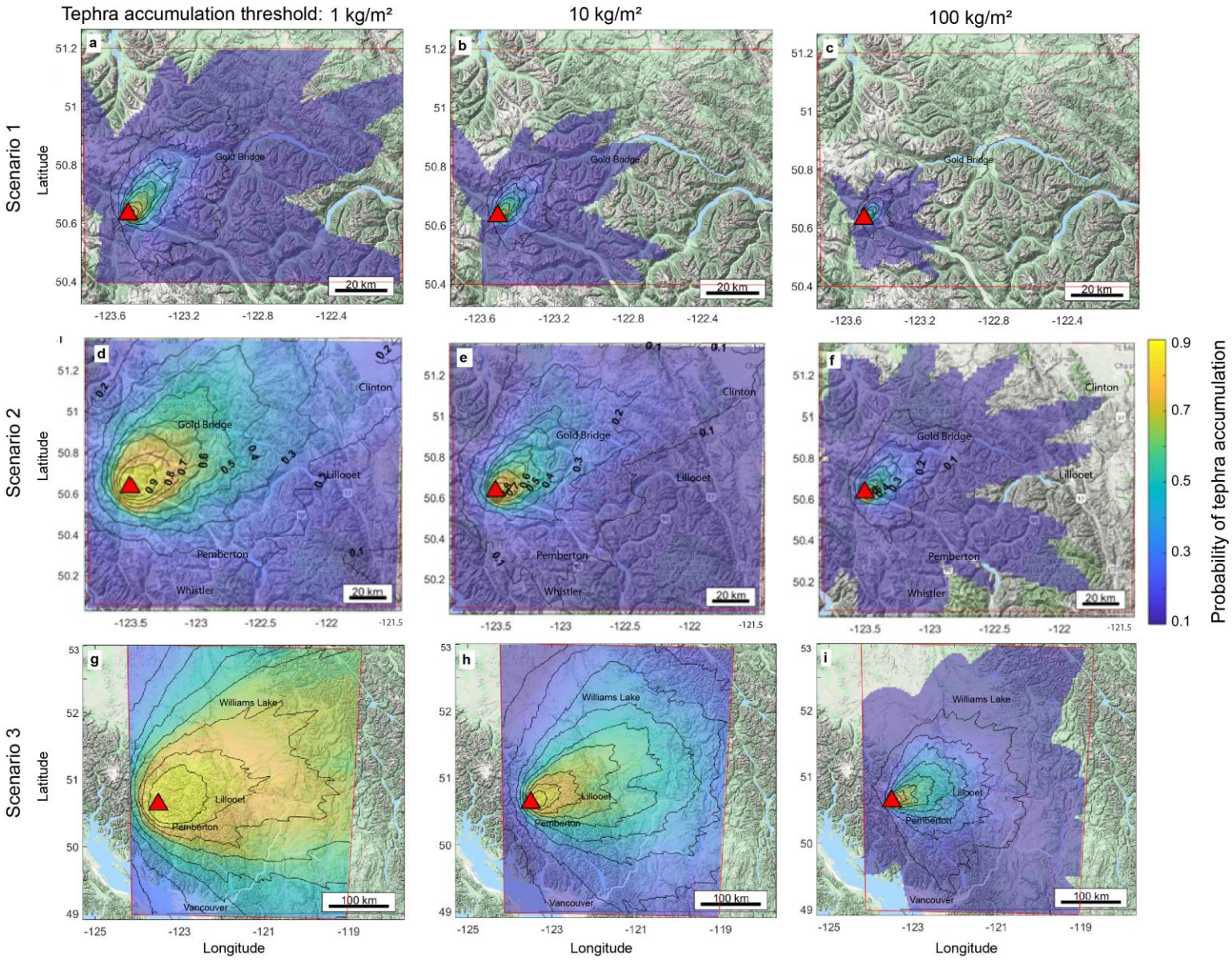


**Figure 3.13 (see next page)**

**Figure 3.13 (See previous page) Mount Meager tephra deposition hazard maps for the probability of exceeding a threshold of tephra accumulation conditional on the eruption scenario where wind profile is unrestricted modelled by TephraProb. Scenario 1 a) for a tephra accumulation of 1 kg/m$^2$, b) 10 kg/m$^2$, c) 100 kg/m$^2$; Scenario 2 d) 1 kg/m$^2$, e) 10 kg/m$^2$, f) 100 kg/m$^2$; Scenario 3 g) 1 kg/m$^2$, h) 10 kg/m$^2$ and i) 100 kg/m$^2$. Contours indicate the probability starting at 0.1 and incrementally increased by an interval of 0.1, red line indicates the boundary of the computed grid and the red triangle locates the eruption vent. Coordinates are WGS 1984.**

**Table 3.6 Unrestricted wind profile results for probability of exceeding the threshold in designated population centres affected by an eruption of Mount Meager**

| | | | Exceedance probability | | |
|---|---|---|---|---|---|
| *Scenario 1* | | | | | |
| Location | Distance | Direction | 1 kg/m$^2$ | 10 kg/m$^2$ | 100 kg/m$^2$ |
| Gold Bridge | 55.5 km | E | 6% | 2% | N/A |
| Upper Lillooet Recreation Site (50.616, -123.392) | 5 km | SE | 12.2% | 11% | 10.1% |
| *Scenario 2* | | | | | |
| Location | Distance | Direction | 1 kg/m$^2$ | 10 kg/m$^2$ | 100 kg/m$^2$ |
| Gold Bridge | 55.5 km | E | 56.03 % | 34.32 % | 8.12 % |
| Lillooet | 111 km | E | 22.0 % | 6.66 % | N/A |
| Pemberton | 65 km | S | 19.36 % | 10.0 % | N/A |
| *Scenario 3* | | | | | |
| Location | Distance | Direction | 1 kg/m$^2$ | 10 kg/m$^2$ | 100 kg/m$^2$ |
| Kamloops | 222 km | E | 72% | 47% | 8% |
| Williams Lake | 195 km | NE | 64% | 34% | 7% |
| Pemberton | 65 km | S | 88% | 50% | 24% |
| Vancouver | 165 km | S | 27% | 12% | 2% |

The uncertainty of contour location, and therefore the coordinate of impact increases with distance away from the source from ±2.5 km to ±10 km.

### *Summary of Volcanic Ash Hazard Results and Limitation*

Dominant prevailing wind patterns across Mount Meager are the westerlies, with some deviation from this norm. This impacts the pattern of ash cloud propagation and ashfall from any potential eruption stemming from Mount Meager. Modelling in both TephraProb and Ash3d shows that the area of southwest British Columbia will be impacted by ashfall (area of spatial extent increasing with increased magnitude of eruption). The area most likely to be affected by a propagating ash cloud would also be southwest British Columbia but ash could extend across North America in any direction (modelled by Ash3d). While a small scale eruption (VEI ≤ 2) will have limited spatial impact, any larger eruption (greater than VEI 3) could have significant regional impact. Other aspects of uncertainty for direction and area of volcanic ash cloud dispersal include, seasonality and local weather condition variation

With both programs, modelled tephra deposition is limited to up to a few 100 kilometres from the edifice. This is due to the extent of effective calculations from the modelling programs used, being vertically stratified but horizontally homogenous.

# Chapter 4.

# Discussion: The preliminary hazard assessment for Mount Meager

The scenarios and accompanying hazard maps serve to show the areas that could be impacted by a future volcanic eruption from Mount Meager. The hazard maps show the extent of each hazard as a solid boundary. In reality, the extent and true coverage of an event are not justified by sharp boundary but are rather gradational contact boundaries, to match their inherent uncertainty. However, with the exception of results from TephraProb, all hazard characteristics were developed from deterministic modelling, which produce definitive boundaries. The ashfall hazard (taken from the results of TephraProb) has been depicted with a dotted line in the following scenario hazard maps in order to communicate the ambiguous boundary inherent from the probabilistic outcomes of this particular hazard modelling.

### *Scenario 1: Small Magnitude Eruption*

In the case of a small explosive eruption (VEI < 2), the research presented here indicates that PDC, lahar and tephra deposition impacts will be limited to the nearby vicinity of the volcano (Figure 4.1). Pyroclastic flows will largely be confined to the region of the massif itself, only extending to the base of the complex with eruptions triggered from Plinth Peak, Mt. Meager or Pylon Peak (Appendix B). Lahar flows will inundate Meager Creek and the Lillooet River up to a maximum runout length of 11.5 km. Simulations show that the tephra cloud may reach areas around southwest British Columbia (depending on the meteorological conditions). However, significant accumulations of tephra will be limited to mostly unpopulated regions around the volcano. The most widespread accumulation of tephra $>$ 1 kg/m$^2$ (1 mm) thickness being deposited up to 30 km from the volcano (greater than 30 % probability). Across all modelled hazards (aside from tephra cloud propagation), no population centres are impacted in this scenario. The areas of impact are restricted to the massif itself and, most importantly, the river systems that surround the volcano.

### *Scenario 2: Mid-Magnitude Eruption*

The areas that could be impacted by a mid-range explosive eruption (VEI 3) exceed the base of the volcanic complex (Figure 4.2). PDC deposits will most likely inundate the main river system (individual simulations initiated from Mt. Job and Capricorn Mountain do not), extending the impact up to ~ 2.5 km beyond the base of the complex. This distance covers roads and building facilities within the upper Lillooet River Valley. Lahar flows will follow the course of Meager Creek and the Lillooet River up to a maximum runout length of 21.5 km, and simulations show they will follow the natural flow path of the river system, flowing towards (but not reaching) the inhabited region of Pemberton Meadows. Simulations show it could take between 2 to 3 minutes from the point of initiation to reach the main water ways that discharge into Meager Creek or Lillooet River, although this timing may be dependent on the point of initial elevation and therefore distance travelled to the main river system. The tephra cloud is most likely to impact southwestern British Columbia, and the northern area of Washington State (USA). However, this information is based on a specific year of meteorological data and has a bias due to the airport database used by Ash3d, the program used for analyzing the ash cloud hazard. Ash fallout of all modelled tephra accumulation thresholds are restricted to southwestern British Columbia, with a low probability of impacting any major population centres. However, the areas of impact do differ from the results of ash fallout with Ash3d and TephraProb. Ash3d simulates, with a probability greater than 30%, that the region within 350 km of Mount Meager may be impacted by tephra accumulation greater than 0.9 mm. Importantly, this includes a potential impact on cities in southern BC (such as Vancouver, Kamloops, and Williams Lake), as well as populations in northern Washington. However, TephraProb, which is based on 10 years of wind data, restricts the furthest extent of impact exceeding 1 kg/m$^2$ (1 mm thickness) to within 100 km from the volcano which only includes the community of Gold Bridge, a small service centre for nearby recreation-residential properties. The region with a probability of impact greater than 30% also includes a section of Pemberton Meadows, an important agricultural area. This deposit value has implications for respiratory irritation of individuals, and some minimal crop damage. Animals, such as cattle may face some irritation due to ashfall of 1 kg/m$^2$ (Thompson et al., 2017).

### *Scenario 3: Large Magnitude Eruption*

In the case of a large explosive eruption (VEI 4-5), inundation from the volcanic hazards could far exceed the perimeter of the massif, impacting infrastructure, agriculture and residential properties (Figure 4.3). As a proximal hazard, pyroclastic density currents will still be confined to the region immediately surrounding the volcanic complex, extending 5 to 6 km beyond the base of the complex, to opposing mountain sides up to an elevation of ~ 1000 m. The potential zone of impact includes the Lillooet River, Meager Creek, logging roads, infrastructure facilities and recreational sites within the vicinity of Mount Meager. Lahar flows could travel up to ~ 30 km beyond the edge of the massif down the Lillooet River valley (this instance occurs from flows stemming from the south-eastern area of the complex). This distance brings the limit of the flow to the edges of Pemberton Meadows, covering about 8 km of agricultural land. This total inundation distance would cover significantly more of the logging and forest service roads beyond that in scenario 1 and 2 lahar inundation. The two main forest service roads that would be impacted and rendered inaccessible are the north and south Lillooet Forest Service Road and Hurley River Forest Service Road. This in turn would cut off road access to facilities in the vicinity of Mount Meager, including those used by logging operations, pumice mining and the run-of-river hydro project on the Upper Lillooet River. Popular back-country recreation sites accessed by these roads would also become inaccessible by road.

The results from modelling the tephra cloud with Ash3d are similar for scenario 2 and 3. The region of impact appears to be the same and the spatial dispersion of cloud impact is heavily biased by the database of airports used by the program. Frequency maps show (Figure 3.11) that for the year of model runs, most of North America could have recorded ash cover. Clearly, the area of highest frequency of recorded ash coverage decreases with distance from the massif. Based on these results, volcanic ash from a large magnitude eruption from Mount Meager would likely impact southwestern British Columbia, and has the potential to travel across North America, with direction being dependent on meteorological conditions at the time.

The region of probable impact from ashfall is expanded from scenario 2. Ash3d results indicate that the furthest extent of impact for tephra accumulation exceeding 0.9 mm thickness could reach 500 km (greater than 30% probability). This region includes

northern Washington, Vancouver Island and all of southwestern British Columbia. Beyond this, with smaller probable values, other notable cities that could be impacted include Portland (25% probability) and Calgary (20% probability). The grid chosen for the spatial probability calculation in TephraProb only extends to ~ 350 km from the volcano. At this limit, TephraProb calculates the probability of exceeding 1 kg/$m^2$ mass load to be greater than 60 %. Within this degree and greater probability, cities such as Kelowna, Kamloops, Williams Lake, Pemberton and surrounding smaller communities and land would be impacted. Vancouver and the Lower Mainland have a 30-40% probability of being impacted by an exceedance of 1 kg/$m^2$ tephra mass load, in this scenario (Ash3d simulates a probability greater than 50% for the same region).

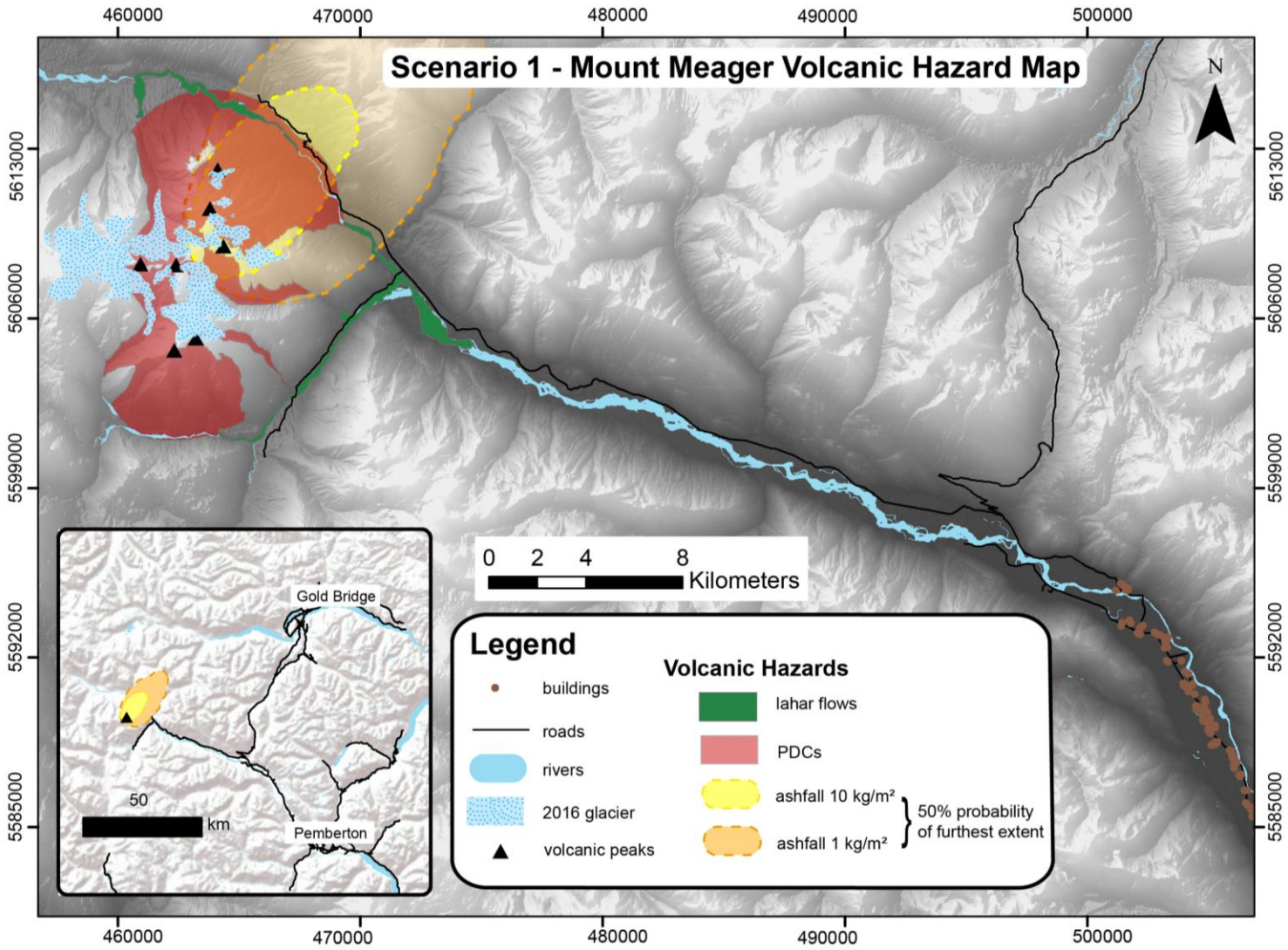


**Figure 4.1** **Hazard Map for scenario 1, conditional on the occurrence of a small scale eruption (VEI ≤ 2). The upper Lillooet River valley will be affected by inundation from lahar flows, pyroclastic density currents and ashfall. Additionally, ashfall may impact areas beyond the Lillooet valley, with deposition affecting mountain ranges north-east of the complex (map inset). All coordinates are in UTM Zone 10N, NAD 83.**

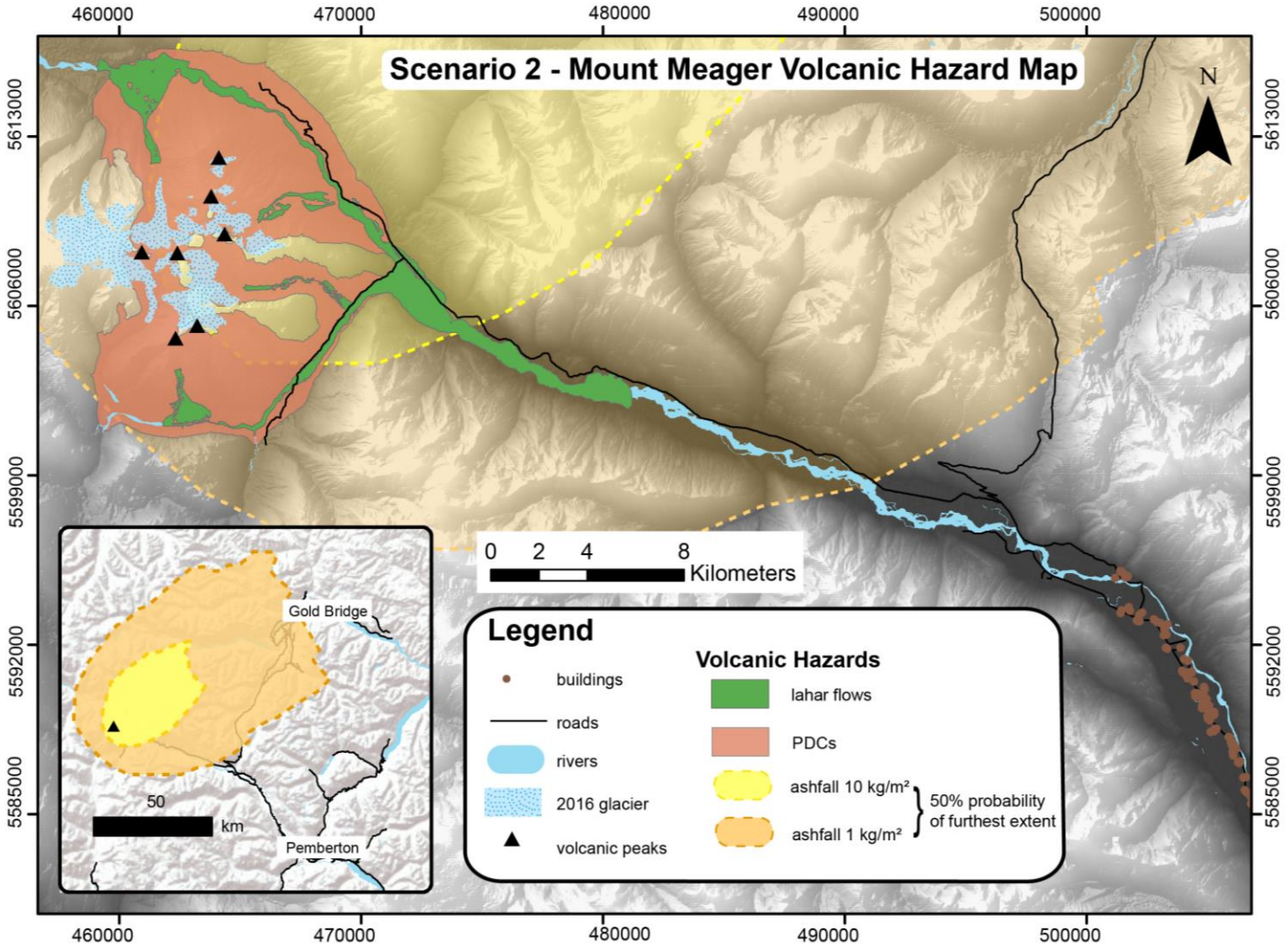


**Figure 4.2** **Hazard Map for scenario 2, conditional on the occurrence of a mid-scale eruption (VEI ≤ 3). Areas affected by lahar flow and pyroclastic density currents include an extension of the upper Lillooet River valley with PDCs fully covering the river channels (Meager Creek and Lillooet River). Ashfall deposit may fully encompass the complex and affect areas up to 90 km NE of the complex (50% probability), see inset map. All coordinates are in UTM Zone 10N, NAD 83.**

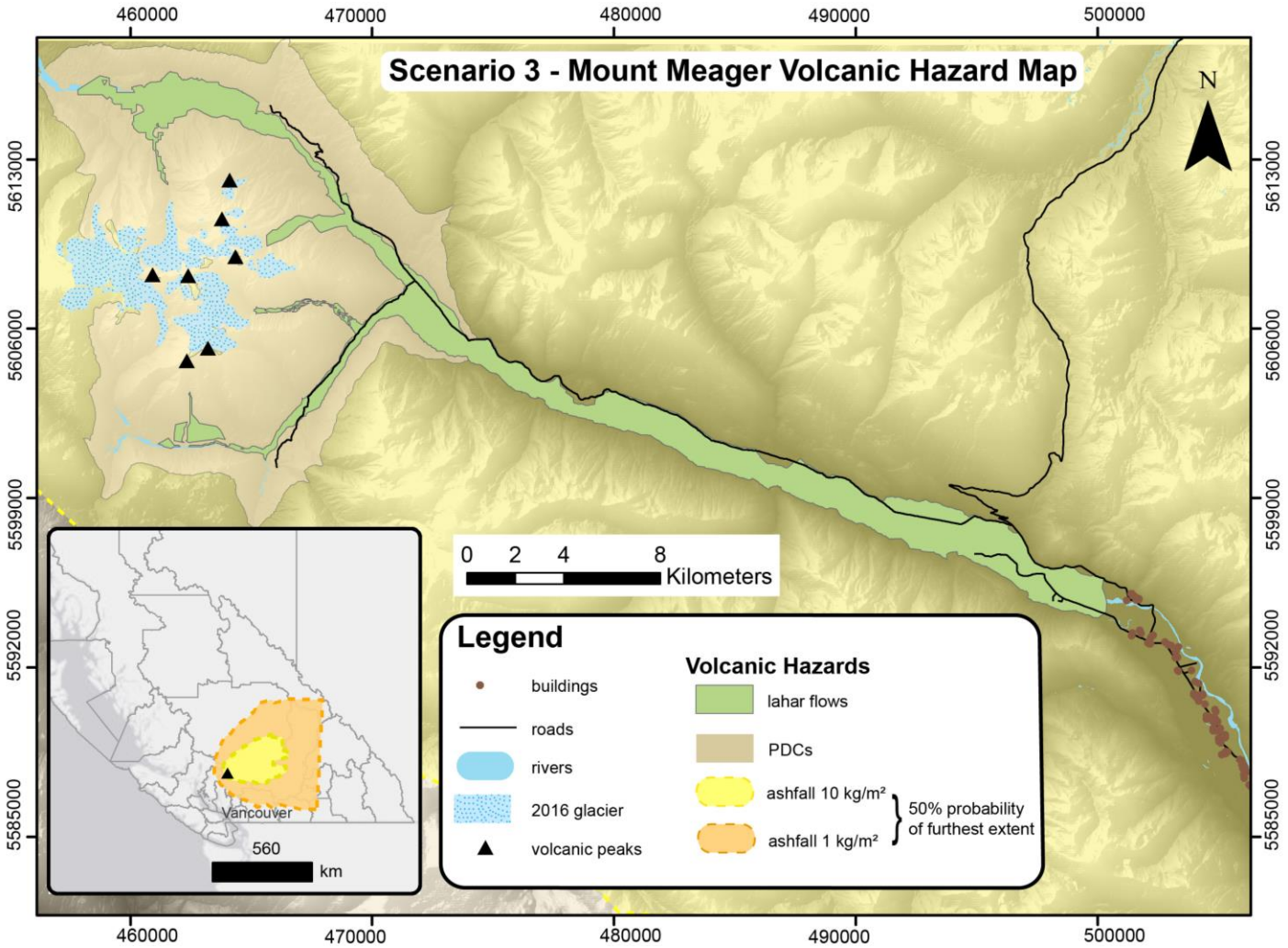


**Figure 4.3** **Hazard Map for scenario 3, conditional on the occurrence of a mid-scale eruption (VEI ≤ 4-5). In addition to the upper Lillooet River valley being affected by all volcanic hazards, Pemberton Meadows, down-valley of the complex may be impacted by lahars and ashfall.The inset depicts the furthest extent of ashfall (50% probability), predominately impacting southwest British Columbia. The furthest extent of 1 kg/m$^2$ tephra accumulation may be more expansive, eastern boundaries were limited by the calculation grid during modelling. All coordinates are in UTM Zone 10N, NAD 83.**

## 4.1. Looking forward: Canadian volcano hazard assessments

Most volcanoes in the Canadian landscape are remote, a key reason for the lack of interest and study of many of them. Being remote, most Canadian volcanoes lack in-depth geologic studies, coupled with limited efforts to discern their eruptive history. Building on the momentum of current interest on Mount Meager and the Garibaldi volcanic belt (e.g., Mullen et al., 2018; Wilson & Russell, 2018; Venugopal, 2019; Grasby et al., 2020), volcanic hazard assessments should be carried out, with the use of numerical models, considering a scenario-based approach in order to capture a range of reasonable hazard characteristics and outcomes. Not all hazard assessments of individual volcanoes will appropriately fit the methods and programs used for this study. For example, a volcanic hazard that was not explored in this study of Mount Meager is lava flows, but they could be very prevalent features from future eruptions of other volcanoes in Canada. Modelling of a past lava flow has been produced for Tseax Volcano, a mafic volcanic system in northwestern BC. This project used VolcFlow to numerically model the emplacement of the lava flow that was deposited onto the landscape over 250 years ago (Le Moigne, 2020).

### 4.1.1. Long-term hazard modelling

A goal of this project has been to use different numerical modelling software programs in order to compare results and to comment on the performance of those programs. This was carried out for the lahar flow and ashfall modelling programs. There are clear benefits and drawbacks for each program used here and the applications for which they perform best. The deliverables and communicability of results from each program differ and may be better suited for different functions. Some differences include probabilistic versus deterministic models, semi-empirical based versus geophysical based or suited-to-crisis situations versus a long-term hazard assessment. In the following section, the programs used for each hazard will be discussed and compared with a comment made for which context they may be best suited for in future Canadian volcanic hazard assessments. The needs for the development of understanding the volcanic landscape across Canada (specifically British Columbia and Yukon) are inherently dynamic, for example, a crisis assessment is unnecessary as there are currently no known or impending explosive eruptions.

### 4.1.2. LAHARZ vs. VolcFlow Comparison

Modelling of lahar flows was completed with LAHARZ and VolcFlow, both producing inundation maps. While LAHARZ is fast and computationally simple, VolcFlow is more powerful with respect to opportunities for investigating the rheological conditions of the flow (thickness, velocity, flow morphology), in addition to the investigation of surface inundation.

In all scenarios, LAHARZ produces longer lahar runout distances than VolcFlow. The differences are on the order of ~ 6 km for equivalent scenario 2 simulations and ~ 10 km for equivalent scenario 3 simulations. As previously noted, LAHARZ is a semi-empirical program based on the observations of 27 previous lahar flows. The environment and physical parameters that are specific to Mount Meager might not be well represented by the statistical analysis of other, unrelated volcanic environments. This is particularly clear for the landscape surrounding Mount Meager, a complex topography, where the mountainous terrane leads to constricted runout paths in mountainous valleys. While this is conducive to channelization which can encourage flow propagation, narrow portions of the valleys may also serve as constriction points encouraging some degree of ponding, or stopping flow movement. It appears that LAHARZ does not capture these “choke points”, especially in the case of large volume flows. In contrast, VolcFlow does since it is a depth-averaged geophysical model, which affects the final runout lengths.

Lahar lengths are also different between the two methods due to the differences in points of measurement. For VolcFlow, the lahar lengths were calculated from a) points close to b) the designated initiation point to the modelled end points. LAHARZ is a semi-empirical model considering deposition, it is not suitable for modelling the entire flow interface including sections of erosion. Lahar length is calculated from a) the point of intersection between stream flow and the energy cone boundary to b) the modelled end points (length of deposition). VolcFlow aims to model the entire flow propagation, which is a fundamental difference between the two modelling methods.

A clear advantage of VolcFlow is the output data that can be extracted and investigated from the program including propagation time, flow thickness, and flow dynamics. These parameters are not inherently available from the LAHARZ program.

These are additional, invaluable details for hazard management considerations and the development of a monitoring system. For this reason, VolcFlow is a beneficial program to utilize in the development of a long-term hazard management strategy. However, VolcFlow is complex, time-consuming and computationally expensive which makes it impractical for use during a crisis situation. LAHARZ would be an effective on-site tool to rapidly produce hazard maps contingent on the current situation requiring limited input data which can be run in a short time frame.

### 4.1.3. Ash3d vs. TephraProb

Part of this study included obtaining probabilistic maps for tephra deposition through the use of TephraProb and Ash3d (basic web interface). An attempt was made to probabilistically model the tephra deposition, as a more rigorous statistically relevant measure of the hazard. This was achieved by TephraProb, but results from Ash3d are considered quasi-probabilistic, as only the wind profile was varied. The obvious difference between the two programs is that the production of probabilistic maps and assessments are built into TephraProb while this is not the case for Ash3d. Using geostatistical tools available in ArcMap, a simplified probabilistic map can be produced from Ash3d tephra deposit results. The end product, however, cannot be accurately compared to the results of TephraProb as the processing is based on fundamentally different results. TephraProb is a probabilistic analysis in that it produces statistics based on multiple iterations of the model choosing from input parameters that include a range of values for eruption height and mass eruption rate. In addition, the software includes a wind data parameter which simulates 10 years of wind patterns. For this project using Ash3d, only 1 year of sporadic simulations were acquired with wind patterns being the only changing parameter and no range given to any other input parameters. Therefore, a comparison of the results, critiquing the probabilistic analysis would be unreasonable, as one model is a probabilistic approach and the other was, in essence, a deterministic approach.

Both TephraProb and Ash3d produce data for the hazard characteristics of ashfall. For Ash3d results, the pattern of deposition across all scenarios is chaotic and shows no trends of preferential directionality. The same is not true for results from TephraProb. This is likely due to the difference in spatial timeframe of the wind data parameter. Ash3d data only represents a year, while wind data was obtained for a longer

time-period for TephraProb, resulting in a more statistically robust outcome. The publically available, web-interface version of Ash3d is clearly more suited to capture the tephra hazard characteristics of a specified day (or current condition). However, the accessibility of the program is not reliable (while running daily models, some days the web-interface was unavailable), in addition Ash3d is not intended for use as an official forecast model without permission and collaboration with the USGS.

A key difference between the two computer models is that Ash3d can also model ash clouds. Over the course of using Ash3D for one year, it was concluded that an ash cloud stemming from an eruption at Mount Meager could be directed in almost any direction, while most prominently affecting the air space of southwest British Columbia. In addition, model outcomes show that ash could travel across North America. However, directionality and impact from the ash cloud is dependent on the airport coordinate database used by Ash3d. As such, ash cloud impact appears to be limited directionally north of Mount Meager, where airport locations may be sparse or non-existent in the Ash3d database.

TephraProb is well suited for long-term hazard analysis, investigating probabilistic ashfall outcomes. Ash3d serves as a simple, user-friendly interface for investigating ash cloud and ashfall hazards as a preliminary investigation of a potentially explosive eruption.

## 4.2. Summary and Conclusions

A suite of preliminary scenario-based volcanic hazard maps have been created for Mount Meager volcano. These hazard maps display a range of hazard phenomena that could reasonably occur from a future explosive eruption stemming from this potentially active system in southwest British Columbia. The range of volcanic hazard phenomena included on maps representing scenarios 1, 2 and 3 (small magnitude to large magnitude eruptions) is appropriate in communicating the multi-hazard phenomena that stem from explosive volcanic eruptions.

These maps and scenario descriptions primarily convey the spatial extent of impacts that could occur from a future phase of volcanism at Mount Meager, which is currently in a phase of relative quiescence, apart from a dynamic fumarole field on Job

Glacier, in the northeast section of the complex and the presence of hot springs in close proximity. Across all scenarios, segments of the upper Lillooet River are impeded by the modelled hazards: lahars, pyroclastic flows and ashfall. The spatial extent naturally extends with greater volume inputs and simulations of larger magnitude eruptions. In scenarios 2 and 3, PDCs (VEI ≥ 3, volume ≥ $1 \times 10^6$ $m^3$) potentially entirely cover and extend past the margins of upper Lillooet River and Meager Creek to a maximum radius of ~12 km from volcanic peaks (precise drainage basin impact would depend on location of eruption vent). Ultimately, lahars are simulated to flow downstream, directed down Meager Creek and/or Lillooet River (depending on origin), with a maximum runout length of ~40 km (scenario 3, volume $1 \times 10^8$ $m^3$). This distance marks the entrance of Pemberton Meadows, an area of agricultural land just north of Pemberton. Ashfall and ash clouds naturally impact proximal-to-distal regions, as tephra is an atmospherically transported volcanic phenomena. Across all scenarios, southwest British Columbia is simulated to receive the bulk of ashfall with regions most likely to be impacted to the NE of Mount Meager.

The challenges faced in this thesis included a lack of geologic data or clearly defined eruptive history and minimal precedent for producing volcanic hazard assessments for the Canadian context. These challenges have been addressed and overcome with the use of numerical models and simulations organized into three scenarios depicting varying eruptive episodes.

# Chapter 5.

# Conclusions and Future Work

To date there has only been one volcanic hazard map developed in Canada, for the Nazko cone region at the eastern end of the Anahim Volcanic Belt (Hickson et al., 2009). The expansion of research for volcanic hazards in Canada and recognition of potentially active systems is much needed to address the vulnerability that volcanic landscapes pose to Canadians (specifically in B.C. and Yukon). This thesis presents the volcanic hazard assessment and scenario-based hazard maps created for Mount Meager Volcanic Complex which communicates the multi-hazard phenomena that could be expected from the next phase of explosive volcanism at this system. This assessment will help us to better understand hazards posed by an explosive eruption from Mount Meager. Importantly, this work can be used to target mitigation strategies and move towards disaster risk reduction and ultimately, community resilience.

Mount Meager is a potentially active volcanic system in southwest British Columbia, 150 km north of Vancouver. There are several reasons for choosing this system for a comprehensive volcanic hazard assessment, including:

- Ongoing surface expressions as evidence of potential volcanic activity (a fumarole field and several geothermal springs in close proximity to the complex) (Roberti, 2018; Venugopal, 2019).
- Status as a known geohazard landscape and the site of Canada's largest landslide (occurred in 2010) as well as ongoing occurrences of slope failure (e.g., Roberti et al., 2018).
- Proximal location to nearby communities (Pemberton, 60 km southwest) including the Lil'wat First Nation and active infrastructure operations within 5 km of the base of the complex (run-of-river hydroelectric project, logging, pumice mining, geothermal interests).
- Well-constrained eruptive hazard characteristics of the last known explosive eruption, occurring in 2360 cal yr B.P. (Stasiuk, et al., 1996; Hickson, et al., 1999; Andrews et al., 2014).

**Figure 5.1 Glacio-volcanic landscape on Job Glacier, NE section of Mount Meager. One of two fumaroles breaching the surface of Job Glacier, as evidence of potential volcanic activity, September 2018.**

The primary objective of this thesis was to create a volcanic hazard assessment and map for Mount Meager, which was achieved with the guidance of a few research questions first introduced in Chapter 1, and summarized answers provided in the following table.

**Table 5.1 Research objectives and summary of outcomes from this thesis**

| Question 1: What are the main hazards of concern for future eruptive activity at Mount Meager? |
| --- |
| Proximal Hazards:<br>• Pyroclastic Density Currents (PDCs): in-situ geologic deposit from the last explosive eruption includes the remnants of a ~ 110 m tall welded block-and-ash flow dam, built-up from the successive deposition of several PDC flows (Andrews et al., 2014).<br>• Lahars: snow and ice covered volcanoes are particularly susceptible to large volume lahars; the Armero tragedy of 1985 eruption of Nevado del Ruiz is a notable example (Voight, 1990). Geologic evidence also suggests the periodic occurrence of large volume debris flows originating from Mount Meager (Friele, et al., 2008). While these are mostly secondary hazards, they are evidence of the capabilities of geophysical flow volumes that could occur during future eruptions.<br>Proximal-to-distal hazards:<br>• Volcanic ash: ash attributed to the 2360 cal yr B.P. eruption has been identified as far away as ~ 500 km east, in Alberta (Stasiuk et al., 1996). As a volcanic hazard transported in the atmosphere, this hazard has the broadest potential impact. While consequences are not often fatal, it can cause immense economic damage, affecting aviation and critical infrastructure. |

| |
|---|
| Question 2: How to develop an effective hazard assessment and map for a relatively remote volcanic system with limited geologic or background volcanic data? |
| • Strategy includes a scenario-based approach utilizing numerical models with input parameters informed by the 2360 cal yr B.P. eruption and well-studied analogous volcanoes.<br>  ○ Characteristics of analogous volcanoes emphasised glacier-clad subduction zone stratovolcanoes. Examples include: Mt. St. Helens, Nevado del Ruiz and Cotopaxi volcanoes.<br>• Largely deterministic, scenario-based approach chosen to capture a range of reasonable eruptive magnitudes and hazard characteristics.<br>• Numerical model-based study rather than classic geological approach in order to address the problem of limited geologic evidence from past eruptions. |
| Question 3: What are reasonable expectations from a future eruption at Mount Meager? |
| • Scenario 1 (small magnitude eruption): impact will be restricted to the immediate vicinity of Mount Meager, no population centres are likely to be directly impacted by lahars, PDCs or ashfall.<br>• Scenario 2 (mid-magnitude eruption): impact region extends beyond that of scenario 1, with Meager Creek and Lillooet River likely to be inundated by both PDCs and lahars but not directly impacting nearby communities. Ashfall may impact the town of Gold Bridge, NE of Mount Meager.<br>• Scenario 3 (large magnitude eruption): PDC deposits have the capacity to fully inundate the main drainage systems at the base of the complex but will not directly inundate any residential communities. Lahars will flow down-stream in the Lillooet River towards Pemberton, potentially affecting the upper portion of Pemberton Meadows (but not directly inundating the community of Pemberton). Ashfall will impact areas of southwest BC, likely directed northeast and east of the complex. |

## 5.1. Additional Hazards

Within the scope of this thesis, only primary volcanic hazards were considered and three hazard phenomena were chosen for the focus of the first iteration of a volcanic hazard assessment for Mount Meager. Volcanic eruptions are multi-hazardous events, as such there are in fact, more than three individual hazards that could result from an eruption, and more phenomena to consider as secondary hazards that could occur outside the time-frame of an eruptive event.

Other hazards to be aware of include: growth/movement of the fumarole field within Job Glacier or extending to other parts of the glacier system, with implications for hazardous volcanic gases. The stability of the glacier is also in question with collapse of ice-caves due to gas accumulation and melting being highly likely; this hazard needs to be considered when people visit the glacier. Lava dome growth and lava flows are also likely features of the next phase of volcanism. These features may only be restricted to the confines of volcano slopes themselves due to the petrological characteristics of the system (dacitic/andesitic composition) and therefore have minimal direct implications to human activity in the vicinity of Mount Meager. They will, however, alter topography, possibly changing the course of the simulated hazards in this thesis. The failure of lava flow fronts and/or dome collapse were also the cause and instigation of PDCs during the last major eruption (Stasiuk et al., 1996), with implications for the propagation of the PDC hazard considered here. Secondary lahars may occur for an indefinite time period following an eruption. As such, lahars are extremely unpredictable and mitigation necessitates the installation of a lahar detection system that monitors the arrival and passage of mass movements. Debris flows, whether considered as separate slope failure events or related to the volcano itself, are known hazards of Mount Meager.

## 5.2. Future Work

The hazard assessment detailed in this thesis acts as one important step towards the development of a robust and reliable disaster risk reduction strategy that should be developed for Mount Meager; this approach should be considered for other volcanic settings in western Canada. This hazard assessment also serves to raise awareness and understanding of the hazards posed by volcanic systems in Canada. With recognition as a multi-geohazard landscape, a monitoring network should be

developed (e.g., regular gas and geochemical sampling of fumaroles and hot springs, automated detection system for mass movement, dedicated seismic station network, analysis of Interferometric Synthetic Aperture Radar (InSAR) images). Not only will this be of immediate benefit for ongoing human activity in the vicinity of the volcano, but data from this network could also be used for further development and improvement of the hazard assessment. This work would also be improved with the addition of accurate knowledge of previous eruptions, in order to constrain eruptive frequencies expected from this system. With the addition of background volcanic signals and eruptive frequency information, a new hazard assessment could be tailored to specific data concerning Mount Meager, rather than depending on analogous volcanic parameters. Periodic updating of the hazard map with new information for Mount Meager, or the advent of new or updated hazard map programs is vital for consideration of successful hazard mitigation and management. Finally, future work should also include a complementary risk analysis which would be beneficial in understanding the scope of impact from the hazards posed by Mount Meager.

# References


Andrews, G. D. M., Russell, J. K., & Stewart, M. L. (2014). The history and dynamics of a welded pyroclastic dam and its failure. *Bulletin of Volcanology*, *76*(4), 1–16. https://doi.org/10.1007/s00445-014-0811-0

Ang, P. S., Bebbington, M. S., Lindsay, J. M., & Jenkins, S. F. (2020). From eruption scenarios to probabilistic volcanic hazard analysis: An example of the Auckland Volcanic Field, New Zealand. *Journal of Volcanology and Geothermal Research*, *397*, 106871. https://doi.org/10.1016/j.jvolgeores.2020.106871

Auker, M. R., Sparks, R. S. J., Siebert, L., Crosweller, H. S., & Ewert, J. (2013). A statistical analysis of the global historical volcanic fatalities record. *Journal of Applied Volcanology*, *2*(2). https://doi.org/10.1186/2191-5040-2-2

Barker, S. J., Van Eaton, A. R., Mastin, L. G., Wilson, C. J. N., Thompson, M. A., Wilson, T. M., … Renwick, J. A. (2019). Modeling ash dispersal from future eruptions of Taupo supervolcano. *Geochemistry, Geophysics, Geosystems*, *20*(7), 3375–3401. https://doi.org/10.1029/2018GC008152

Bernard, B., Battaglia, J., Proaño, A., Hidalgo, S., Vásconez, F., Hernandez, S., & Ruiz, M. (2016). Relationship between volcanic ash fallouts and seismic tremor: quantitative assessment of the 2015 eruptive period at Cotopaxi volcano, Ecuador. *Bulletin of Volcanology*, *78*(11), 1–11. https://doi.org/10.1007/s00445-016-1077-5

Bernstein, R. S., Baxter, P. J., Falk, H., Ing, R., Foster, L., & Frost, F. (1986). Immediate public health concerns and actions in volcanic eruptions: Lessons from the Mount St. Helens eruptions, May 18-October 18, 1980. *American Journal of Public Health*, *76*, 25–37. https://doi.org/10.2105/AJPH.76.Suppl.25

Biass, S., Todde, A., Cioni, R., Pistolesi, M., Geshi, N., & Bonadonna, C. (2017). Potential impacts of tephra fallout from a large-scale explosive eruption at Sakurajima volcano, Japan. *Bulletin of Volcanology*, *79*(10). https://doi.org/10.1007/s00445-017-1153-5

Biass, Sébastien, Bonadonna, C., Connor, C., & Connor, L. (2016a). *TephraProb User Manual*. https://doi.org/10.5281/zenodo.3590721

Biass, Sébastien, Bonadonna, C., Connor, L., & Connor, C. (2016b). TephraProb: a Matlab package for probabilistic hazard assessments of tephra fallout. *Journal of Applied Volcanology*, *5*(1). https://doi.org/10.1186/s13617-016-0050-5

Bonadonna, C., Connor, C. B., Houghton, B. F., Connor, L., Byrne, M., Laing, A., & Hincks, T. K. (2005). Probabilistic modeling of tephra dispersal: Hazard assessment of a multiphase rhyolitic eruption at Tarawera, New Zealand. *Journal of Geophysical Research B: Solid Earth*, *110*(3), 1–21. https://doi.org/10.1029/2003JB002896

Bonadonna, C., Folch, A., Loughlin, S., & Puempel, H. (2012). Future developments in modelling and monitoring of volcanic ash clouds: Outcomes from the first IAVCEI-WMO workshop on Ash Dispersal Forecast and Civil Aviation. *Bulletin of Volcanology*, *74*(1), 1–10. https://doi.org/10.1007/s00445-011-0508-6

Bovis, M. J., & Jakob, M. (2000). The July 29, 1998, debris flow and landslide dam at Capricorn Creek, Mount Meager Volcanic Complex, southern Coast Mountains, British Columbia. *Canadian Journal of Earth Sciences*, *37*(10), 1321–1334. https://doi.org/10.1139/e00-042

Brown, S. K., Loughlin, S. C., Sparks, R. S. J., Vye-Brown, C., Barclay, J., Calder, E., … Valentine, G. (2015). Global volcanic hazard and risk. In S. C. Loughlin, R. S. J. Sparks, S. K. Brown, S. F. Jenkins, & C. Vye-Brown (Eds.), *Global Volcanic Hazards and Risk* (pp. 81–172). Cambridge: Cambridge University Press.

Budd, L., Griggs, S., Howarth, D., & Ison, S. (2011). A Fiasco of Volcanic Proportions? Eyjafjallajökull and the Closure of European Airspace. *Mobilities*, *6*(1), 31–40. https://doi.org/10.1080/17450101.2011.532650

Burgisser, A., & Bergantz, G. W. (2002). Reconciling pyroclastic flow and surge: The multiphase physics of pyroclastic density currents. *Earth and Planetary Science Letters*, *202*(2), 405–418. https://doi.org/10.1016/S0012-821X(02)00789-6

Calder, E. S., Wagner, K., & Ogburn, S. E. (2015). Volcanic hazard maps. In S. C. Loughlin, R. S. J. Sparks, S. K. Brown, S. F. Jenkins, & C. Vye-Brown (Eds.), *Global Volcanic Hazards and Risk* (pp. 335–341). Cambridge: Cambridge University Press.

Campbell, M. E., Porritt, L., & Russell, J. K. (2016). Forensic recovery of transient eruption parameters for the 2360 BP fall deposit, Mount Meager, British Columbia. *Journal of Volcanology and Geothermal Research*, *312*, 11–25. https://doi.org/10.1016/j.jvolgeores.2016.01.013

Carey, S., Sigurdsson, H., Mandeville, C., & Bronto, S. (1996). Pyroclastic flows and surges over water: An example from the 1883 Krakatau eruption. *Bulletin of Volcanology*, *57*(7), 493–511. https://doi.org/10.1007/BF00304435

Carey, S., & Sparks, R. S. J. (1986). Quantitative models of the fallout and dispersal of tephra from volcanic eruption columns. *Bulletin of Volcanology*, *48*, 109–125. https://doi.org/10.1007/BF01046546

Carrivick, J. L., Manville, V., & Cronin, S. J. (2009). A fluid dynamics approach to modelling the 18th March 2007 lahar at Mt. Ruapehu, New Zealand. *Bulletin of Volcanology*, *71*(2), 153–169. https://doi.org/10.1007/s00445-008-0213-2

Charbonnier, S. J., Connor, C. B., Connor, L. J., Sheridan, M. F., Oliva Hernández, J. P., & Richardson, J. A. (2018). Modeling the October 2005 lahars at Panabaj (Guatemala). *Bulletin of Volcanology*, *80*(1). https://doi.org/10.1007/s00445-017-1169-x

Clague, J. J., Evans, S. G., Rampton, V. N., & Woodsworth, G. J. (1995). Improved age estimates for the White River and Bridge River tephras, western Canada. *Canadian Journal of Earth Sciences*, *32*, 1172–1179. https://doi.org/10.1139/e95-096

Clague, John J., & Ward, B. (2011). Pleistocene Glaciation of British Columbia. In J. Ehlers, P. L. Gibbard, & P. D. Hughes (Eds.), *Developments in Quaternary Science* (Vol. 15, pp. 563–573). Amsterdam, The Netherlands: Elsevier Inc. https://doi.org/10.1016/B978-0-444-53447-7.00044-1

Denlinger, R. P. (1987). A Model for Generation of Ash Clouds by Pyroclastic Flows, With Application to the 1980 Eruptions at Mount St . Helens, Washington. *Journal of Geophysical Research*, *92*(B10), 10,284-10,298.

Druitt, T. H. (1998). Pyroclastic density currents. In J. S. Gilbert & R. S. J. Sparks (Eds.), *The Physics of Explosive Volcanic Eruptions* (pp. 145–182). London: Geological Society, Special Publications.

Edwards, B. R., & Russell, J. K. (1999). Northern Cordilleran volcanic province: A northern Basin and range? *Geology*, *27*(3), 243–246. https://doi.org/10.1130/0091-7613(1999)027<0243:NCVPAN>2.3.CO;2

Evans, S. G. (1987). A rock avalnche from the peak of Mount Meager, British Columbia. In *Current Research, Part A* (Paper 87-1, pp. 929–934). Geological Survey of Canada. https://doi.org/10.1017/CBO9781107415324.004

Fagents, S. A., & Baloga, S. M. (2006). Toward a model for the bulking and debulking of lahars. *Journal of Geophysical Research: Solid Earth*, *111*(10), 1–21. https://doi.org/10.1029/2005JB003986

Falkenstrøm, J., Bell, N., Kotsia, R. M., Taleb, F., Kamal, Z. A., & Marco, S. H. (2014). *Assessing the risk of fluorine poisoning of Icelandic livestock by an explosive eruption from Hekla volcano*. Roskilde University College. Retrieved from http://rudar.ruc.dk:8080/handle/1800/22706

Farley, K. A., Rusmore, M. E., & Bogue, S. W. (2001). Post-10 Ma uplift and exhumation of the northern Coast mountains, British Columbia. *Geology*, *29*(2), 99–102. https://doi.org/10.1130/0091-7613(2001)029<0099:PMUAEO>2.0.CO;2

Fisher, R. (1964). Maximum Size, Median Diameter, Sorting of Tephra. *Journal of Geophysical Research*, *69*(2), 341–355. https://doi.org/10.1029/JZ069i002p00341

Fisher, R. V., & Schmincke, H.-U. (1984). *Pyroclastic rocks*. Berlin: New York: Springer-Verlag.

Friele, P. (2012). *Volcanic Landslide Risk Management, Lillooet River Valley, BC: Start of north and south FSRs to Meager Confluence, Meager Creek and Upper Lillooet River .* Retrieved from https://www.for.gov.bc.ca/dsq/Engineering/VolcanicLandslideRiskManagement.pdf

Friele, P. A., Clague, J. J., Simpson, K., & Stasiuk, M. (2005). Impact of a Quaternary volcano on Holocene sedimentation in Lillooet River valley, British Columbia. *Sedimentary Geology*, *176*(3–4), 305–322. https://doi.org/10.1016/j.sedgeo.2005.01.011

Friele, P., Jakob, M., & Clague, J. (2008). Hazard and risk from large landslides from Mount Meager volcano, British Columbia, Canada. *Georisk: Assessment and Management of Risk for Engineered Systems and Geohazards*, *2*(1), 48–64. https://doi.org/10.1080/17499510801958711

Friele, Pierre A., & Clague, J. J. (2004). Large Holocene landslides from Pylon Peak, southwestern British Columbia. *Canadian Journal of Earth Sciences*, *41*, 165–182. https://doi.org/10.1139/E03-089

Global Volcanism Program. (1980). *Report on St. Helens (United States)*. (D. Squires, Ed.), *Scientific Event Alert Network Bulletin* (Vol. 5). Smithsonian Institution. https://doi.org/10.5479/si.GVP.SEAN198005-321050

Global Volcanism Program. (2016). *Report on Cotopaxi (Ecuador)*. *Bulletin of the Global Volcanism Network* (Vol. 41). Retrieved from https://doi.org/10.5479/si.GVP.BGVN201604-352050

Grasby, S. E., Ansari, S. M., Bryant, R., Calahorrano-DiPatre, A., Chen, Z., Craven, J. A., … Williamson, A. . (2020). *Garibaldi Geothermal Energy Project: Mount Meager 2019 - Field Report*. Retrieved from http://www.geosciencebc.com/projects/2018-004/

Green, N. L., Armstrong, R. L., Harakal, J. E., Souther, J. G., & Read, P. B. (1988). Eruptive history and K-Ar geochronology of the late Cenozoic Garibaldi volcanic belt, southwestern British Columbia. *Bulletin of the Geological Society of America*, *100*(4), 563–579. https://doi.org/10.1130/0016-7606(1988)100<0563:EHAKAG>2.3.CO;2

Green, N. L., & Harry, D. L. (1999). On the relationship between subducted slab age and arc basalt petrogenesis, Cascadia subduction system, North America. *Earth and Planetary Science Letters*, *171*(3), 367–381. https://doi.org/10.1016/S0012-821X(99)00159-4

Griswold, J. P., & Iverson, R. M. (2008). *Mobility statistics and automated hazard mapping for debris flows and rock avalanches*. Reston, VA. https://doi.org/10.3133/sir20075276

Gueugneau, V. (2014). *Evaluation du logiciel VolcFlow pour la simulation numérique de lahars et application aux risques associés* (Master's Thesis). Université Blaise Pascal Clermont II.

Guffanti, M., Mayberry, G. C., Casadevall, T. J., & Wunderman, R. (2009). Volcanic hazards to airports. *Natural Hazards*, *51*(2), 287–302. https://doi.org/10.1007/s11069-008-9254-2

Guthrie, R. H., Friele, P., Allstadt, K., Roberts, N., Evans, S. G., Delaney, K. B., … Jakob, M. (2012). The 6 August 2010 Mount Meager rock slide-debris flow, Coast Mountains, British Columbia: Characteristics, dynamics, and implications for hazard and risk assessment. *Natural Hazards and Earth System Science*, *12*(5), 1277–1294. https://doi.org/10.5194/nhess-12-1277-2012

Herd, D. G. (1986). The 1985 Ruiz Volcano Disaster. *Eos Trans. AGU*, *67*(19), 457–460. https://doi.org/10.1029/EO067i019p00457-03

Hetherington, R. (2014). *Slope Stability Analysis of Mount Meager, South-Western British Columbia, Canada* (Master's thesis). Michigan Technological University. Retrieved from http://digitalcommons.mtu.edu/etds/764

Hickson, C. J. (1994). Volcanic hazards and volcanism in the Canadian Cordillera. In T. J. Casadevall (Ed.), *Volcanic Ash and Aviation Safety: Proceedings of the First International Symposium on Volcanic Ash and Aviation Safety* (pp. 47–56). Seattle: United States Geological Survey, Bulletin 2047.

Hickson, C. J., Kelman, M. C., Chow, W., Shimamura, K., Servranckx, R., Bensimon, D., … Wiliams-Jones, G. (2009). Nazko Region Volcanic hazard Map. *Geological Survey of Canada Open File 5978*. https://doi.org/10.4095/247379

Hickson, C. J., Russell, J. K., & Stasiuk, M. V. (1999). Volcanology of the 2350 B.P. eruption of Mount Meager volcanic complex, British Columbia, Canada: Implications for hazards from eruptions in topographically complex terrain. *Bulletin of Volcanology*, *60*(7), 489–507. https://doi.org/10.1007/s004450050247

Horwell, C. J., & Baxter, P. J. (2006). The respiratory health hazards of volcanic ash: A review for volcanic risk mitigation. *Bulletin of Volcanology*, *69*(1), 1–24. https://doi.org/10.1007/s00445-006-0052-y

Iverson, R. M. (1997). The Physics of Debris Flows. *Reviews of Geophysics*, *35*(3), 245–296. https://doi.org/10.1029/97RG00426;

Iverson, R. M., Schilling, S. P., & Vallance, J. W. (1998). Objective delineation of lahar-inundation hazard zones. *Bulletin of the Geological Society of America*, *110*(8), 972–984. https://doi.org/10.1130/0016-7606(1998)110<0972:ODOLIH>2.3.CO;2

Jensen, B. J. L., Beaudoin, A. B., Clynne, M. A., Harvey, J., & Vallance, J. W. (2019). A re-examination of the three most prominent Holocene tephra deposits in western Canada: Bridge River, Mount St. Helens Yn and Mazama. *Quaternary International*, *500*, 83–95. https://doi.org/10.1016/j.quaint.2019.03.017

Jordan, R. P. (1994). *Debris Flows in the Southern Coast Mountains , British Columbia : Dynamic Behaviour and Physical Properties* (Doctoral dissertation). University of British Columbia. Retrieved from https://circle.ubc.ca/handle/2429/8796

Kataoka, K. S., Matsumoto, T., Saito, T., Kawashima, K., Nagahashi, Y., Iyobe, T., … Suzuki, K. (2018). Lahar characteristics as a function of triggering mechanism at a seasonally snow-clad volcano: contrasting lahars following the 2014 phreatic eruption of Ontake Volcano, Japan. *Earth, Planets and Space*, *70*(1). https://doi.org/10.1186/s40623-018-0873-x

Kelfoun, K., & Vallejo Vargas, S. (2016, January). VolcFlow capabilities and potential development for the simulation of lava flows. (A. J. L. Harris, T. De Groeve, F. Garel, & S. A. Carn, Eds.), *Detecting, Modelling and Responding to Effusive Eruptions*. Geological Society of London. https://doi.org/10.1144/SP426.8

Le Moigne, Y. (2020). *Chapter 5 - Dynamics of the 1700 CE Tseax Lava Flow - Insights from Numerical Modelling* (Doctoral dissertation). Simon Fraser University.

Lindsay, J. M., & Robertson, R. E. A. (2018). Integrating Volcanic Hazard Data in a Systematic Approach to Develop Volcanic Hazard Maps in the Lesser Antilles. *Frontiers in Earth Science*, *6*(42), 1–17. https://doi.org/10.3389/feart.2018.00042

Mastin, L. G., Randall, M. J., Schwaiger, H. F., & Denlinger, R. P. (2013). *User's Guide and Reference to Ash3d — A Three-Dimensional Model for Eulerian Atmospheric Tephra Transport and Deposition*. *U.S. Geological Survey Open-File Report 2013-1122*. Retrieved from https://pubs.usgs.gov/of/2013/1122

Mastin, L. G., Schwaiger, H., Schneider, D. J., Wallace, K. L., Schaefer, J., & Denlinger, R. P. (2013). Injection, transport, and deposition of tephra during event 5 at Redoubt Volcano, 23 March, 2009. *Journal of Volcanology and Geothermal Research*, *259*, 201–213. https://doi.org/10.1016/j.jvolgeores.2012.04.025

Michol, K. A., Russell, J. K., & Andrews, G. D. M. (2008). Welded block and ash flow deposits from Mount Meager, British Columbia, Canada. *Journal of Volcanology and Geothermal Research*, *169*(3–4), 121–144. https://doi.org/10.1016/j.jvolgeores.2007.08.010

Mingo, L., & Flowers, G. E. (2010). Instruments and Methods An integrated lightweight ice-penetrating radar system. *Journal of Glaciology*, *56*(198), 709–714. https://doi.org/10.3189/002214310793146179

Mullen, E. K., & Weis, D. (2013). Sr-Nd-Hf-Pb isotope and trace element evidence for the origin of alkalic basalts in the Garibaldi Belt, northern Cascade arc. *Geochemistry, Geophysics, Geosystems*, *14*(8), 3126–3155. https://doi.org/10.1002/ggge.20191

Mullen, E., Paquette, J.-L., Tepper, J. H., & McCallum, I. S. (2018). Temporal and spatial evolution of Northern Cascade Arc magmatism revealed by LA-ICP-MS U-Pb zircon dating. *Canadian Journal of Earth Sciences*, *55*(5), 443–462. https://doi.org/10.1139/cjes-2017-0167

Muñoz-Salinas, E., Castillo-Rodríguez, M., Manea, V., Manea, M., & Palacios, D. (2009). Lahar flow simulations using LAHARZ program : Application for the Popocatépetl volcano , Mexico. *Journal of Volcanology and Geothermal Research*, *182*, 13–22. https://doi.org/10.1016/j.jvolgeores.2009.01.030

Newhall, C. G., & Self, S. (1982). The volcanic explosivity index (VEI) an estimate of explosive magnitude for historical volcanism. *Journal of Geophysical Research*, *87*(C2), 1231. https://doi.org/10.1029/JC087iC02p01231

Ogburn, S., Berger, J., Calder, E., Lopes, D., Patra, A., Pitman, E. B., … Wolpert, R. (2016). Pooling strength amongst limited datasets using hierarchical Bayesian analysis, with application to pyroclastic density current mobility metrics. *Statistics in Volcanology*, *2*, 1–26. https://doi.org/10.5038/2163-338x.2.1

Ogburn, S. E. (2012). FlowDat - Mass flow database. Vhub Database. Retrieved from https://vhub.org/groups/massflowdatabase

Ogburn, S. E., & Calder, E. S. (2017). The Relative Effectiveness of Empirical and Physical Models for Simulating the Dense Undercurrent of Pyroclastic Flows under Different Emplacement Conditions. *Frontiers in Earth Science*, *5*(83). https://doi.org/10.3389/feart.2017.00083

Patra, A. K., Bauer, A. C., Nichita, C. C., Pitman, E. B., Sheridan, M. F., Bursik, M., … Renschler, C. S. (2005). Parallel adaptive numerical simulation of dry avalanches over natural terrain. *Journal of Volcanology and Geothermal Research*, *139*(1–2), 1–21. https://doi.org/10.1016/j.jvolgeores.2004.06.014

Pierson, T. C., Janda, R. J., Thouret, J. C., & Borrero, C. A. (1990). Perturbation and melting of snow and ice by the 13 November 1985 eruption of Nevado del Ruiz, Colombia, and consequent mobilization, flow and deposition of lahars. *Journal of Volcanology and Geothermal Research*, *41*(1–4), 17–66. https://doi.org/10.1016/0377-0273(90)90082-Q

Pierson, T. C., Wood, N. J., & Driedger, C. L. (2014). Reducing risk from lahar hazards: Concepts, case studies, and roles for scientists. *Journal of Applied Volcanology*, *3*(1), 1–25. https://doi.org/10.1186/s13617-014-0016-4

Prata, F., & Rose, B. (2015). Volcanic Ash Hazards to Aviation. In H. Sigurdsson, B. Houghton, S. McNutt, H. Rymer, & J. Stix (Eds.), *The Encyclopedia of Volcanoes* (2nd ed., pp. 911–934). Elsevier Science & Technology. https://doi.org/10.1016/b978-0-12-385938-9.00052-3

Pyle, D. M. (1989). The thickness, volume and grainsize of tephra fall deposits. *Bulletin of Volcanology*, *51*(1), 1–15. https://doi.org/10.1007/BF01086757

Read, P. B. (1990). Mount Meager Complex, Garibaldi Belt, Southwestern British Columbia. *Geoscience Canada*, *17*(3), 167–170. Retrieved from https://journals.lib.unb.ca/index.php/GC/article/view/3672

Roberti, G., Ward, B., van Wyk De Vries, B., Falorni, G., Menounos, B., Friele, P., … Freschi, S. (2018). Landslides and glacier retreat at Mt. Meager volcano: hazard and risk challenges. In *Geohazards 7 Conference*. Canmore, Alberta: Canadian Geotechnical Society.

Roberti, Gioachino. (2018). *Mount Meager, a glaciated volcano in a changing cryosphere: hazard and risk challenges* (Doctoral dissertation). Simon Fraser University.

Roberti, Gioachino, Friele, P., van Wyk de Vries, B., Ward, B., Clague, J. J., Perotti, L., & Giardino, M. (2017). Rheological evolution of the mount meager 2010 debris avalanche, southwestern british columbia. *Geosphere*, *13*(2), 1–22. https://doi.org/10.1130/GES01389.1

Roberti, Gioachino, Ward, B., van Wyk de Vries, B., Friele, P., Perotti, L., Clague, J. J., & Giardino, M. (2018). Precursory slope distress prior to the 2010 Mount Meager landslide, British Columbia. *Landslides*, *15*(4), 637–647. https://doi.org/10.1007/s10346-017-0901-0

Rouwet, D., Constantinescu, R., & Sandri, L. (2017). Deterministic Versus Probabilistic Volcano Monitoring: Not “or” But “and.” In J. Gottsmann, J. Neuberg, & B. Scheu (Eds.), *Advances in Volcanology* (pp. 35–46). Springer, Cham. https://doi.org/10.1007/11157_2017_8

Scheidegger, A. E. (1973). On the prediction of the reach and velocity of catastrophic landslides. *Rock Mechanics Felsmechanik Mécanique Des Roches*, *5*(4), 231–236. https://doi.org/10.1007/BF01301796

Schilling, S. P. (1998). *LAHARZ; GIS programs for automated mapping of lahar-inundation hazard zones*. *Open-File Report*. https://doi.org/10.3133/ofr98638

Schwaiger, H. F., Denlinger, R. P., & Mastin, L. G. (2012). Ash3d: A finite-volume, conservative numerical model for ash transport and tephra deposition. *Journal of Geophysical Research: Solid Earth*, *117*(4), 1–20. https://doi.org/10.1029/2011JB008968

Scollo, S., Tarantola, S., Bonadonna, C., Coltelli, M., & Saltelli, A. (2008). Sensitivity analysis and uncertainty estimation for tephra dispersal models. *Journal of Geophysical Research*, *113*(B6), 1–17. https://doi.org/10.1029/2006jb004864

Scott, A. C., Sparks, R. S. J., Bull, I. D., Knicker, H., & Evershed, R. P. (2008). Temperature proxy data and their significance for the understanding of pyroclastic density currents. *Geology*, *36*(2), 143–146. https://doi.org/10.1130/G24439A.1

Sheridan, M. F. (1979). Emplacement of pyroclastic flows: A review. In C. E. Chapin & W. E. Elston (Eds.), *Ash-flow Tuffs* (Vol. 180, pp. 125–136). Geological Society of America Special Paper. https://doi.org/https://doi.org/10.1130/SPE180-p125

Simpson, K. A., Stasiuk, M., Shimamura, K., Clague, J. J., & Friele, P. (2006). Evidence for catastrophic volcanic debris flows in Pemberton Valley, British Columbia. *Canadian Journal of Earth Sciences*, *43*(6), 679–689. https://doi.org/10.1139/e06-026

Smith, G. A., & Fritz, W. J. (1989). Volcanic influences on terrestrial sedimentation. *Geology*, *17*(4), 375–376. https://doi.org/10.1130/0091-7613(1989)017<0375:VIOTS>2.3.CO;2

Stasiuk, Mark V., Hickson, C. J., & Mulder, T. (2003). The vulnerability of Canada to volcanic hazards. *Natural Hazards*, *28*(2–3), 563–589. https://doi.org/10.1023/A:1022954829974

Stasiuk, M V, Russell, J. K., & Hickson, C. J. (1996). Distribution, Nature, and Origins of the 2400 BP Eruption Products of Mount Meager, British Columbia: Linkages Between Magma Chemistry and Eruption Behaviour. *Geological Survey of Canada Bulletin*, (486).

Stewart, M L, Russell, J. K., & Hickson, C. J. (2003). Discrimination of hot versus cold avalanche deposits: Implications for hazard assessment at Mount Meager, B.C. *Natural Hazards and Earth System Sciences*, *3*, 713–724. https://doi.org/10.5194/nhess-3-713-2003

Stewart, Martin L. (2002). *Dacite block and ash avalanche Hazards in mountainous terrain: 2360 yr. bp eruption of Mount Meager, British Columbia* (Master's thesis). The University of British Columbia.

Thompson, M. A., Lindsay, J. M., & Leonard, G. S. (2017). More than Meets the Eye: Volcanic Hazard Map Design and Visual Communication. In C. J. Fearnley, D. K. Bird, K. Haynes, W. J. McGuire, & G. Jolly (Eds.), *Advances in Volcanology* (pp. 621–640). Springer, Cham. https://doi.org/10.1007/11157_2016_47

Thompson, M. A., Lindsay, J. M., Wilson, T. M., Biass, S., & Sandri, L. (2017). Quantifying risk to agriculture from volcanic ashfall: a case study from the Bay of Plenty, New Zealand. *Natural Hazards*, *86*(1), 31–56. https://doi.org/10.1007/s11069-016-2672-7

Valentine, G. A. (1987). Stratified flow in pyroclastic surges. *Bulletin of Volcanology*, *49*(4), 616–630. https://doi.org/10.1007/BF01079967

Vallance, J. W. (2000). Lahars. In H. Sigurdsson, B. F. Houghton, S. R. McNutt, H. Rymer, & J. Stix (Eds.), *Encyclopedia of Volcanoes* (pp. 601–616). New York: Elsevier.

Vallance, J. W., & Scott, K. M. (1997). The Osceola Mudflow from Mount Rainier: Sedimentology and hazard implications of a huge clay-rich debris flow. *Bulletin of the Geological Society of America*, *109*(2), 143–163. https://doi.org/10.1130/0016-7606(1997)109<0143:TOMFMR>2.3.CO;2

Vasconez, F., Vasconez, R., & Mothes, P. (2017). *Reconstruccion de los flujos de lodo del volcan Carihuairazo originados por el terremoto de 1698 utilizando el codigo VolcFlow*. https://doi.org/10.13140/RG.2.2.14488.19209

Venugopal, S. (2019). *Magmatic Sources To Volcanic Gas Emissions: Insight From the Garibaldi Volcanic Belt, Western Canada* (Doctoral dissertation). Simon Fraser University.

Venugopal, Swetha, Moune, S., Williams-Jones, G., Wilson, A., & Russell, K. (2017). Gas emissions and magma source of the Mount Meager Volcanic Complex, Garibaldi Volcanic Belt, BC. In *IAVCEI Scientific Assembly Abstracts*. Portland, Oregon.

Voight, B. (1990). The 1985 Nevado del Ruiz volcano catastrophe: anatomy and retrospection. *Journal of Volcanology and Geothermal Research*, *42*(1), 151–188. https://doi.org/10.1016/0377-0273(90)90075-Q

Wadge, G., Voight, B., Sparks, R. S. J., Cole, P. D., Loughlin, S. C., & Robertson, R. E. A. (2014). An overview of the eruption of Soufrière Hills Volcano, Montserrat from 2000 to 2010. *Geological Society Memoir*, *39*(1), 1–39. https://doi.org/10.1144/M39.1

Waythomas, C. F. (2014). Water, ice and mud: Lahars and lahar hazards at ice- and snow-clad volcanoes. *Geology Today*, *30*(1), 34–39. https://doi.org/10.1111/gto.12035

Widiwijayanti, C., Voight, B., & Hidayat, D. (2009). Objective rapid delineation of areas at risk from block-and-ash pyroclastic flows and surges. *Bulletin of Volcanology*, *71*, 687–703. https://doi.org/10.1007/s00445-008-0254-6

Williams, R., Stinton, A. J., & Sheridan, M. F. (2008). Evaluation of the Titan2D two-phase flow model using an actual event: Case study of the 2005 Vazcún Valley Lahar. *Journal of Volcanology and Geothermal Research*, *177*(4), 760–766. https://doi.org/10.1016/j.jvolgeores.2008.01.045

Wilson, A. M., & Russell, J. K. (2018). Quaternary glaciovolcanism in the Canadian Cascade volcanic arc – paleoenvironmental implications. In M. Poland, M. Garcia, V. Camp, & A. Grunder (Eds.), *Field Volcanology: A Tribute to the Distinguished Career of Don Swanson* (Special Pa, pp. 133–157). The Geological Society of America. https://doi.org/10.1130/2018.2538(06)

Wilson, T. M., Stewart, C., Sword-Daniels, V., Leonard, G. S., Johnston, D. M., Cole, J. W., … Barnard, S. T. (2012). Volcanic ash impacts on critical infrastructure. *Physics and Chemistry of the Earth, Parts A/B/C*, *45–46*, 5–23. https://doi.org/10.1016/j.pce.2011.06.006

Wolfe, E. W., & Pierson, T. C. (1995). *Volcanic-hazard zonation for Mount St. Helens, Washington*. *U.S. Geological Survey Open-File Report 95-497*. Retrieved from https://pubs.usgs.gov/of/1995/0497/

Woodward, J., & Burke, M. J. (2007). Applications of ground-penetrating radar to glacial and frozen materials. *Journal of Environmental and Engineering Geophysics*, *12*(1), 69–85. https://doi.org/10.2113/JEEG12.1.69

# Appendix A.

# Individual Lahar flow simulations with LAHARZ

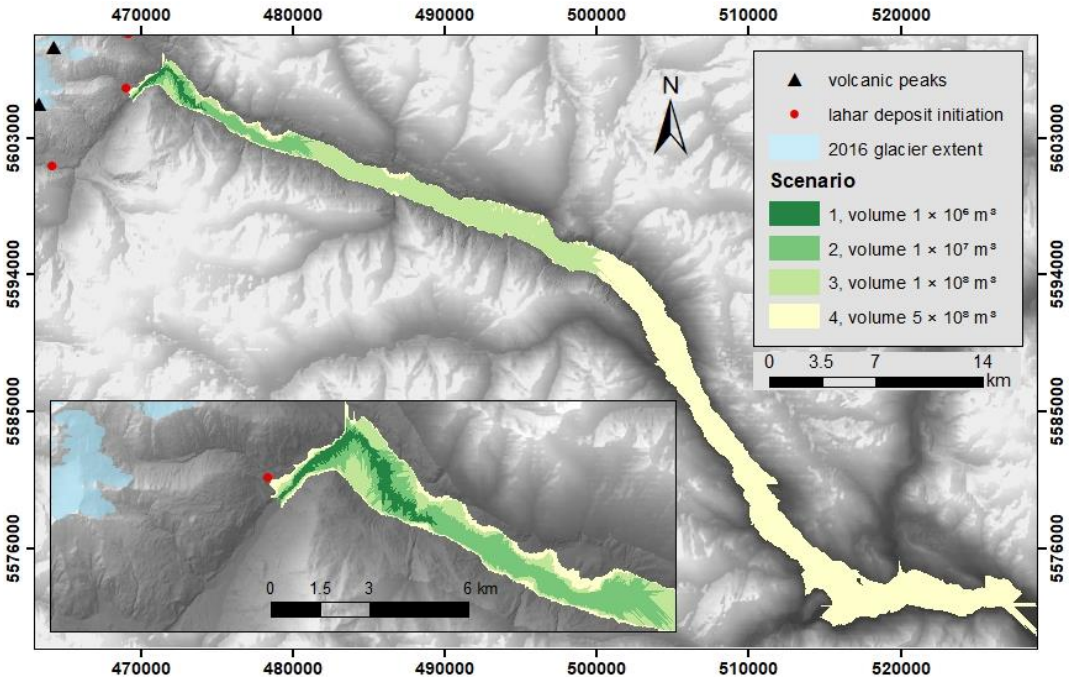


**Figure A.1 Lahar flow output from Capricorn creek basin**

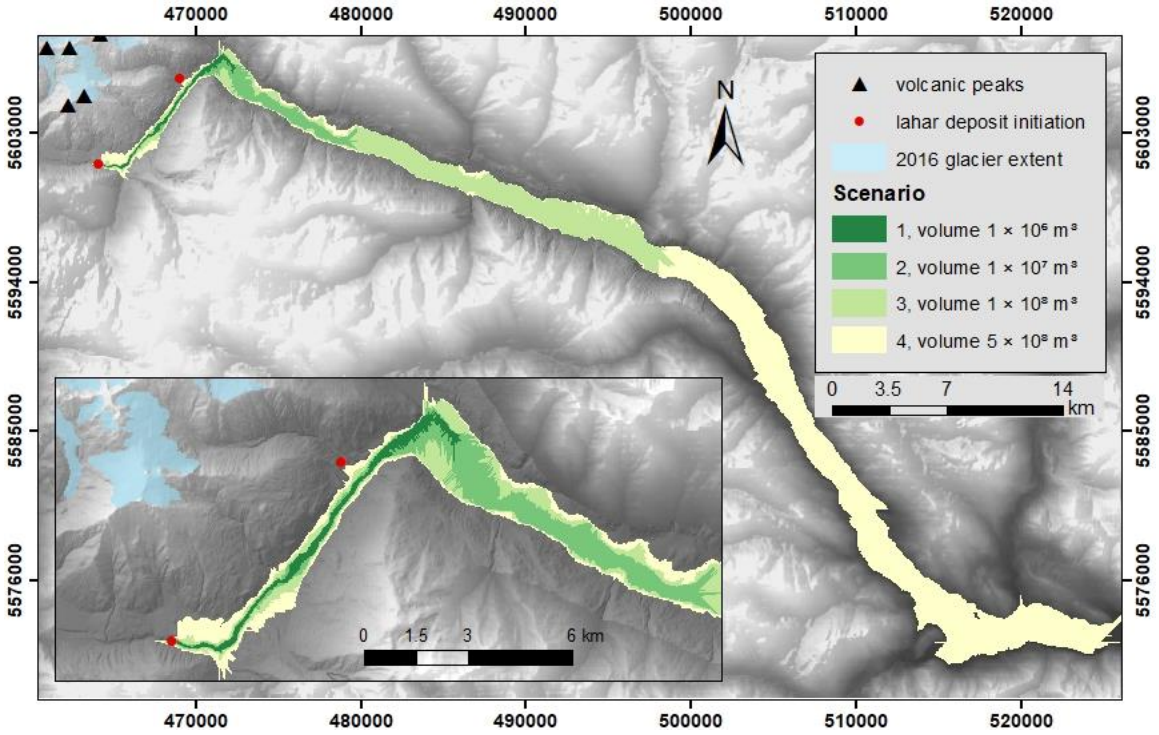


**Figure A.2 Lahar flow output from Devastator Peak basin**

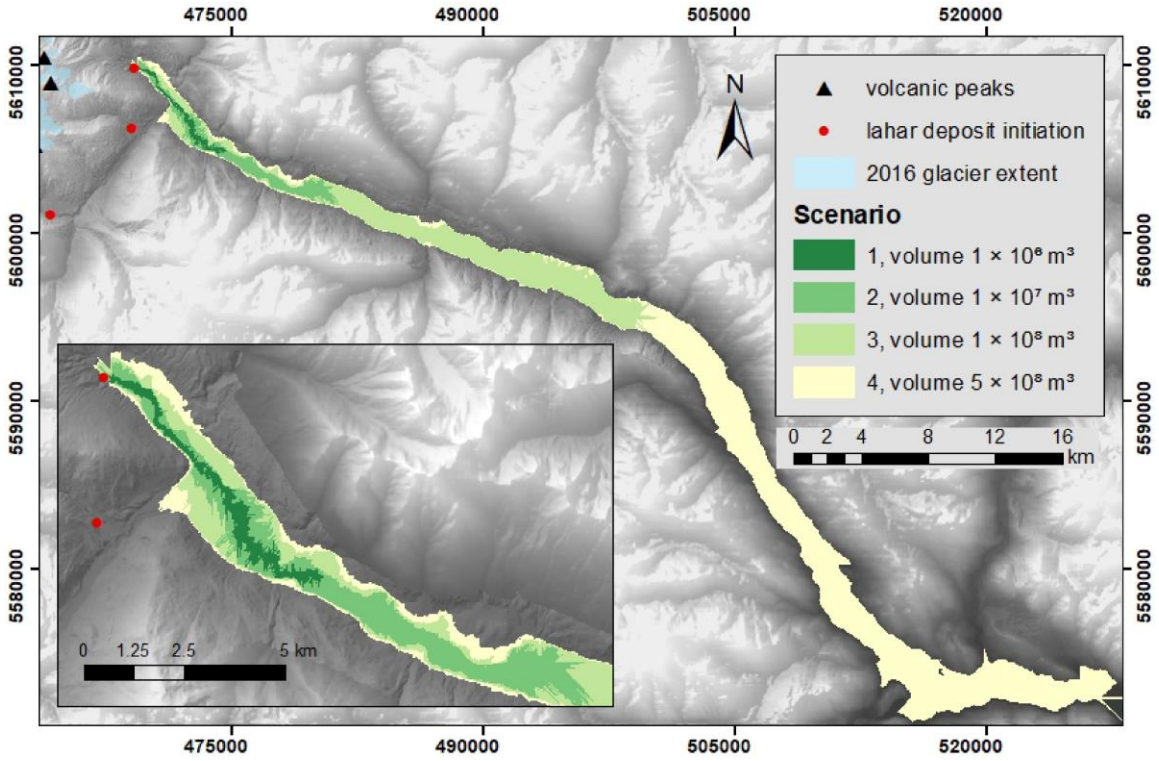


**Figure A.3 Lahar flow output for Mount Meager drainage area**

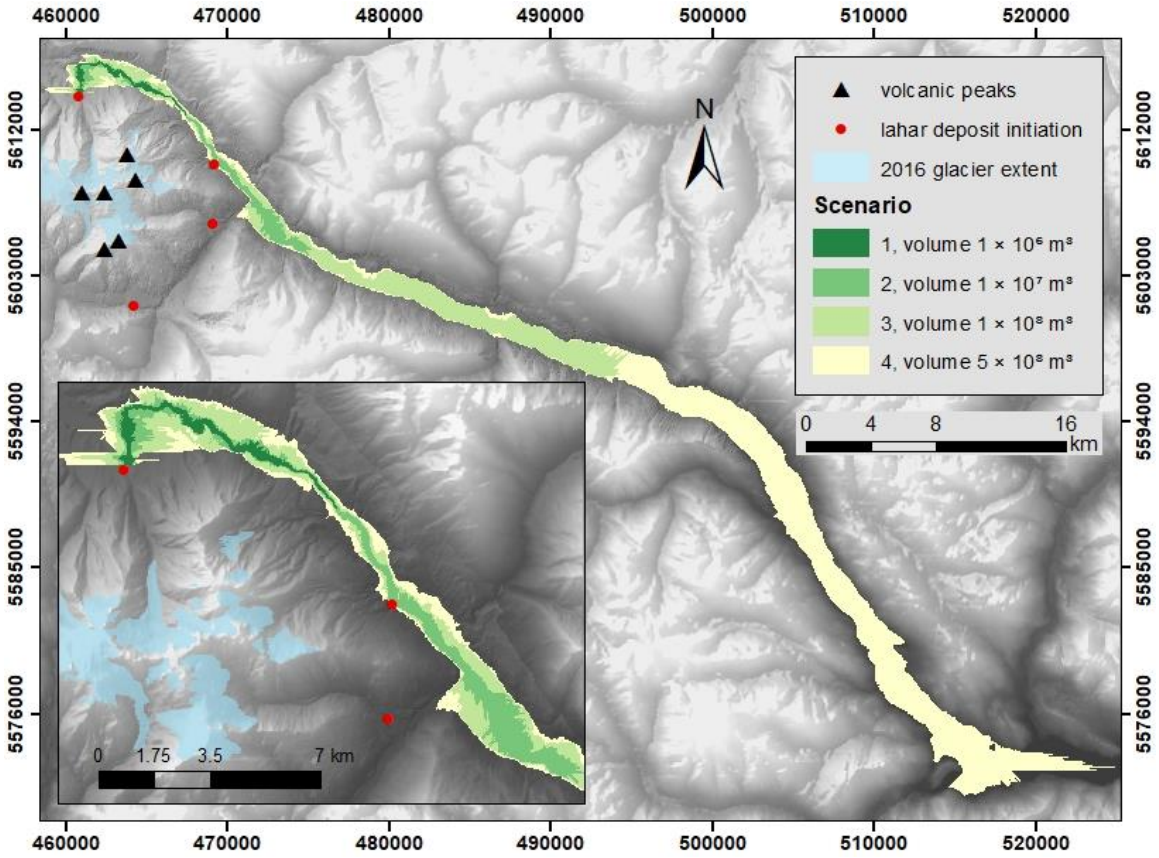


**Figure A.4 Lahar flow output from Job Creek basin**

# Appendix B.

# Pyroclastic Density Current simulations with ΔH/L method

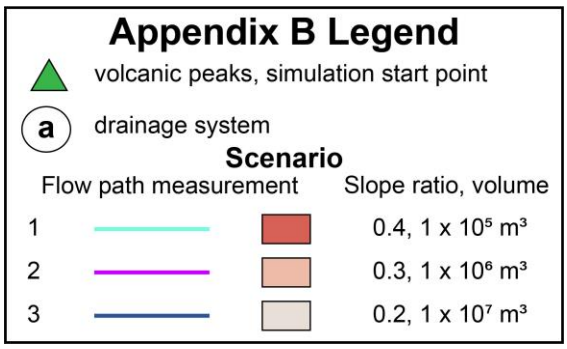


**Drainage code for identification of drainage systems affected in PDC simulations**

| Letter code | Drainage basin |
|---|---|
| a | Job Creek |
| b | No name creek |
| c | Capricorn creek |
| d | East flank drainage system |
| e | Devastator creek |

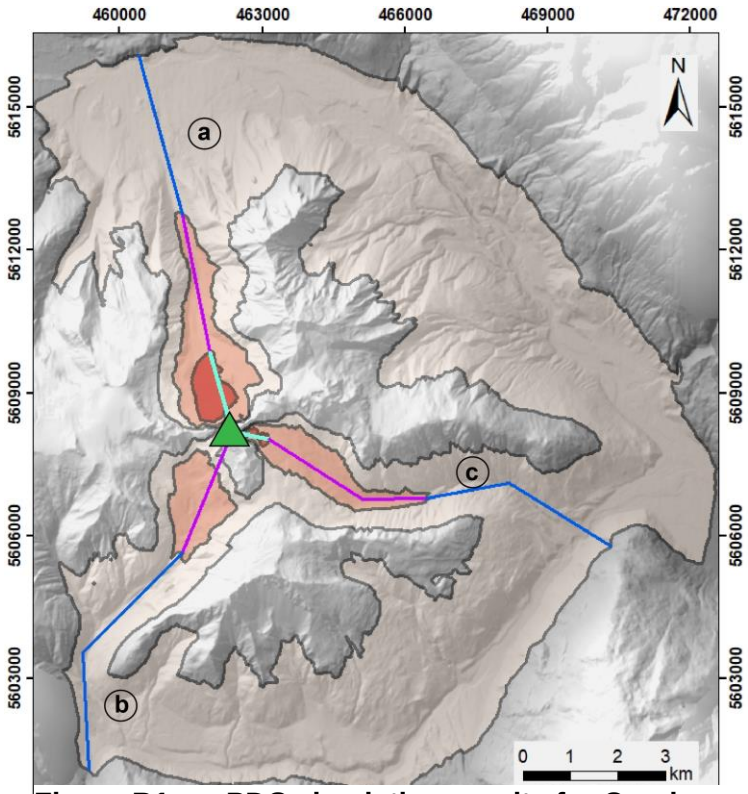


**Figure B1. PDC simulation results for Capricorn Mountain**

| | Scenario | | |
|---|---|---|---|
| Drainage system | 1 | 2 | 3 |
| a | 1.6 km | 4.6 km | 8.0 km |
| b | N/A | 2.8 km | 8.2 km |
| c | 0.6 km | 4.3 km | 8.4 km |

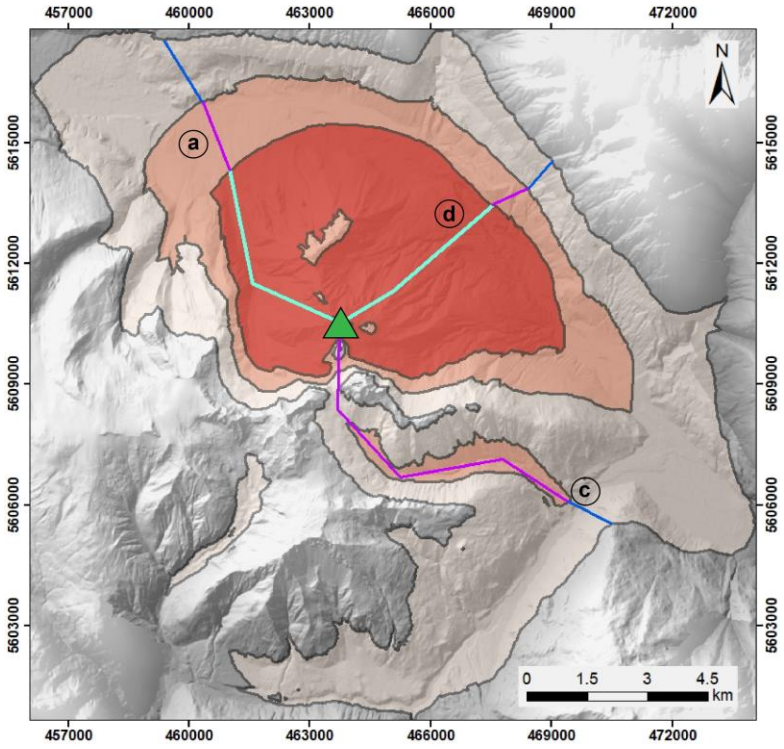


| | Scenario | | |
|---|---|---|---|
| Drainage system | 1 | 2 | 3 |
| a | 5.2 km | 7.0 km | 8.8 km |
| c | N/A | 8.8 km | 10.0 km |
| d | 4.7 km | 5.7 km | 6.6 km |

**Figure B2. PDC simulation results for Plinth Peak**

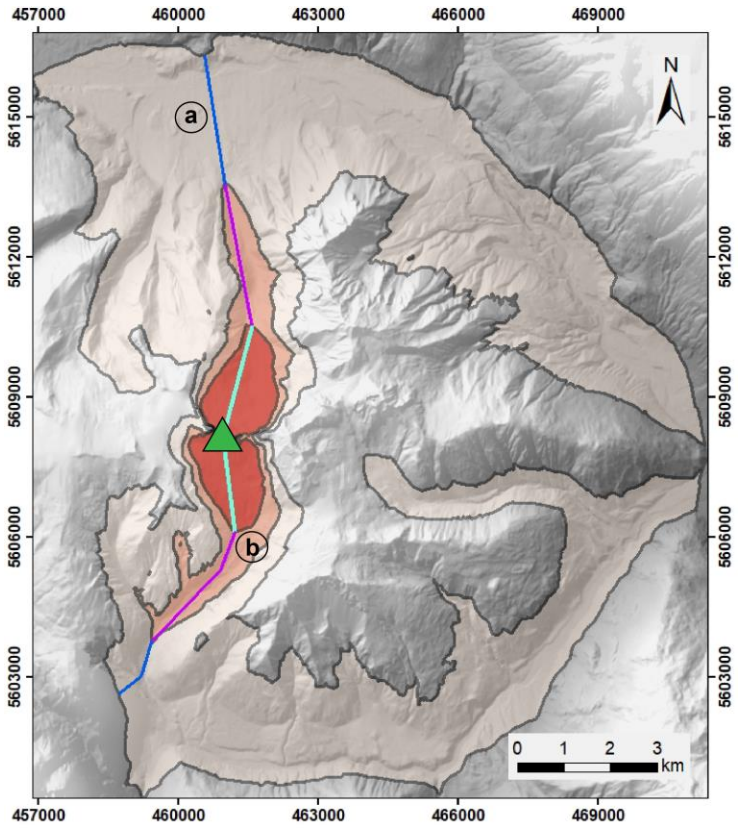


| | Scenario | | |
|---|---|---|---|
| Drainage system | 1 | 2 | 3 |
| a | 2.3 km | 5.4 km | 8.2 km |
| e | 2.1 | 5.1 km | 6.5 km |

**Figure B3. PDC simulation results for Mt. Job**

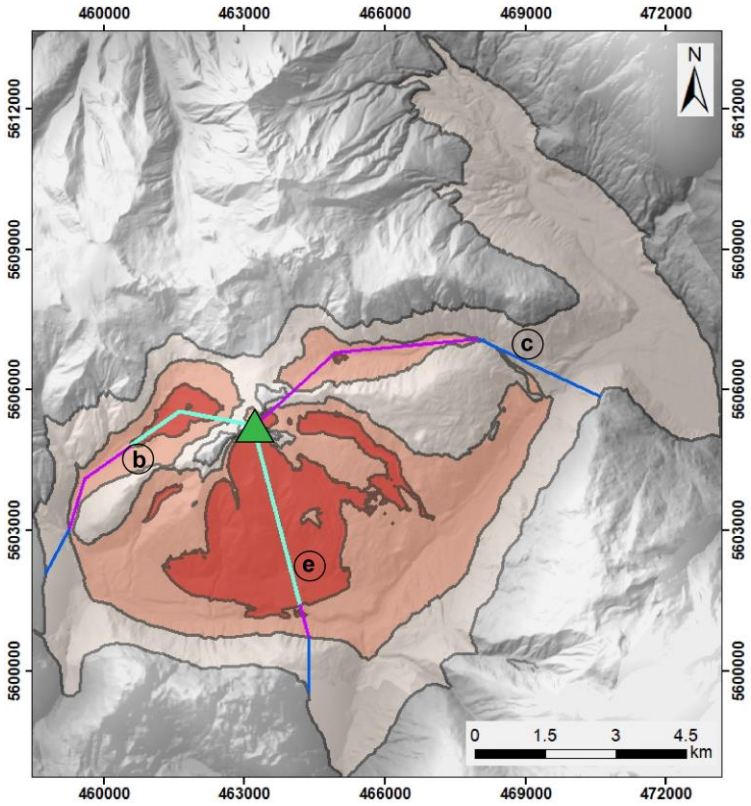


| | Scenario | | |
|---|---|---|---|
| Drainage system | 1 | 2 | 3 |
| e | 2.9 km | 5.2 km | 6.2 km |
| c | N/A | 5.4 km | 8.2 km |
| f | 3.9 km | 4.5 km | 5.7 km |

**Figure B4. PDC simulation results for Pylon Peak**

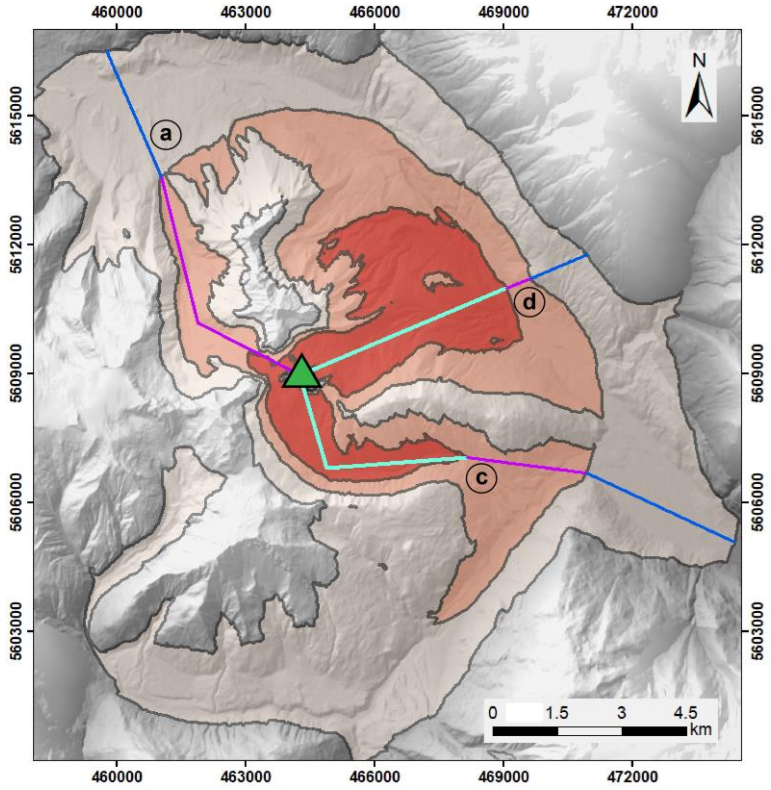


| | Scenario | | |
|---|---|---|---|
| Drainage system | 1 | 2 | 3 |
| a | N/A | 6.1 km | 9.2 km |
| c | 5.3 km | 8.2 km | 12.0 km |
| d | 5.2 km | 6.6 km | 7.8 km |

**Figure B5. PDC simulation results for Mt. Meager**

# Appendix C.

# Comparison of results for Ash3d

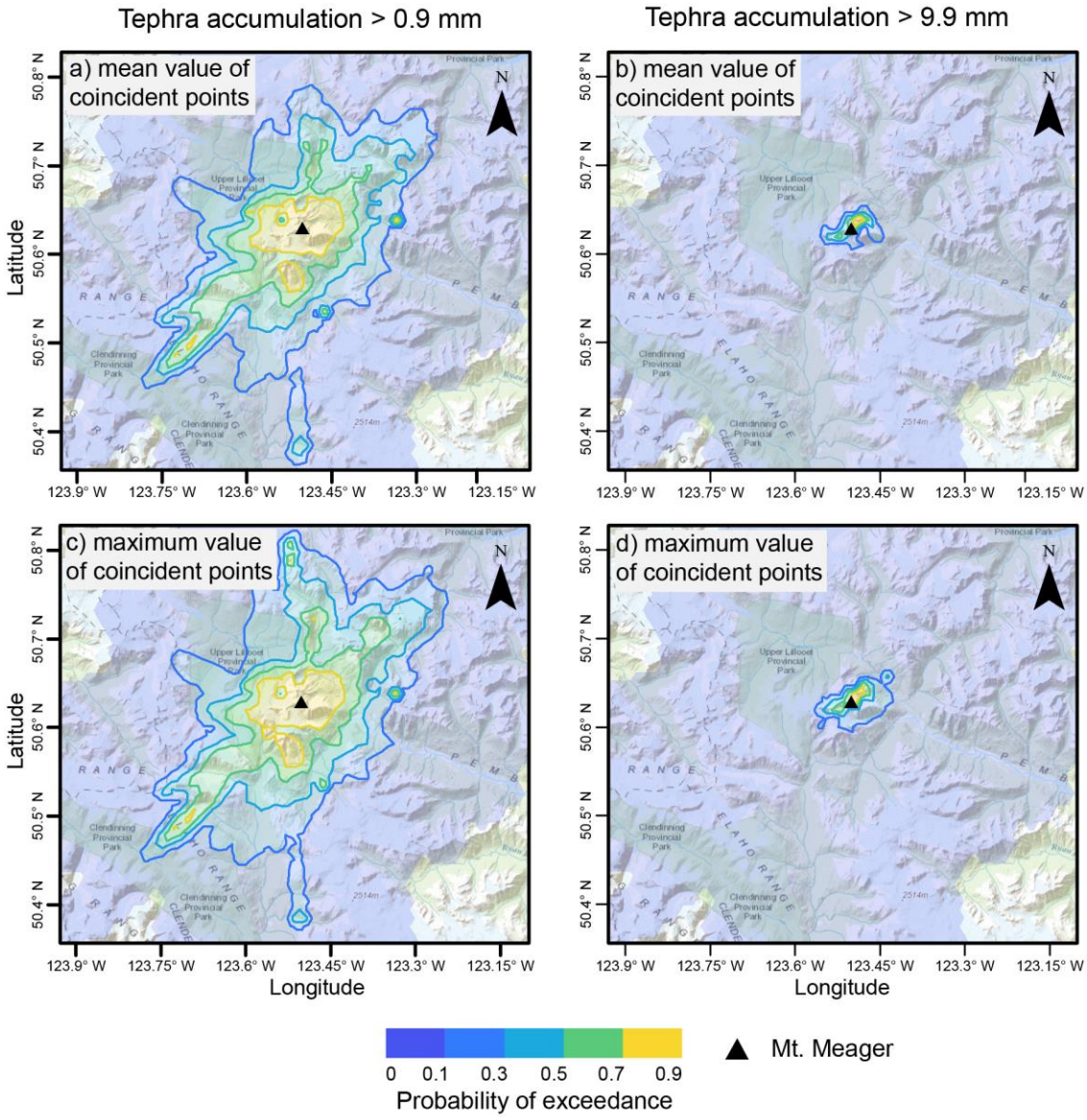


**Figure C1.** **The probability of exceeding the designated tephra accumulation threshold for scenario 1. Compares the results for scenario 1, designating the value of thickness at coordinates with coincident points be the mean value (a,b) or maximum value (c,d). Map scale is 1:860,000, WGS 1984, UTM Zone 10N.**

# Appendix D.

# Tephra deposition with TephraProb

In this appendix the results of simulations in TephraProb reproducing the 2360 cal yr B.P. eruption are presented. The recreation of tephra deposition from this eruption was fit to unpublished isopach maps, although recent work by Jensen delineates updated tephra deposition extent from the past eruption (Jensen et al., 2019). Plume height, total mass, median grain size diameter and sorting are based on parameters specific to the 2360 cal yr B.P. eruption of Mount Meager from Campbell et al. (2016).

**Table D1. TephraProb input parameters for simulation of 2360 cal yr B.P. eruption**

| Parameter | 2360 eruption |
|---|---|
| Grid size | 2500 m |
| Plume height (km asl) | 15-35 |
| Erupted Mass (kg) | $1 \times 10^{11}$ – $1 \times 10^{13}$ |
| TGSD range (Φ) | -6 - 8 |
| Median diameter (Φ) | -4 - 0 |
| Sorting (Φ) | 2.5 |
| Aggregation coefficient | 0.3-0.7 |
| Lithic density (km/m3) | 2500 |
| Pumice density (kg/m3) | 500 |
| Diffusion coefficient (m/s2) | 2000 |
| Fall-time threshold (s) | 5000 |
| Eruption duration (hours) | 6-12 |
| Wind direction | 50°-80° |

The wind directions (table below) tested for Scenario 2, 3 and the 2360 cal yr B.P. eruption scenario represent key target regions of interest for this study concerning where major populations reside and/or locations involving important infrastructure and agricultural resources.

**Table D2. Wind restrictions tested for areas of interest while modelling tephra deposition in TephraProb.**

| Wind direction | Region of interest |
|---|---|
| 30° - 70° | Kootenays |
| 60° - 120° | Lillooet |
| 120° - 175° | Sea-to-Sky Corridor |
| 180° - 360° | West Coast (including northern portion of Vancouver Island) |

**Table D3. Unrestricted wind profile results for probability of exceeding the threshold in designated population centres affected by an eruption of Mount Meager conditional on 2360 cal yr B.P. eruption parameters**

| | | | Exceedance probability | | |
|---|---|---|---|---|---|
| *2360 Cal. Yr. eruption scenario* | | | | | |
| Location | Distance | Direction | 1 kg/m$^2$ | 10 kg/m$^2$ | 100 kg/m$^2$ |
| Gold Bridge | 55.5 km | E | 70% | 40 % | 19.7% |
| Lillooet | 111 km | E | 29.47% | 15.67% | 1% |
| Pemberton | 65 km | S | 32% | 17.18% | 4.53% |

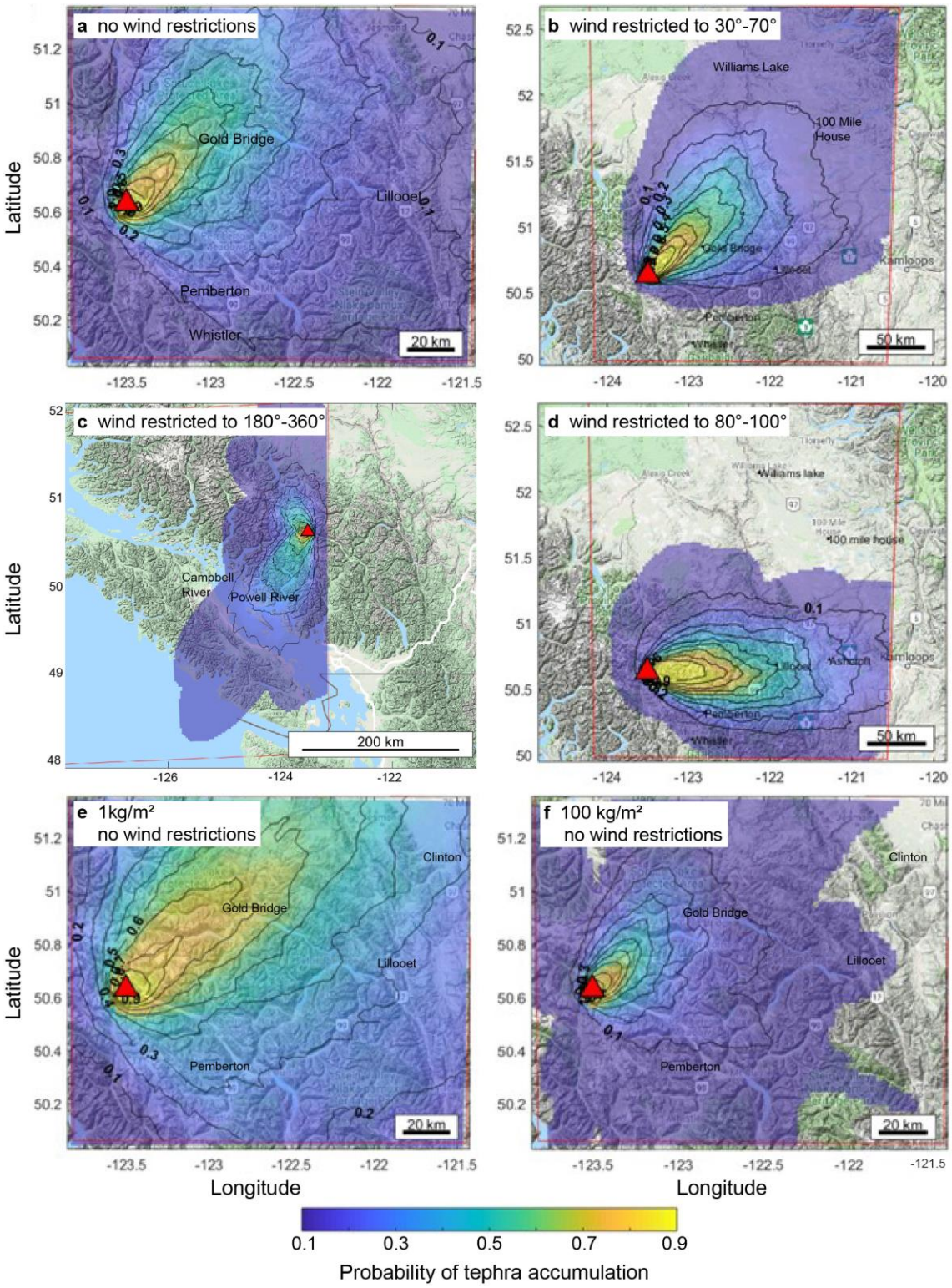


**Figure D1.** **Probability maps based on parameters simulating the 2360 cal yr B.P. eruption for the exceedance of tephra accumulation of 10 kg/m$^2$ with a) no wind restriction, and winds restricted to b) 30°-70°, c) 180°-360°, d) 80°-100° and e) 1 kg/m$^2$ with no wind restrictions and 100 kg/m$^2$ with no wind restrictions. Coordinates are WGS 1984.**

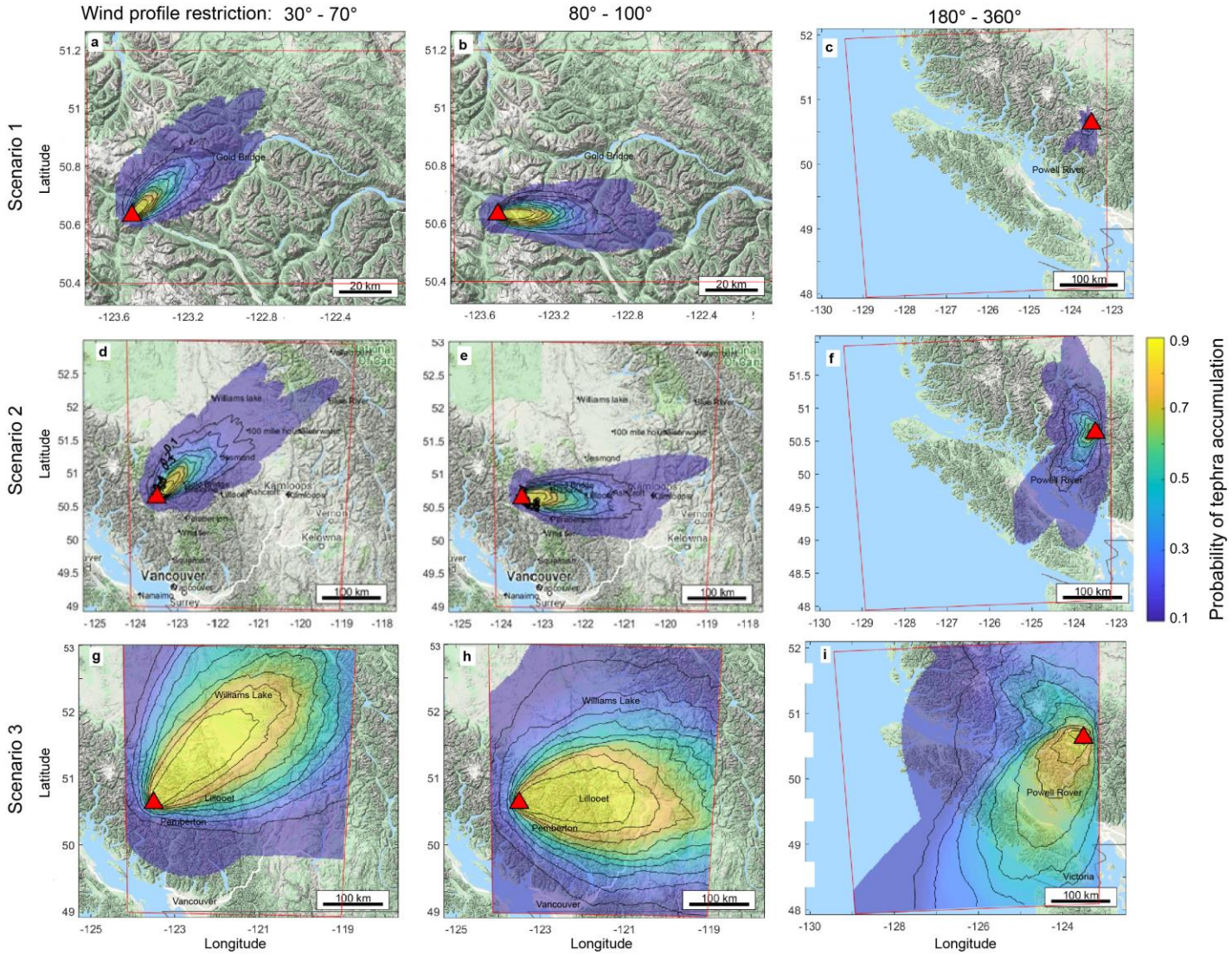


**Figure D2. (See figure description below)**

**Figure D2.** **(See figure above) Mount Meager tephra deposition hazard maps for the probability of exceeding a threshold of 1 kg/m$^2$tephra accumulation modelled in TephraProb with restricted wind profiles. Scenario 1 a) wind restricted to 30° – 70°, b) 80° – 100°, c) 180° – 360°. Scenario 2 d) 30° – 70°, e) 80° – 100°, f) 180° – 360°. Scenario 3 g) 30° – 70°, h) 80° – 100°, i) 180° – 360°. Contours indicate the probability starting at 0.1 and incrementally increased by an interval of 0.1, red line indicates the boundary of the computed grid and the red triangle locates the eruption vent. Coordinates are WGS 1984.**

# Appendix E.

# Glacier Volume calculations for Job Glacier

## Field Work with Ice Penetrating Radar

To estimate glacier volume for validation of the fluid volume input parameter used for the volcanic debris flow modelling, ice-penetrating radar (IPR) was used at Job Glacier. IPR data were collected using the common-offset survey method to produce profiles of Job Glacier ice thickness. Over the course of one day, September 24$^{th}$ 2018, a series of transects (radar lines) were completed.

The common-offset method involves a receiver and transmitter being moved together down a straight line path, with data acquired as traces (Woodward & Burke, 2007). The radar system used for this survey was the Blue System Integration (BSI) IceRadar with antennas of 10 MHz centre frequency. Position control was obtained with an on-board single frequency GPS receiver. The systems hardware and software is described by Mingo & Flowers (2010). The survey lines were planned prior to arriving in the field with the orientation of each line being straight and aligned roughly perpendicular to the ice-flow direction (determined through visual observations of glacier imagery). The total distance covered by the survey was 1.7 kilometres, an area of about 0.19 km$^2$ of the surface of Job Glacier, which itself is about 2.7 km$^2$. The survey was therefore only able to cover about 7% of the total glacier (as mapped from 2016 imagery). Due to logistics and difficult terrain, much of the glacier is inaccessible. Time constraints also limited the amount of area able to be covered by the field team. This amounted to five line segments, four of which were oriented to profile the cross section of the glacier and one longitudinal line oriented to sample the middle underlying structural morphology (north-south orientation on Job Glacier). While all line data collected was used in the calculation of the total glacier volume, longitudinal profiles are known to underestimate ice depth in u-shaped valleys. The entire dataset was used in this exercise due to the reality of its small size in comparison to the actual size of the glacier.

The glacier bed was apparent in all radar sections with minimal post-processing, and the bed was picked using the BSI IceRadar Analyzer (Mingo & Flowers, 2010).

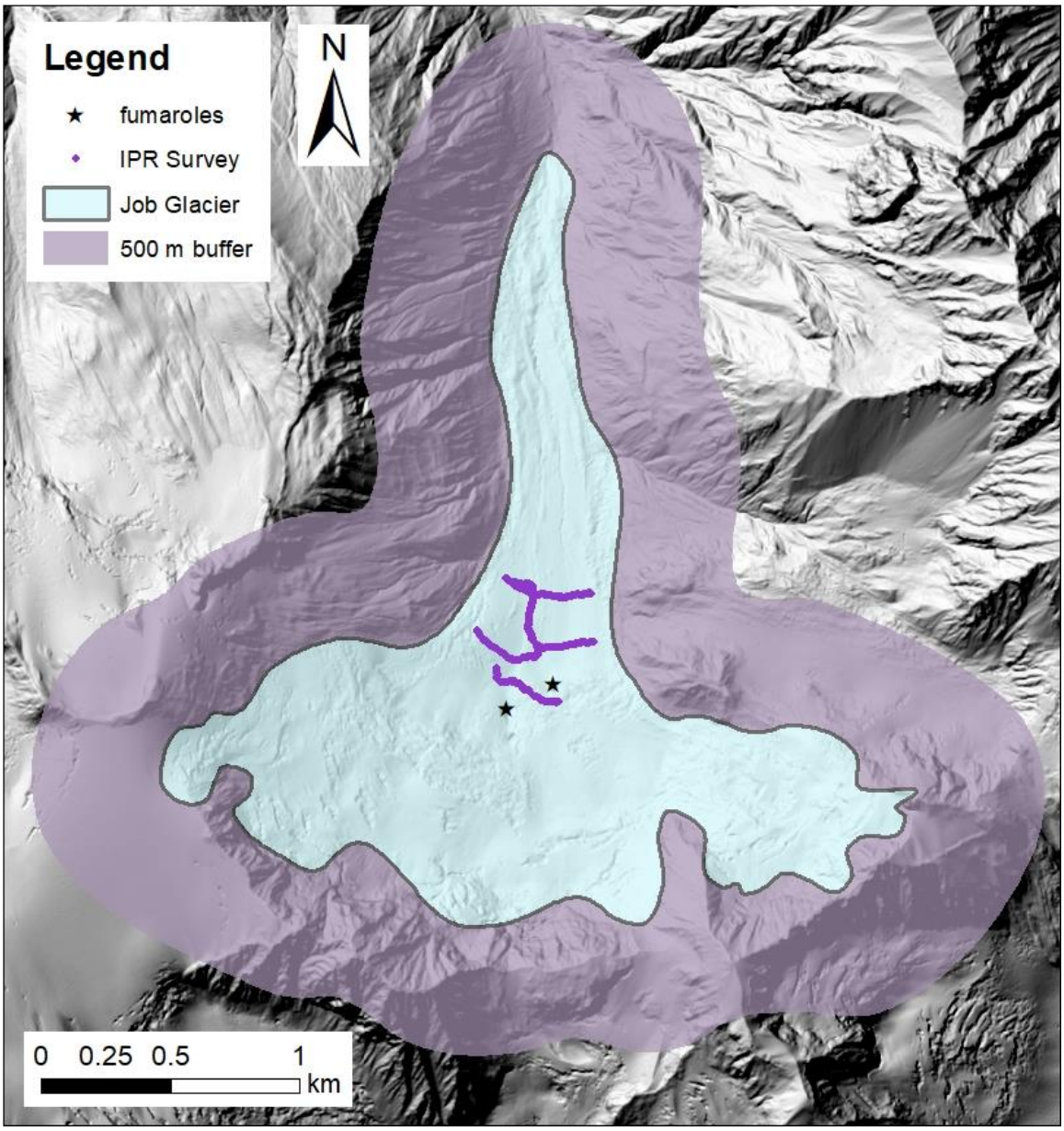


**Figure E1. Ice penetrating radar survey orientation on Job Glacier**

## Interpolation Methodology

Interpolation methods were used in order to calculate an estimated volume of Job Glacier from thickness values obtained by the ice penetrating radar survey. Although the coverage of the survey was minimal across the entire glacier, utilizing interpolation calculations in Matlab, along with including additional points to capture ground slope geometry surrounding the glacier, a preliminary estimate of volume for Job Glacier could be obtained. The buffer included elevation points from the 1 metre resolution LiDAR, for

500 metre zone surrounding the glaciers outline, as mapped by 2016 glacier extent. This buffer includes the geometry of slopes surround the glacier, which acted to inform the interpolation calculations for the geometry of the bed beneath glacier cover. Errors are involved in this methodology, as not all areas surrounding Job glacier are without glacier cover (neighbouring glaciers are within the designated buffer).

The interpolation methods, provided by Matlab functions, that were used include: linear interpolation, natural neighbour interpolation, cubic interpolation, and biharmonic interpolation. Interpolation was performed for ice bed thickness, based on a grid size of 20 m by 20 m, across the extent of data (buffer in glacier extent included). The volume calculation included the interpolated thickness values and known elevations of ice (from LiDAR data). The interpolated thickness values and assuming thickness values of points extending into the buffer zone were 0 metres thick. Volume was calculated using the covhull method in Matlab for each interpolation method.

## Results

The volume of Job Glacier is estimated to be $7.5 \times 10^7$ $m^3$ based on interpolated calculations of ice thickness values obtained from an ice radar survey of the glacier, performed in September 2018. This work was carried out in order to derive constraints for the volume of fluid potentially available for lahar flows stemming from this drainage basin. Calculations were made in Matlab using several interpolation functions (Table E1).

**Table E1. Interpolated ice volumes of Job Glacier**

| Interpolation method | Grid spacing (m) | Volume ($m^3$) |
|---|---|---|
| Cubic | 20 | $8.85 \times 10^7$ $m^3$ |
| Natural Neighbour | 20 | $7.07 \times 10^7$ $m^3$ |
| Biharmonic | 19.2 | $1.58 \times 10^8$ $m^3$ |
| Linear | 19.2 | $6.83 \times 10^7$ $m^3$ |

Aside from the biharmonic interpolation method all other methods result in the same order of magnitude of ice volume. Errors are large due to the fact that the IPR survey only covered a small portion of the glacier (7%). This glacier is also retreating

(common for most alpine glaciers around the world) which means the glacier volume is actively being reduced as time passes.

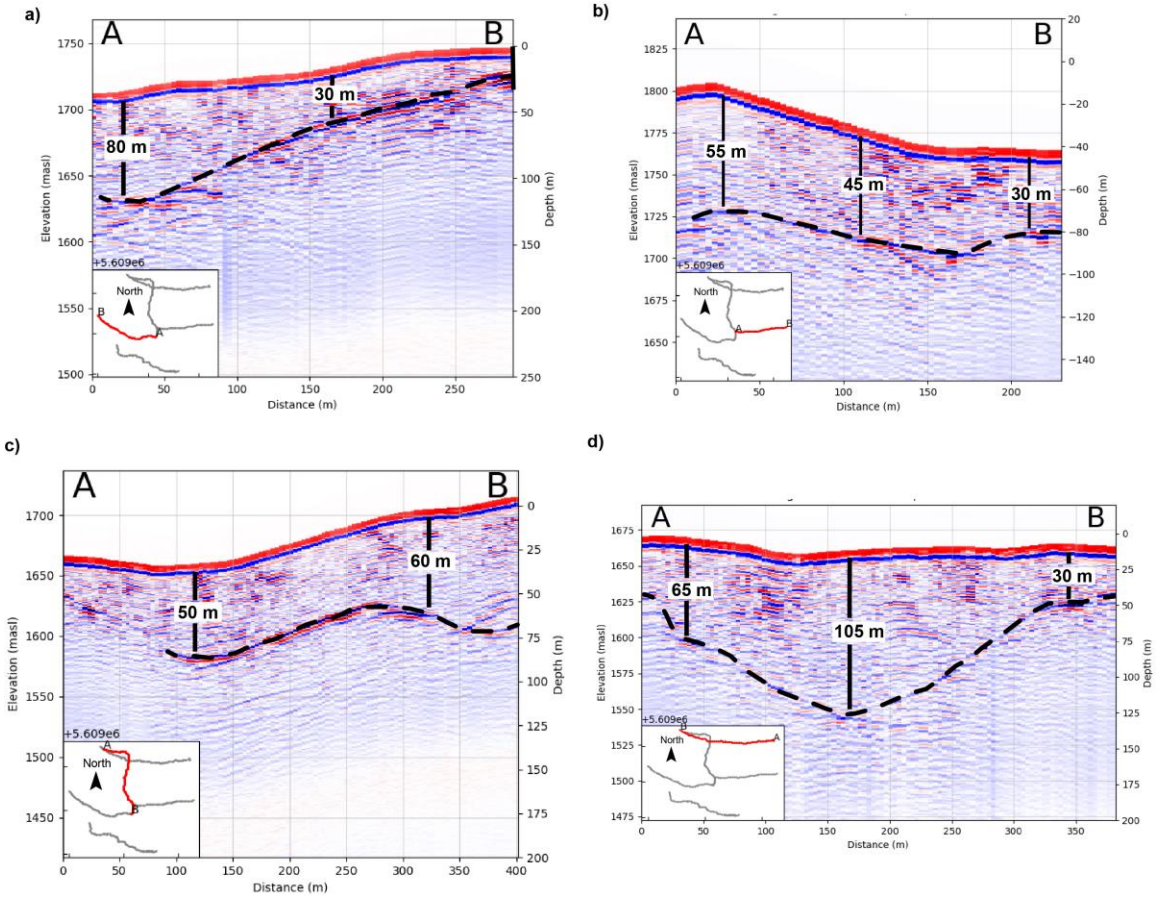


**Figure E2. Bed thickness values along four lines of the ice penetrating survey on Job Glacie collected September 2018.**